A Response Surface Exit Crown Model Built from the Finite Element Analysis of a Hot-Rolling Mill

William E. Stewart

Thesis submitted to the Faculty of the
Virginia Polytechnic Institute and State University
in partial fulfillment of the requirements for the degree of

Master of Science
in
Mechanical Engineering

Robert L. West, Co-chair
William T. Baumann, Co-chair
James E. Atkinson

October 3, 2011
Blacksburg, Virginia

A Response Surface Exit Crown Model Built from the Finite Element Analysis of a Hot-Rolling Mill

William E. Stewart

(ABSTRACT)

Nine independent and four dependent variables are used to build a response surface to calculate strip crown using the difference in the industry standard strip height measurements. The single element response surface in use provides the advantages of continuous derivatives and decouples rolling load from the determination of exit height. The data points to build the response surface are the product of a calibrated finite element model. The rolling dynamics in the finite element model creates a transient that requires nonlinear regression to find the system steady-state values.

Weighted-least squares is used to build a response surface using isoparametric interpolation with the non-rectangular domain of the mill stands represented as a single element. The regression statistics, the 1-D projections, comparisons against other response surface models and the comparisons against an existing strip crown model are part the validation of the response surface generated.

A four-high mill stand is modeled as a quarter-symmetry 3-D finite element model with an elastic-plastic material model. A comparison of the pressure distribution under the arc of contact with existing research supports the pressure distribution found with experiments conducted by Siebel and Lueg [16] and it also suggests the need for one improvement in the initial velocity for the strip in the finite element model.

The strip exit heights show more sensitivity to change than strip exit crown in seven out of the nine independent variables, so a response surface built with the strip exit height is statistically superior to using the derived dependent variable strip exit crown. Sensitivity of strip exit crown and the strip exit heights to changes in work-roll crown are about equal. Backup-roll diameter sensitivity is small enough that oversampling for the mean trend has to be considered or ignore backup-roll altogether. Strip entry velocity is a new independent variable, unless the response surface is built from the derived variable, strip exit crown.

A problem found is that the sensitivity of strip entry crown and work-roll crown requires a larger than typical incremental change to get a reliable measure of the change strip exit crown. A narrow choice of high and low strip entry crowns limits the usefulness of the final response surface. A recommendation is to consider the use of the strip cross-section as an exit crown predictor.

Acknowledgments

I would like to thank my advisory committee: Dr. Robert L. West, Jr., Dr. William T. Baumann, and James Atkinson.

Special thanks go to my advisor, Dr. West, for his patience, expertise and guidance in completing this work; and to James Atkinson and Thomas Ranger of Industrial Process Support Services for their expertise and for sponsoring this project. I would also like to thank Derek Slaughter for the development of the finite element model used.

Contents

List of Figures

List of Tables

List of Symbols
Uppercase Symbols

A	dummy parameter for steady-state nonlinear fit
$[\mathbf{A}]$	state-space A matrix
B	dummy parameter for steady-state nonlinear fit
$[\mathbf{B}]$	state-space B matrix
B_s	pre-strain amount in the Swift equation
C	dummy parameter for steady-state nonlinear fit
C	condition number for regressor matrix
C^0	interpolation functions continuous at the nodes
C^1	interpolation functions first derivative continuous at the nodes
$[\mathbf{C}]$	state-space C matrix
C_e	strip entry diametrical crown
C_x	strip exit diametrical crown
$C_{x,obs}$	strip exit diametrical crown calculated from observation
$C_{x,prod}$	strip exit diametrical crown derived from current crown model
$\{C_{x,k}\}$	vector of response surface nodal value ($k \times 1$)
$\{C_{x,obs}\}$	vector of steady-state exit crown values ($n \times 1$)
C_{RS}	roll-stack damping factor
C_{std}	stand-frame damping factor
C_{stp}	strip damping factor
C_{wr}	work-roll diametrical crown
$C_{x,1}$	strip diametrical exit crown derived from the exit height difference
$C_{x,2}$	strip diametrical exit crown based on the strip cross section polynomial fit
$C_{x,RS}$	strip diametrical exit crown derived directly from the response surface
$C_{x,obs}$	strip diametrical exit crown derived from the observation exit height difference
C_{x0}	starting value from a Taylor series approximation of exit crown
D	dummy parameter for steady-state nonlinear fit
$[\mathbf{D}]$	state-space D matrix
E	modulus of elasticity
$ExMu$	excitation multiplier
F_{α,ν_1,ν_2}	F-test statistic with degrees of freedom ν_1 and ν_2
$F_{\alpha,k-1,n-k}$	F-test statistic with degrees of freedom $k-1$ and $n-k$
H	Ramberg-Osgood stress constant
J	jacking load
K_{dw}	Gizburg's work roll effect on strip exit crown
K_{std}	mill stand frame stiffness
K_{stp}	strip stiffness

Uppercase Symbols

L	undeformed strip length
L'	deformed strip length along strip surface
$[\mathbf{M}]$	mapping matrix between isoparametric and natural values
M_1	$mass_1$ (work roll)
M_2	$mass_2$ (backup roll)
$N_{1,1}$	example interpolation shape function #1 for the h_{ef} variable
$N_{1,2}$	example interpolation shape function #2 for the h_{ef} variable
$N_{2,1}$	example interpolation shape function #1 for the gap variable
$N_{2,2}$	example interpolation shape function #2 for the gap variable
$N_{l,1}$	quadratic shape function #1 for the "l^{th}" variable
$N_{l,2}$	quadratic shape function #2 for the "l^{th}" variable
$N_{l,3}$	quadratic shape function #3 for the "l^{th}" variable
$N_{i,1}$	interpolation shape function #1 for the "i^{th}" variable
$N_{i,2}$	interpolation shape function #2 for the "i^{th}" variable
P	rolling load
$\{P_k\}$	vector of response surface nodal value ($k \times 1$)
$\{P_{obs}\}$	vector of dependent variable values from n observations
$\{P_{obs}\}$	vector of steady-state rolling load values ($n \times 1$)
$[\mathbf{P}]$	transformation matrix
R'	deformed work roll radius
R'_0	initial work roll radius
R^2	coefficient of determination
$R_{i,i}$	regressor matrix diagonal
$RuMu$	finite element model run-time multiplier
Rx	strip reduction
S	sample standard deviation
SNR	signal to noise ratio
$SNRdb$	signal to noise ratio in decibels
SSE	sum of the squares due to error
SSR	sum of the squares due to regression
S^2	sample variance
S_a^2	larger F-test variance with a degrees of freedom
S_b^2	smaller F-test variance with b degrees of freedom
S_x^2	strip centerline exit height variance
S_{xf}^2	strip exit height at the feather variance
S_{cx}^2	strip exit crown variance

Uppercase Symbols

S_n^2	noise mean square sum
S_s^2	signal mean square sum
S_i^2	sample variance for observation i
S_y	strip yield stress
$S_{y,mult}$	elliptical yield curve yield multiplier
T	lumped mass model time period
U	unit-strip crown
U_1	displacement in the direction of the x-axis
$U_{2,br}$	backup roll center displacement in the direction of the y-axis
$U_{2,wr}$	work roll center displacement in the direction of the y-axis
$U_{2,excit}$	vertical work-roll displacement during *excitation phase*
U_2	displacement in the direction of the y-axis
U_3	displacement in the direction of the z-axis
$U_{3,excit}$	horizontal work-roll displacement during *excitation phase*
Y_0	material constant for the Swift equation
Y_s	material constant for the Swift equation
$[\mathbf{W}]$	least squares weights matrix
Z_2	entry crown effect on strip diametrical exit crown

Lowercase Symbols

a	dummy parameter for steady-state nonlinear fit
avg_i	average natural values of variable i in example
b	dummy parameter for steady-state nonlinear fit
b_{ell}	elliptical strain constant
c	dummy parameter for steady-state nonlinear fit
c_0	two degree of freedom equation steady-state exit height
c_1	generic constant for two degree of freedom generic equations
c_2	generic constant for two degree of freedom generic equations
c_3	generic constant for two degree of freedom generic equations
c_4	generic constant for two degree of freedom generic equations
d	dummy parameter for steady-state nonlinear fit
d_1	point 1 at entry with excess deformation of work roll
d_2	point 2 at exit with excess deformation of work roll
d_{br}	diameter of the backup roll
d_{wr}	diameter of the work roll
$d_{wr,1}$	diameter of the work roll, 625 [mm]
$d_{wr,2}$	diameter of the work roll, 775 [mm]
gap	finite element model gap measured work-roll surface to work-roll surface
$\widehat{gap}$	finite element model gap after pre-scaling
gap_0	gap search initial estimate
gap_i	nodal value of natural gap values
gap_j	nodal value of natural gap values
$\{gap_k\}$	vector of nodal values for natural gap
gap_{model}	finite element model gap
gap_{std}	industry standard gap measured from work-roll center to work-roll center
h_e	strip centerline entry height
h_{ee}	strip entry height at the edge
h_{ef}	strip entry height at the feather
$\{h_{ef,k}\}$	vector of nodal values for natural strip entry height
$\widehat{h_{ef}}$	strip entry height at the feather after pre-scaling
$h_{ef,i}$	example response surface nodal natural entry height at the feather value
$\{h_{rl,obs}\}$	vector of pseudo-strip heights from rolling load
h_{last}	last strip exit height used in steady-state determination
h_{prj}	projected strip exit height at run time $\times 1.5$
h_x	strip centerline exit height
$h_{x,cross}$	strip centerline exit heights not used to build response surface
$\{h_{x,k}\}$	vector of response surface nodal value ($k \times 1$)
$h_{x,obs}$	strip centerline exit heights used to build the response surface

Lowercase Symbols

$\{h_{x,obs}\}$	vector of steady-state centerline exit height values ($n \times 1$)
$h_{x,n}$	steady-state search ending exit height data point (y-axis)
$h_{x,RS}$	strip centerline exit height from the response surface
$h_{x,targ}$	gap search strip exit height desired
h_{x0}	initial strip centerline exit height
$h_{x,0}$	steady-state search starting exit height data point (y-axis)
h_{xe}	strip exit height at the edge
h_{xf}	strip exit height at the feather
$h_{xf,cross}$	strip exit heights at the feather not used to build response surface
$h_{xf,obs}$	strip exit heights at the feather used to build the response surface
$h_{xf,RS}$	strip exit height at the feather from the response surface
$\{h_{xf,k}\}$	vector of response surface nodal value ($k \times 1$)
$\{h_{xf,obs}\}$	vector of steady-state exit height at the feather values ($n \times 1$)
$h_{xf,1}$	strip exit height at the feather from steady-state determination
$h_{xf,2}$	strip exit height at the feather based on polynomial fit from $\pm wid_{fea}/2$
$h_{xf,3}$	strip exit height at the feather based on polynomial fit centerline to start of deformation,
k	number of degrees of freedom in tensor product
m	slope for the equation for a line
m_1	minor stress peak number 1
m_2	minor stress peak number 2
n	number of observations used to build response surface
n	the Ramberg-Osgood exponent
n_1	number of nodes for the dimension 1 variable in the response surface
n_2	number of nodes for the dimension 2 variable in the response surface
n_3	number of nodes for the dimension 3 variable in the response surface
n_{q-1}	number of nodes for the dimension $q-1$ variable in the response surface
n_s	the Swift strain hardening exponent
q	number of dimensions in response surface
$\{r\}$	vector of residuals after weighted-least squares fit
$retNatCoor$	function name to convert isoparametric to natural coordinates
rng_i	natural value range of variable i in example
s	draft curve height
s_0	final draft curve height to raise strip to set gap
t	time
t_0	discrete time zero
t_1	discrete time at index 1
t_i	discrete time at index i
t_n	discrete time for end of run

Lowercase Symbols

t_{exc}	excitation time
t_{run}	run time
$tolerance$	gap search completion tolerance
v_1	figure strip velocity, 1284 [mm/s]
v_2	figure strip velocity, 4018 [mm/s]
v_3	figure strip velocity, 6753 [mm/s]
vel_e	strip entry velocity at strip entry point under work roll
vel_{NP}	work roll tangential velocity at neutral point
vel_x	strip exit velocity at strip exit under work roll
vel_{wr}	work roll tangential velocity
wid	strip width
wid_{fea}	strip width less the feather offset (typically 40 [mm])
$wid_{fea,3}$	strip width less a feather offset determined by edge deformation
x	x-axis
x_i	natural coordinate
$x_{i,0}$	initial value of natural coordinate in model comparisons
$\{x_{targ}\}$	vector of desired natural variables
$\{y_n\}$	set of steady-state of exit heights
y	y-axis
$\{y\}$	state-space vector
$\{\hat{y}\}$	state-space output vector after transformation
y_1	state-variable 1
y_2	state-variable 2
y_3	state-variable 3
y_4	state-variable 4
$\{x\}$	vector of natural coordinates of dimension $q \times 1$
$\{x_{1,k}\}$	vector of natural coordinates mapped to isoparametric coordinates
$\{x_{2,k}\}$	vector of natural coordinates mapped to isoparametric coordinates
$\{x_{q,k}\}$	vector of natural coordinates mapped to isoparametric coordinates
z	z-axis
$\{z\}$	state-space output vector
z_0	two degree of freedom starting position on z-axis
z_e	z-axis position in millimeters of strip and work roll at strip entry
z_n	two degree of freedom ending position on z-axis
z_x	z-axis position in millimeters of strip and work roll at strip exit

Greek Symbols

α	hand tuned parameter to improve the gap search
$\bar{\epsilon}$	true stress
Δ	a small change in the variable
ϵ_{max}	maximum strain
γ	damping factor for a under or over damped system
γ_1	damping factor for sub-system 1
γ_2	damping factor for sub-system 2
$[\mathbf{\Lambda}]$	diagonal matrix of eigenvalues or spectral matrix
ϕ_1	Lagrangian two variable linear shape function
ϕ_2	Lagrangian two variable linear shape function
ϕ_3	Lagrangian two variable linear shape function
ϕ_4	Lagrangian two variable linear shape function
$[\phi_{4x1}]$	sample two variable linear 4×1 tensor product vector
λ_0	smallest eigenvalue found for regressor matrix
λ_1	eigenvalue of generic two degree of freedom equation
λ_2	eigenvalue of generic two degree of freedom equation
λ_3	eigenvalue of generic two degree of freedom equation
λ_4	eigenvalue of generic two degree of freedom equation
λ_{k-1}	largest eigenvalue found for regressor matrix
$\{\lambda\}$	vector of eigenvalues found for regressor matrix
η_1	scaled h_{ef} natural coordinate in example
η_2	scaled gap natural coordinate in example
ν	Poisson's ratio
ω	under damped frequency or over damped pseudo-frequency
ω_1	frequency for sub-system 1
ω_2	frequency for sub-system 2
ω_d	damped frequency in radians
ω_n	natural frequency in radians
$[\phi(\{\boldsymbol{\zeta}\})]$	isoparametric response surface tensor product
$[\Phi]$	isoparametric tensor product for all observations
$[\Phi]^T$	transpose of $[\Phi]$
ρ	strip density
σ_y	strip yield strength
σ_{wr}	average work roll stress at strip boundary
σ_1	average strip stress for first layer of strip elements
σ_2	average strip stress for second layer of strip elements
σ_3	average strip stress for third layer of strip elements
θ	generic angle in radians

Greek Symbols

ζ_i isoparametric coordinates
$\{\zeta\}$ vector of isoparametric coordinates of dimension $q \times 1$
ζ_1 isoparametric coordinate 1 for two-dimensional example
ζ_2 isoparametric coordinate 2 for two-dimensional example

Chapter 1

Introduction

1.1 Research Objective

Based on a quick survey of the literature, the most commonly used crown model is a beam model. All of the beam models have to make assumptions about how to model contact and about how to model the strip or to use compatibility equations to model the expected strip deformation. Therefore, a model that eliminates some of these simplifications is at the very least an incremental improvement.

A solution to produce hot-rolled strip for five to seven stand mill is not necessarily optimal. One option is to run simulations as the search progresses, in which case minimizing simulation run time is important. The other option is saving the results of each simulation to reuse in a future search, which makes simulation run times less critical. Populating the search space in a planned manner makes a response surface practical and a response surface with continuous gradients provides the kind of functional continuity to make searches for optimal mill setup straightforward. Additional simulations are only needed to extend the search space. Estimating the physics with a response surface can also decouple dependent variables, namely, the mutual dependence between exit height and rolling load.

Domanti and McElwain [6] list three world conferences concerned with the problem of producing better strip shape and metallurgical properties. They also review some of the advances in rolling models made using the Finite Element Method, which eliminates the need to make many of the simplifying assumptions used in other solutions, especially how to model the strip. The problem becomes a choice of a material model (constitutive relationship) for the roll stack and the strip; whether to solve for the deformed strip using a Lagrangian or Eulerian frame; the use of two- or three-dimensional elements; and whether or not to model the work roll or backup roll with finite elements or as a rigid-body.

1.2 Solution Hypothesis

This research is designed around a building a response surface model of a four-high hot-rolling mill stand to use in mill stand setup. Instead collecting actual mill data, which is a costly and an impractical proposition, a response surface is built taking a design-of-experiments approach and using the data collected from a dynamic-explicit solution of a finite-element mill-stand model. The mill-stand model uses a discretized (meshed) roll stack and strip; and includes the dynamics of rolling the strip. The finite-element mill-stand model used is the product of prior research [21]. The response surface approach developed makes mill setup applicable to either new or existing strip products.

1.3 Implementation

The biggest challenge to implementing a finite element model is balancing run times against meshing all of the stand components with the finest mesh possible and the use of the most detailed material model possible. A larger mesh size or replacing meshed components with a mathematical construct must take place to balance accuracy against the costs. The finite element model in use solves for the strip rolling dynamics using Abaqus explicit. The major components of the four-high mill-stand model are the strip, the work rolls and backup rolls. The mill stand is replaced with a linear spring and damper. The work rolls are driven at a specified angular velocity and there is work roll to strip contact and work roll to backup roll contact. Strip yielding is modeled as elastic-plastic and strip crown is represented with a parabolic curve. There is complete control of nine model variables and this can be extended to include any of the work roll, backup roll or strip parameters. The simulation limitations or drawbacks are:

- The stand frame is replaced with a linear spring and damper combination.
- The model needs to be calibrated against a real mill stand.
- The run times are significant (run times in hours and minutes versus minutes and seconds).
- Convergence is a function of mesh size, so run times must be balanced against simulation convergence.

The independent variables chosen to build the response surface from are

- strip width,
- strip yield strength,
- strip entry diametrical crown,
- strip entry height at the feather,
- jacking load,

- work-roll diameter,

- work-roll diametrical crown,

- backup-roll diameter,

- work-roll gap (gap).

The remaining parameters are configured for a specific mill. Table 1.1 illustrates the poor scaling that exists between many of the variables and the relatively large change in range for a single variable. Another drawback to building a response surface for a hot-rolling mill, besides the scaling issues, is that the variable domain is not rectangular, for instance,

- as gap and strip height change, the useful minimum and maximum changes for many of the other independent variables,

- some variable value combinations are meaningless, like a gap value greater than the entry height,

- some variable value combinations are not used in practice, like a gap close to zero with an entry height greater than 30 [mm].

Table 1.1: Estimates of Variable Relative Scales.

Variable	Upper limit	Lower limit	Ratio
Strip width, [mm]	1700	900	1.9
Strip crown, [mm]	0.4	0.04	10.0
Strip height, [mm]	45	1	45.0
Strip yield strength, [tonne/mm^2]	0.00344	0.0008	4.3
Work-roll diameter, [mm]	800	600	1.3
Work-roll gap, [mm] (surface-to-surface)	30	0.01	3,000.0
Work-roll crown, [mm]	0.14	0.001	140.0
Backup-roll diameter, [mm]	1700	1400	1.2
Jacking load, [tonne]	300	0.01	30,000.0
Rolling load, [tonne]	2500	500	5.0
Worst case numeric scaling	2500	0.0008	3,125,000.0

The response surface will be implemented using a nine-dimensional isoparametric formulation to reduce the effects of the scaling issues and the non-rectangular domain. A response surface is built for the four-dependent variables: strip exit crown, centerline strip height, strip exit height at the feather, and rolling load.

1.4   The Study Scope

The primary focus is

- identifying the run and meshing parameters needed to run the dynamic-explicit solution for the different stands,

- creating a sampling plan that for the finite element model simulations,

- determining the exit height and rolling values from extracted simulation data,

- implementing a response surface to calculate the strip exit crown based on the centerline strip exit height and the strip exit height at the feather,

- validating the choice of polynomial order for the response surface.

Short comings of the proposed crown model or any needed improvements to the finite-element simulation are also explored.

Out of scope for this project is the development of a mill setup optimization procedure using a gradient-based method for all seven mill stands. Development of alternative crown definitions or a separate response surface model just for rolling load is also out of scope of this research. Crown control using backup-roll crown is not dealt with.

1.5   Discussion Organization

This thesis starts with a brief description of a four-high mill stand along with the stand components that vary with rolling or that are under user control. This includes identification of the important points of measurement on the strip. Next, the quarter-symmetry finite element (FE) model is introduced and its boundary conditions and constraints enumerated.

Simulating the model dynamics requires a compromise between how a real stand feeds the strip and the problems that occur solving for a discretized model. The method of loading the strip and setting the gap is described along with the rationale for not employing the same method as a real mill stand. A two degree of freedom lumped-mass model is developed as a basis to identify the steady-state exit heights and rolling loads. Possible improvements in the choice of new simulation setup time and damping parameters for 1.6 [mm] strip are discussed too.

The discussion moves on to provide additional details about how well the FE simulation compares to behavior found in prior research. A needed change to initial conditions of the strip is pointed out. Also, a means of identifying the initial conditions issue is presented using a visual of what happens under the work roll.

Additional evidence for the choice of a two-degree of freedom lumped-mass model is presented using the Fast-Fourier Transform of collected data. The derivation of the equations of motion follows and finishes up with a simplified-generic equation. Next, the selection of data points from the simulation and their reformulation into the time domain and the two methods of finding the coefficients for the above equation is covered. The solution provides the steady-state values necessary to build the response surface.

The response surface discussion begins with the choice of the nine-independent and four-dependent variables and introduces an alternative method for calculating strip exit crown that works well at the finishing stands. The method of generating simulation samples follows, including the initial miss steps and the final sampling plan.

The mathematics behind the interpolation function based response surface is presented, starting with the interpolation functions for un-scaled and untransformed variables using a two-dimensional example. Continuing with the example, variable scaling and isoparametric formulations for the interpolation functions are developed. Another option, variable pre-scaling is covered, which also leads into how to get the partial derivatives in terms of the original independent variable. Finally, a quick derivation of the method of weighted-least squares and how it is used to compute the unknown response surface coefficients or coordinates is presented.

The next section discusses how one- and two-dimensional projections are used to take the guess work out of determining the polynomial order for an independent variable. The highlights of this section are that four variables are quadratic and support is found for the choice of a strip exit crown model. The functional form of the backup-roll diameter with its mixed results is discussed last.

The nine-dimensional response surface is evaluated with the statistics and found to have one unnecessary variable, the backup-roll diameter. The process to validate three candidate eight-dimensional response surfaces follow, as well as listing the three criteria necessary to make the correct response surface choice. An additional response surface tool is introduced that provides a means to find response surface nodes without enough samples.

Both the original nine-dimensional response surface and the improved eight-dimensional response surface are compared to a production model. Strip exit crown from both models is plotted for perturbations of eight independent variables for three representative mill stands. A sampling problem with strip entry crown and the solution is identified.

The summary, conclusions and recommendations complete the write up.

Chapter 2

Literature Review

2.1 Rolling Load and Neutral Point

Orowan [16] develops a graphical method to calculate the pressure distribution along the arc of contact. Once the pressure distribution is known calculating the rolling load and rolling torque is possible. He also identifies some simplifications to make the equations easier to work with:

1. Dividing the strip up into many thin vertical strips between the two work rolls, the stresses are modeled as a normal and shear force exerted at a slight incline top and bottom, and as a normal force on each side without any shear (*homogeneous compression*).

2. Dynamic friction, *slipping*, is assumed between the strip and work roll and the strip shear force is equal to the work-roll normal force times the coefficient of sliding friction. The assumption is a problem in hot rolling where the calculated forces can easily exceed the maximum shear stress of the material being rolled, in which case viscous friction is a better model.

3. The yield stress is constant though the roll gap, which in hot rolling ignores the effect of strain rate on the yield stress, while in cold-rolling strain-hardening is a more important factor than the strain-rate effects.

4. The arc of contact can be modeled as a circular arc, which ignores localized roll flattening or even multiple regions with different flat or curvilinear sections [6].

5. Mathematical approximations like the small angle approximation, $sin\theta \approx \theta$, etc.... are used to make the equations tractable.

Orowan calculates the force distribution with the same conditions and material as experiments conducted by Siebel and Lueg [16], and does the calculations using the *homogeneous compression*, the *slipping* assumption and Hitchcock's formula that calculates the flattening

on the work roll due to the contact between the strip and work roll. The *slipping* simplification is usable for cold-rolling with a low coefficient of friction, in other cases this assumption results in too much calculated stress. In general, a coefficient of friction, μ, of 0.4 sticks for hot rolling and a μ of less than 0.2 to 0.25 slips. The *homogeneous compression* simplification is usable. Hitchcock's formula is accurate enough for rolling load, but not very usable for calculating rolling torque.

Orowan does experiments to discover the profile of the work roll deformation and the final strip contours support larger work roll deformation at the neutral point, which is inconsistent with an elliptical roll flattening predicted with Hitchcock's formula. To accurately calculate the rolling torque, the precise location of the neutral point and the force distribution under work roll is required. A graphical comparison seen in Figure 2.1 of the force distribution for experimental measurements and Hitchcock's formula are quite different. The force distribution for Hitchcock's formula rounds off the peak forces found in the experimental measurements at the neutral point and overstates the forces at the strip entry and exit. This difference in force distribution explains the large discrepancy found when using Hitchcock's formula to calculate rolling torque, which is very sensitive to incorrect force calculations, especially at the entry and exit work roll contact points.
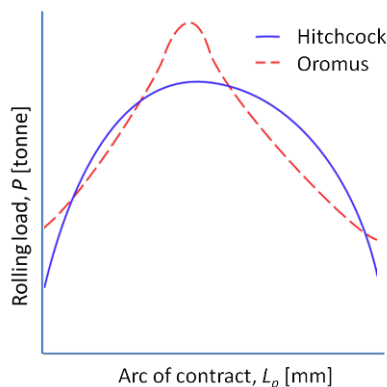
Figure 2.1: A likeness of the plot in Orowan [16] that compares the force distribution under work roll using the Hitchcock formula and experimental results.

Alexander [1] develops a numerical solution for the Kármán equation. Alexander does not include the correction for strain rate developed by Orowan, but uses the simplification of *homogeneous compression* for the strip. He discusses the effects of simplifications introduced by Orowan and used in the calculation of rolling load and rolling torque made by Bland and Ford (1948, 1952), Sims (1954), Alexander and Ford (1963), which produce small errors in rolling load, but large errors in rolling torque.

Freshwater [8, 9] improves on Alexander's solution by replacing the gradient of stress-strain relation with a yield-stress function, which is much easier to determine empirically. Freshwater uses the Swift yield-stress equation, $Y_s = Y_0(1 + B_s\bar{\epsilon})^{n_s}$ where B_s is a material constant, Y_0 is a yield strength constant and n_s is a strain hardening exponent found from an ex-

perimental fit and $\bar{\epsilon}$ is the true strain. Using this improvement Freshwater compares the inhomogeneous Orowan and a modified Kármán, which all agree very well with each other on the calculated rolling load. Good values for rolling torque and the neutral point are also calculated.

The use of the neutral point calculation is recommended to solve a simulation setup issue where knowledge of two different strip velocities are necessary to more closely simulate mill stand conditions.

2.2 Mill Stand Beam Models

Shohet and Townsend [20] use seven-factor sampling in a four-high mill to determine the strip exit crown sensitivities to mill width, strip width, reduction, work roll (2 types: JWW and JWB) and backup roll bending (JBB), and work roll camber. The three kinds of work-roll bending (JWW, JWB and JBB) are discussed in detail in section 3.2. They also introduce a beam model that is the starting point for many subsequent researchers.

The need to use many of the simplifications for the strip is no longer necessary with the use of finite elements. The work rolls and backup rolls no longer need to be modeled as beams.

2.3 Finite Element Analysis Models

Domanti and McElwain [6] tabulate research on a total of 33 two-dimensional (2-D) and three-dimensional (3-D) finite element (FE) models. Fifteen of these models are 2-D where plain strain is assumed in the third dimension. Nine are 3-D models with a rigid-body roll-stack and the velocities are decoupled in one dimension in the element. Four are 3-D models with a rigid-body roll-stack model, and in one 3-D model the general details are unknown. The 3-D models can improve accuracy and eliminate the plane strain assumption. Both the 2-D and 3-D models are quasi-static solutions and use a rigid-body roll-stack that cannot model the deformation of contact between the two roll or between the strip and work roll.

Finite element models of the strip allow yield models like rigid-plastic and elastic-plastic, which are a big improvement over the use of discrete springs and elastic foundations commonly used in beam-model implementations. Strip models based viscoplastic and elastoviscoplastic properties are possible choices when the strain-rate effects are important.

Slaughter [21] develops a 3-D dynamic-rolling simulation using an explicit-dynamic solver with an elastic-plastic material model running under the commercial package Abaqus (©Dassault Systèmes). This 3-D finite element simulation uses a finite-element roll-stack, instead of a rigid-body. Dynamic contact like the work roll and the strip friction is modeled. The strip is meshed, so assumptions like *homogeneous compression* do not need to be made and modeling

strain-rate effects become an option.

Chapter 3

Four-High Rolling Mill Finite Element Model

3.1 Strip Description

An ideal strip cross section, modeled with a parabolic profile and positive diametrical crown, is shown in Figure 3.1. Strip measurements width, wid, feather length, L_f, strip entry height at the feather, h_{ef} and strip entry centerline height, h_e are the industry standards. Another parameter, not shown, is feather width, $wid_{fea} = wid - 2L_f$, which is the location where the entry height at the feather, h_{ef}, is measured. One common L_f value is 40 [mm]. The strip entry height at the edge, h_{ee}, is portrayed with the assumption that excessive rolling deformation has occurred between the width, wid, and the width at the feather, wid_{fea}.

The strip diametrical entry crown, C_e, is the difference between the strip entry centerline height, h_e, and the strip entry height at the feather, h_{ef}. A parabolic profile is often assumed to exist between the centerline and wid_{fea} points on the rolled strip. The finite element strip model is built with the measurements: wid, L_f, h_{ef}, and C_e.

The notation used for the above dimensions are for the entry side of the stand. On the exit side of the work roll, the strip exit crown is identified as C_x, the strip exit centerline height as h_x and strip exit height at the feather as h_{xf}.

An important number in planning strip reduction is the ratio of C_e to h_e, or unit-strip crown. The same ratio is calculated for the exit side of the work roll using C_x and h_x. Figure 3.2 is a conceptual plot of the change in unit-strip crown between the entry and exit of each stand versus the stand number taken from Wang [22]. Generally, at the entry stands, 1 through 3, there is latitude to change the unit-strip crown without altering flatness, but once the strip enters the finishing stands, any changes in strip exit crown has to be confined to a narrow band of unit-strip crown changes.
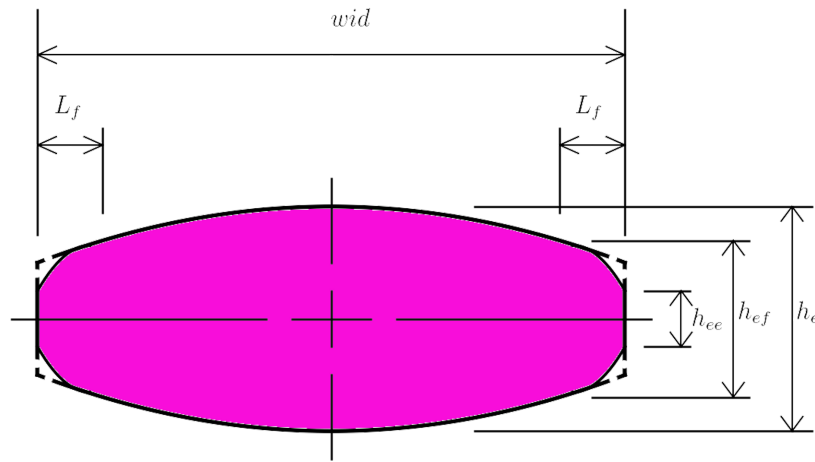
Figure 3.1: A strip cross-sectional view.
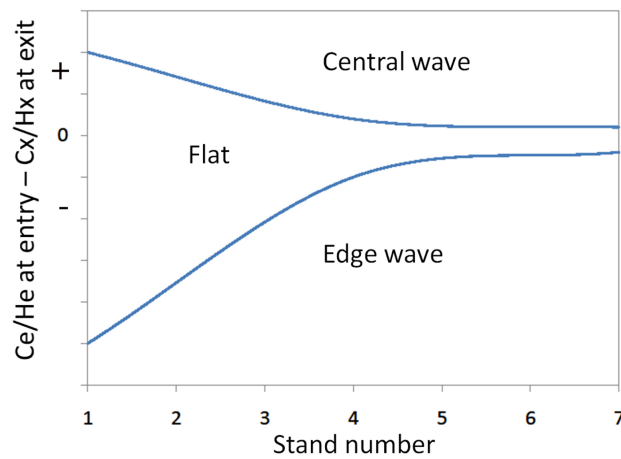
Figure 3.2: A conceptual plot of flatness as calculated from the difference of entry and exit unit-strip crown versus the stand number [22].

3.2   Four-high Mill Overview

A typical hot-rolling finishing mill has five to seven stands. The diagram in Figure 3.3 is a side view of a seven-stand mill with the stand frames omitted. Each stand reduces the strip a planned percentage of the entry height, commonly referred to as reduction. The entry stands (stands 1 through 3 in the diagram) typically take a large reduction in strip height (50 to 60 percent) and sets the unit-strip crown to a planned value. The intermediate stands also take large reductions, but they have less latitude to change unit-strip crown. The final finishing stands (stand 6 and 7) take between 10 to 25 percent reduction, but they must preserve unit-strip crown.
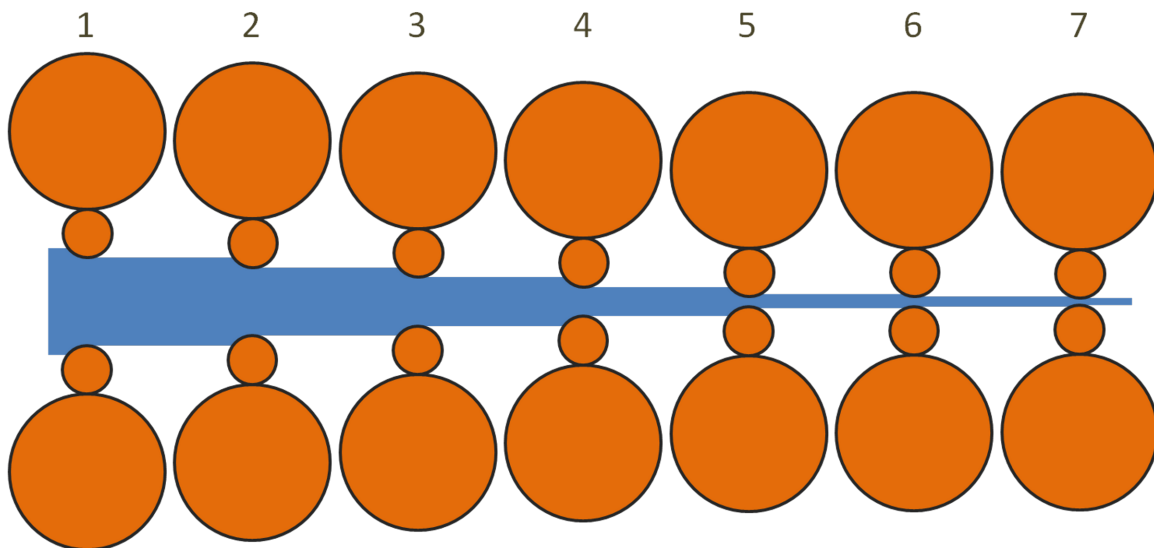
Figure 3.3: Diagram of a seven-stand mill with the assigned stand number showing the backup and work rolls and strip.

The mill modeled with the response surface is a seven-stand mill using simulations for four out of the seven stands – stands 1, 3, 5 and 7. The similarity in function between stands 2 and 3; 4 and 5; and 6 and 7 make simulations at stands 2, 4, and 6 redundant, so where appropriate, the term stand group 1 is used to refer to stand 1, stand group 3 is used in place of stand 2 and 3, etc.

Figure 3.4 shows a simplified four-high hot-rolling mill stand. The two backup rolls provide extra stiffness to the work rolls, which in turn do the work of reducing the height of the strip. The combination of the work and backup rolls is called the roll stack. For a given mill the dimensions of new rolls are fixed. Diametrical work-roll crown, C_{wr}, is the difference in diameters measured at the work-roll center and the work-roll edge (labeled $C_{wr}/2$ in Figure 3.4). A work roll with crown viewed from front is often represented as a parabolic profile and it is chosen to influence the final strip exit crown value. While a backup roll may be

designed with diametrical crown or develop crown through wear, this behavior of the rolling process is not modeled in the finite element simulations run. The work-roll and backup-roll diameters change because of scheduled turning to remove defects and wear, so both diameters are variables.
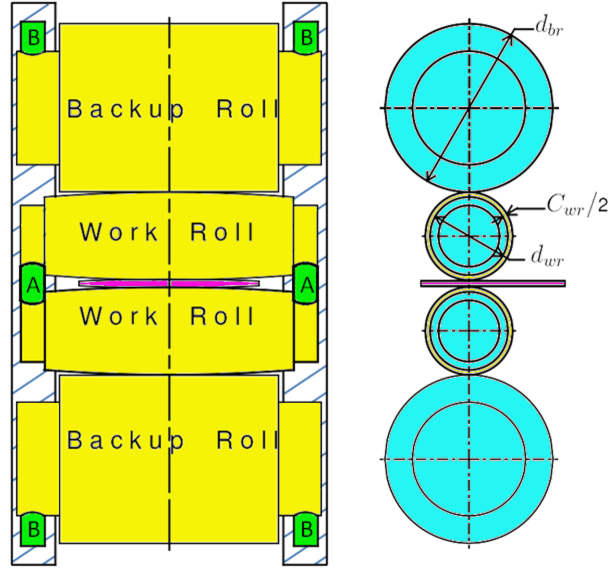
Figure 3.4: Unloaded mill stand cut away and side view the top roll stack (work and backup rolls) and strip.

The work-roll gap is set with actuators located at **B** in Figure 3.4. The work rolls are driven by electric motors (not shown), which pulls the strip through the gap. Because of the forces generated through deforming the strip, the roll stack has larger vertical displacements in the center than at the strip edge. This strip height difference is strip diametrical exit crown,

$$C_x = h_x - h_{xf} \tag{3.1}$$

where h_x is the strip centerline exit height and h_{xf} is strip exit height measured at the strip feather width (see Figure 3.1). The strip edge is not used because of rounding at the strip edge that is not consistent with the parabolic or higher polynomial profile assumed to exist between the centerline and feather widths (the rounded corners in Figure 3.1 between wid_{fea} and wid).

One way to control the final exit crown is to use actuators at **A** in Figure 3.4, which apply an opposing force to the two work rolls. These opposing forces or jacking loads, J, develop a bending moment on the work roll (JWW) that reduces strip crown. Another form of work roll bending applies a tension force between the work roll and backup roll (actuators not shown) to develop work-roll bending (JWB). The least effective method is to apply bending indirectly to the work roll by bending the backup roll, (JBB) [20, 19].

3.3 Finite-Element Model

3.3.1 Quarter-Symmetry Model

The calibration and development of the Abaqus finite element model used to generate samples for the different mill stand configurations is documented in detail by Slaughter [21] in *Strip Crown Prediction: Developing a Refined Dynamic Roll-Stack Model for the Hot Rolling Process.* Some of the important points are repeated here, since they bear upon the choices made to determine steady-state values for the strip exit heights and the rolling load.

A quarter-size model of the mill stand is possible if the forces, the geometry, and the material properties are symmetric about the vertical and horizontal axes. The requirements met for a mill stand are:

- The forces seen at the ends of each backup roll at actuators **B** in Figure 3.4 are the same and the location of the actuators is symmetric about two axes.

- The jacking load applied to both the top-and-bottom actuators at **A** in Figure 3.4 is the same and symmetric left and right.

- The top-and-bottom halves of the roll-stacks are identical and have the same geometric and material properties left and right.

- The strip also has left and right and top and bottom geometric and material property symmetries.

A quarter-size stand is shown in Figure 3.5.

The displacement boundary conditions for the quarter model along the vertical plane of symmetry are

- the roll stack and strip are allowed to move vertically, U_2 (displacement along the y-axis),

- the same co-planar nodes are allowed to move in the direction of strip motion, U_3 (displacement along the z-axis),

- all surface points on the centerline U_2 and U_3 plane are prevented from moving normal, U_1 (displacement along the x-axis), to this plane.

The displacement boundary conditions for the quarter model along the horizontal plane of symmetry only affect the strip. The strip nodes on the U_1 and U_3 horizontal centerline plane can move parallel to the plane of symmetry, but not off the plane of symmetry.

The backup-roll and work-roll displacement attachment boundary conditions (see Figure 3.5) are

- the backup-roll and work-roll ends ($x = L_{br}/2 + L_{brn}$ and $x = L_{wr}/2 + L_{wrn}$ respectively) are connected to a rigid plate with centers of rotation at $U_{2,br}$ for the backup roll and
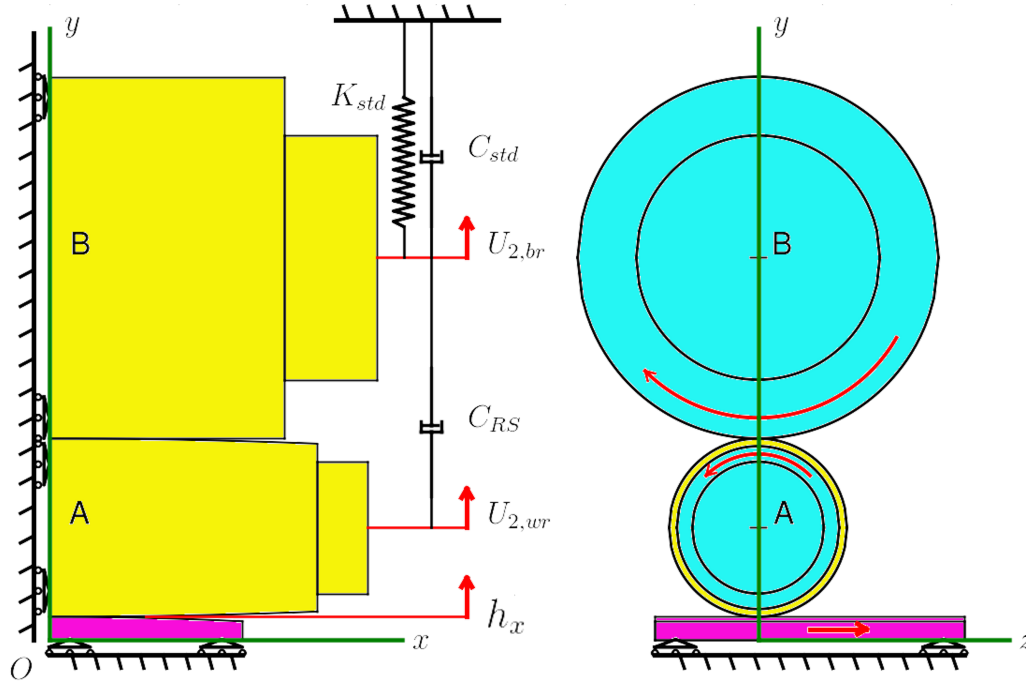
Figure 3.5: Quarter model with a front and a side view.

$U_{2,wr}$ for the work roll (like a cantilever beam with the freedom to rotate),

- those same two points are only allowed to move vertically and deflections in the remaining two directions are prevented.

Backup-roll and work-roll lengths L_{br} and L_{wr} are measured between the start of the necks. Backup-roll and work-roll neck lengths are L_{brn} and L_{wrn} respectively.

Since the forces on the stand at either connection to the backup roll (**B** in Figure 3.4) develop the same forces (ignoring gravity), a fixed point P and the parallel spring, K_{std} and damper, C_{std}, combination connected to the backup roll at $U_{2,br}$ take the place of the stand frame. The mill-stand spring is modeled as a linear spring and calibrated for a specific stand and since the seven stands are identical, this spring constant is used for all four stand-groups modeled. Because the actual stand connection to the work roll is naturally damped, a second damper, C_{RS}, between the work roll and backup roll models this. The two dampers are modeled with proportional damping values that are calculated from estimate of the lowest natural frequency using a lumped-mass model like that in Figure 3.9. Slaughter [21] provides more details.

3.3.2   Initial Conditions

The strip velocity parameter is used to calculate the initial angular velocities for the backup roll and the work roll. The tangential work-roll velocity is the same velocity assigned to the strip as its initial velocity effective at the start of the simulation, the *excitation phase*. The calculated velocity for the work roll is a prescribed velocity, which simulates a pair of motors driving each work roll and is in effect for the duration of the simulation.

The dynamic simulation requires careful loading of the strip to prevent loss of contact between the backup and the work roll; and between the work roll and the strip, which at time zero can be only a single point of contact. The bottom surface of the strip starts below the horizontal-centerline plane and it is moved up flush to the horizontal centerline plane using prescribed vertical displacements as shown in Figure 3.6. The strip is also given an initial velocity in the horizontal direction. The time interval to move the strip into position is proportional to the total run time. The strip setup portion of the simulation is called the *excitation phase*.
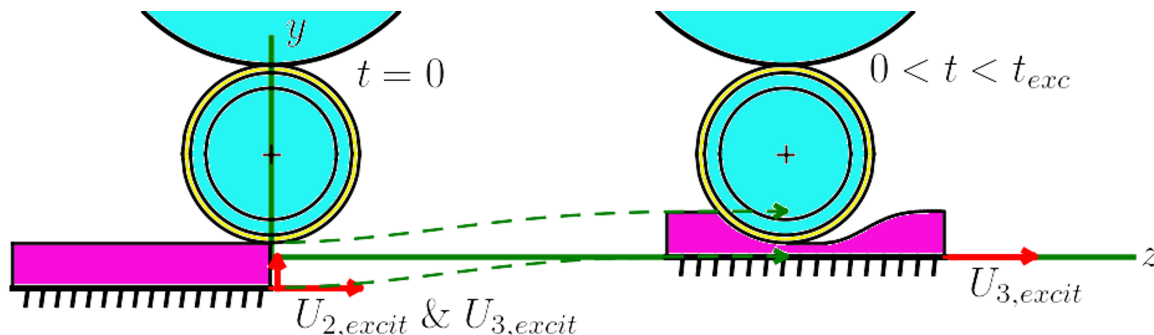
Figure 3.6: Quarter-stand model side view of strip loading to reduce roll-stack excitation.

Both the work-roll and strip meshes use the same element length in the direction of strip motion (U_3) and across the width of the strip (U_1). The closer the work roll and strip nodes remain during the simulation, the easier it is to solve for contact.

There are no vertical strip movements in a mill, except for inter-stand tensioning during rolling, so the strip encounters the work roll as shown in Figure 3.7. Modeling the initial strip contact this way has two problems: first, contact of the work roll with the strip is a sharp edge, so there is the probability of a singularity (the forces approaching infinity) at these nodes. Second, the work roll could have a tendency to walk up the strip before settling down, which extends the time to reach steady-state.

This figure also illustrates another model parameter – FE gap. The industry standard gap, gap_{std}, measurement is the centerline distance between work rolls, while in the FE model, the work-roll gap or FE gap, *gap*, is the distance between the inner surfaces of the two work rolls. The FE gap is independent of work roll dimensions, which makes the partial derivatives of

gap easier to work with, since gap_{std} would include the partials for the work-roll diameter in addition to *gap*.
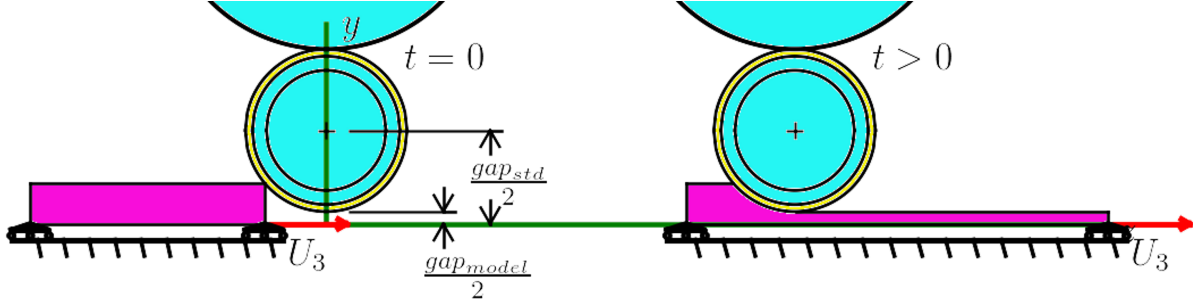
Figure 3.7: Model for standard strip rolling.

3.4 Simulation Excitation phase

3.4.1 Strip Setup Draft Curve

The roll stack has a net vertical acceleration of zero after setting the gap. The vertical motion of the strip during the *excitation phase* of the simulation uses a double-harmonic cam curve [21],

$$s = \frac{s_0}{2} \left(\left(1 - cos \left(\frac{t_i \pi}{t_{exc}} \right) \right) - \frac{1}{4} \left(1 - cos \left(\frac{t_i 2\pi}{t_{exc}} \right) \right) \right) \tag{3.2}$$

where $s_0 = (h_e - gap)/2$, t_{exc} is the duration of the cam action (excitation time), and t_i is the time for the current data point. The dashed lines in Figure 3.6 show the draft curve as a function of time from the initial state at $t = 0$ and at the end of the excitation step at $t = t_{exc}$. Using the cam motion in Equation 3.2 the net vertical strip acceleration is zero when the strip is released to seek dynamic equilibrium. The work roll is close to its steady-state vertical position when the strip is allowed to roll freely on the x-z plane as in the $t > 0$ case in Figure 3.7.

3.4.2 Zero Net Vertical Acceleration

Figure 3.8 is a plot of the *excitation phase* displacement and velocity curves from an FE simulation or observation. The strip properties used are $h_{ef} = 6.4337$ [mm], $C_e = 0.05$ [mm], and $gap = 3.48$ [mm]. At the end of the *excitation phase* the strip velocity is zero.
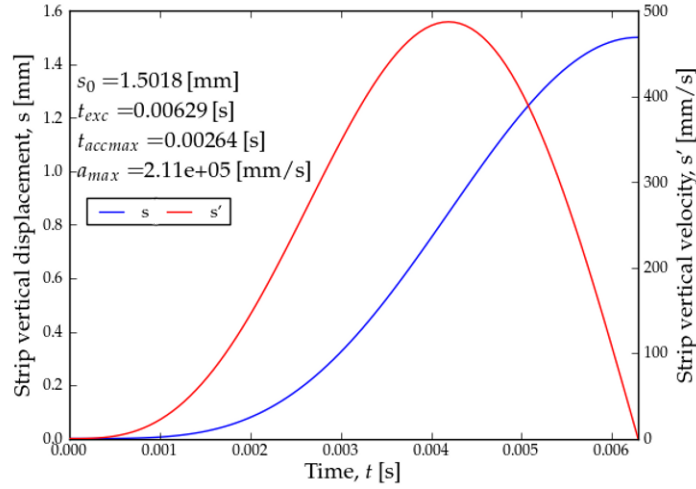
Figure 3.8: Excitation phase displacement and velocity curves for the example.

Integrating the second derivative of the draft curve over the excitation time from 0 [s] to t_{exc} [s],

$$\int_0^{\Delta t} \frac{1}{2} s_0 \left(\frac{\pi^2 \cos\left(\frac{\pi t}{\Delta t}\right)}{\Delta t^2} - \frac{\pi^2 \cos\left(\frac{2\pi t}{\Delta t}\right)}{\Delta t^2} \right) dt = 0 \tag{3.3}$$

which demonstrates that the net vertical velocity is zero. To find the point of maximum positive acceleration involves taking one more derivative and then finding the stationary points,

$$\frac{1}{2} s_0 \left(\frac{2\pi^3 \sin\left(\frac{2\pi t}{\Delta t}\right)}{\Delta t^3} - \frac{\pi^3 \sin\left(\frac{\pi t}{\Delta t}\right)}{\Delta t^3} \right) = 0 \tag{3.4}$$

which for this sample is 0.00264 [s] with a maximum acceleration of 21,100 [mm/s^2]. Based on the rolling load data for this sample, the maximum rolling load occurs at 0.00358 [s] after 63 percent of the full vertical displacement necessary to put the bottom of the half-strip flush with the horizontal plane of symmetry. The lag time between maximum acceleration and maximum force is due to the damping used in the model.

3.4.3　Simulation Run and Excitation Times

The two model parameters that control the duration of the simulation and the vertical strip movement to set the gap (*excitation phase*) are the run-time multiplier, $RuMu$ and the excitation multiplier, $ExMu$, which are found after some experimenting. The basic time step, T, is based on the calculated period of the lowest natural frequency of a lumped-mass model like that in Figure 3.9 where M_2 is the backup-roll mass and M_1 is work-roll mass. The details of how T is calculated is covered in detail in Slaughter[21]. The run time is calculated as $t_{run} = (RuMu)(T)$ and the excitation time as $t_{exc} = (ExMu)(T)$.
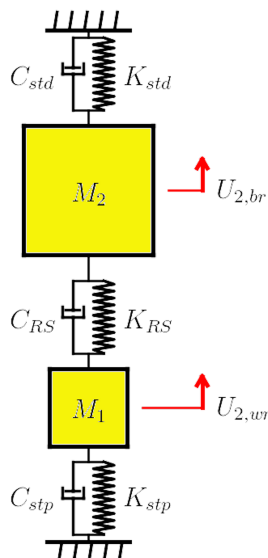
Figure 3.9: Two-degree of freedom (2DOF) lumped-mass model of a mill stand.

The effect of varying the excitation multiplier and holding the run-time multiplier and the other stand variables constant is seen in Figure 3.10 for a 6.4 [mm] high strip. The smallest excitation multiplier of 0.50 penetrates an extra 0.18 [mm] into the strip before the *excitation phase* ends and using too large a multiplier, like 1.5, reduces the number of post *excitation phase* data points that can be used to determine the final steady-state exit heights, h_x and h_{xf}. For the chosen run-time multiplier and excitation multiplier, all five curves essentially converge on the same steady state curve. The inset shows a blow up of a 0.004 [mm] by 30 [mm] section of the post excitation-phase run. This is evidence that with long enough run times, the simulations for the 6.4 [mm] strip heights are not very sensitive to changes in excitation multiplier.

Unlike the 6.4 [mm] strip, the choice of excitation multipliers for 1.6 [mm] strip is complicated by the significant increase in strip stiffness. Figure 3.11 is a comparison of strip centerline exit heights, h_x, for two excitation multipliers with one of the excitation multipliers having three different damping values. The smoothest curve (least amount of vibration) has additional damping with a γ of 1.25 and an excitation multiplier of 1.5. The value of γ is a scalar used by the model generation routines to compute proportional damping values for C_{RS} and C_{std}.

Figure 3.12 varies the same parameters as Figure 3.11 and it is from the same simulation, but the strip exit heights at the feather, h_{xf}, are used. The smoothest curve has the higher excitation time multiplier, 2.0, so a better solution is likely to be compromise with an excitation multiplier close to 2.0 in combination with damping multiplier between 1.0 and 1.25. The run-time multiplier is chosen to be just long enough for at least 35 post excitation data points to be produced out of the Abaqus simulations.
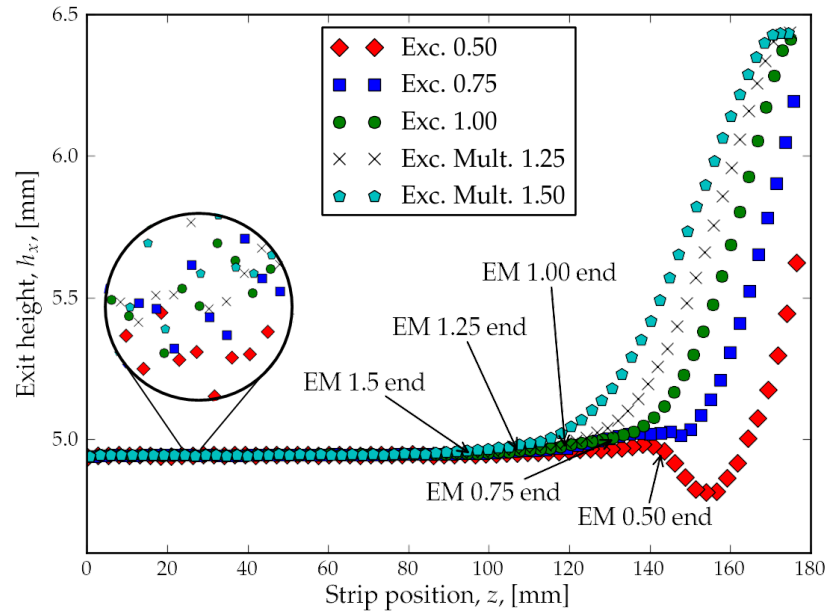
Figure 3.10: Excitation-multiplier effect on steady-state for a 6.4 [mm] high strip.
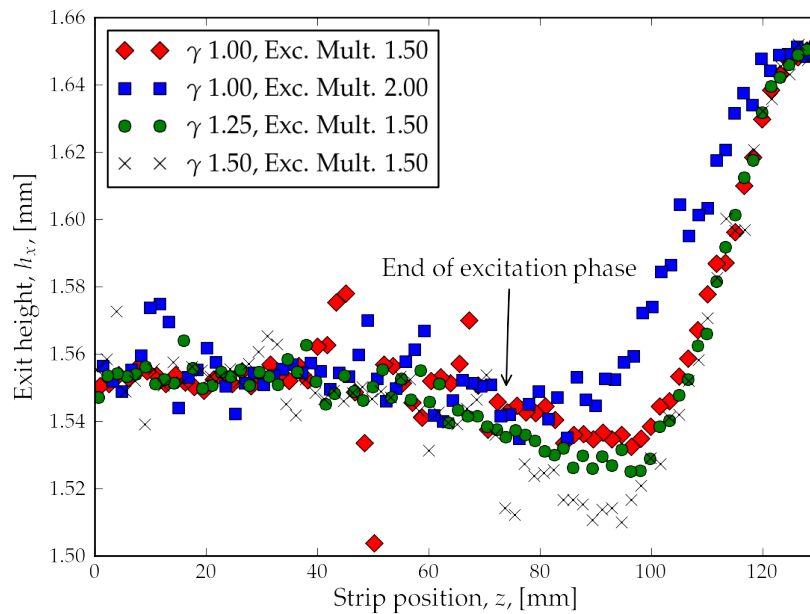
Figure 3.11: Excitation-multiplier effect on steady-state centerline exit height for a 1.6 [mm] high strip.
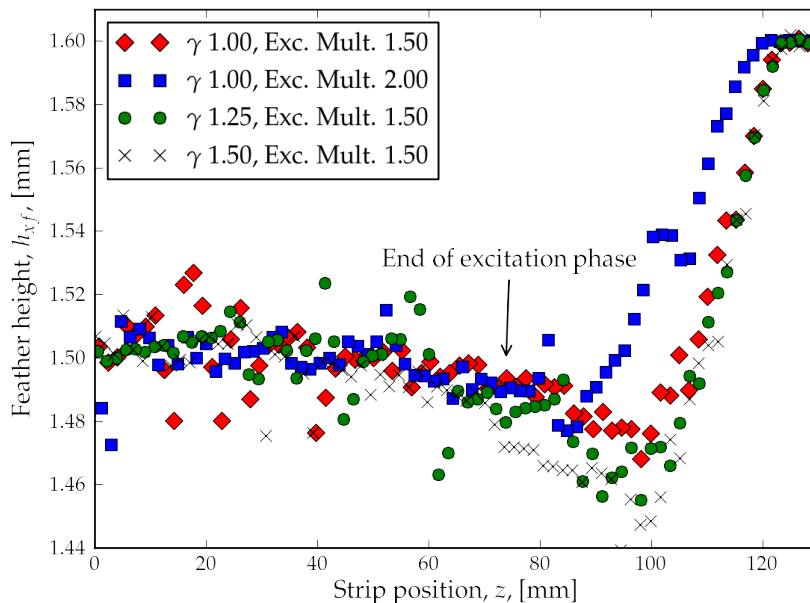
Figure 3.12: Excitation multiplier effect on steady-state exit height at the feather for a 1.6 [mm] high strip.

3.5   Post-Excitation Phase

3.5.1   Post-Excitation Phase Run Conditions

Figure 3.13 illustrates three important features found in the simulations. The first is the neutral point where the shear forces between the strip and work roll go to zero and change orientation; the normal force on the work roll is at its maximum; and the velocity of the strip relative to the work roll is zero [16]. The second-and-third features found are two minor stress peaks at m_1 and m_2. Figure 3.14 is a plot of the work-roll stress using estimated values from the legend and includes m_1 and m_2, plus the stresses from the first three rows of strip elements. Moving in just one node towards the center from m_1, the stress on the strip is reduced enough that the strip stress is less than the yield stress, which suggests the work roll is being pushed up and back at m_1 far enough to ease stresses on the strip.

The neutral-point stress peak in the center of Figure 3.14 should be a sharp-but-rounded peak [16]. A more refined mesh would improve the transition from the shoulders to the stress peak and provide a more detailed outline.

Equations that are a function of strip entry height and exit height at the neutral point are needed to calculate separate strip initial velocity and work-roll tangential velocity. The strip width to height aspect ratio is large enough to assume plane strain and there is very little
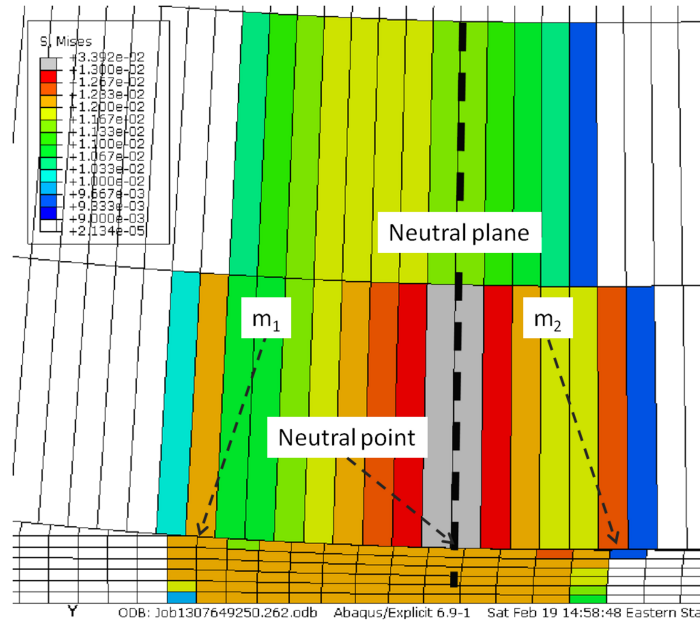
Figure 3.13: Von Mises stress for stand group 5 centerline work roll and strip contact.
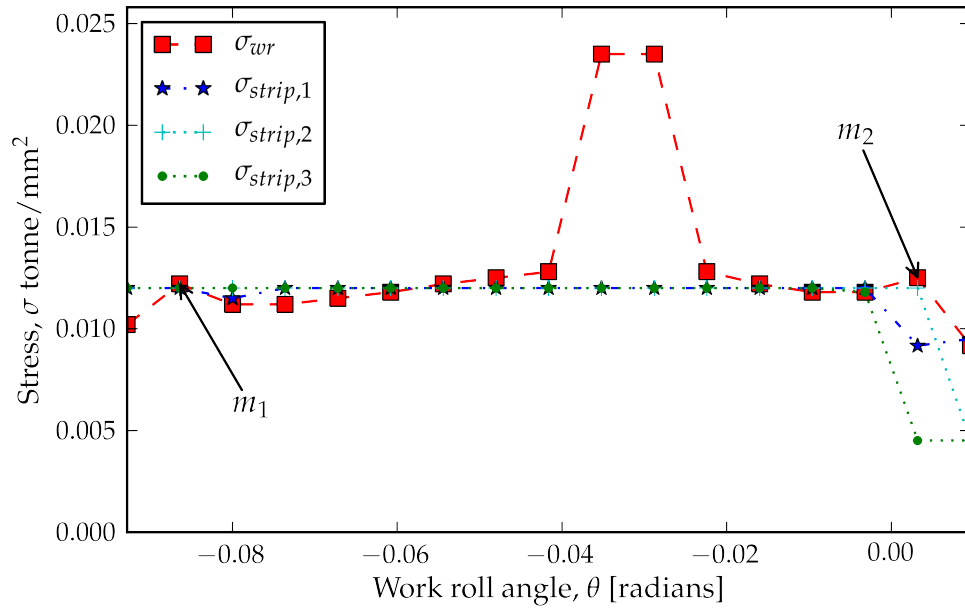
Figure 3.14: Plot of work-roll stress, σ_{wr}, and the stress from first three strip rows, σ_1, σ_2 and σ_3.

change in strip width going through the rolls. The equation for a mass balance between the entry and exit is,

$$\rho \; wid \; h_e \; \Delta z_e = \rho \; wid \; h_x \; \Delta z_x \tag{3.5}$$

where ρ is the strip density, wid is the strip width, h_e and h_x are the strip entry and exit heights respectively ignoring crown, and Δz_e and Δz_x are small longitudinal changes at the work-roll entry and exit points. Eliminating common terms and computing the related rates,

$$h_e \frac{dz_e}{dt} = h_x \frac{dz_x}{dt} \tag{3.6}$$

where strip heights are not considered functions of time. Then making the substitution $h_x = (1 - Rx)h_e$ and dividing both sides by h_e gives,

$$vel_e = (1 - Rx)vel_x \tag{3.7}$$

where $vel_e = dz_e/dt$, $vel_x = dz_x/dt$, Rx is the reduction in strip centerline entry height and $0 < Rx < 1$. The limits on Rx ensures entry velocity, vel_e, is always less than the exit velocity, vel_x, and because the strip velocity at the neutral point equals the work roll velocity, the follow relation holds:

$$vel_e < vel_{NP} = vel_{wr} < vel_x \tag{3.8}$$

where vel_{NP} is the strip velocity at the neutral point, vel_{wr} is the tangential work roll velocity.

An example of the difference in the three different velocities given the following information:

- $vel_{wr} = 2650$ [mm/s] a nominal stand 3 velocity.
- $Rx = .50$.
- A simple assumption that neutral point is located midway between the strip entry height and the strip exit height or $Rx = .25$, which is conservative if there is no tension on the strip and strip reduction is 50% or better.

The unknown entry velocity, vel_e, using Equation 3.7 is 1767 [mm/s] and the strip exit velocity, vel_x, is 3533 [mm/s]. The 883 [mm/s] difference in the strip-entry and work-roll velocity gives the mass on strip entry side additional momentum, or an extra push through the rolls. This extra push is the cause of the two stress peaks at m_1 and m_2. It is unknown whether or not with a longer run time this is transient condition or not.

The strip exit velocity is the strip entry velocity of the next stand. Since both vel_{NP} and vel_x depend on the reduction taken, neither is a good candidate as a independent variable. Estimations of vel_{NP} and vel_{wr} requires that the strip reduction is determined on just the independent variables. Otherwise the response surface is a function of at least one dependent variable.

3.5.2 Work-roll Velocity Estimation

Currently, an estimate of draft is made using a fixed number of iterations with the Ford-and-Alexander force Equation 6.1 and a static estimate of strip exit height with Equation 3.10. First, a simple percentage of the entry height is used as the starting exit height, h_x, then the force is calculated,

$$P = FA(k, d_{wr}, h_e, h_x, E, \nu, wid) \tag{3.9}$$

where $k = S_y/\sqrt{3}$, S_y is the yield strength, d_{wr} is the diameter of the work roll, $h_e = h_{ef} + C_e$ is the centerline entry height, $h_x = h_{xf} + C_x$ is the centerline exit height, E is the work-roll modulus of elasticity, ν is Poisson's ratio for the work-roll and wid is the strip width. This force is used to estimate the exit height with

$$h_x = gap + P/K_{std} \tag{3.10}$$

where gap is the FE gap and K_{std} is the stand stiffness constant. The average of the new and the old h_x values are used to estimate the next exit height to recalculate force, P. The final exit-height estimate is used to compute an estimate of the strip-exit modulus for the lumped-mass model. An new use would be to estimate the neutral-point exit height and to calculate the neutral-point velocity with Equation 3.7 to set the work-roll velocity, vel_{wr}.

The numerical methods discussed in Freshwater's [8, 9] research do locate the neutral point, while the above estimate does not. The use of the Freshwater equations and Equation 3.10 should improve the final work-roll velocity value.

Separate strip and work-roll initial velocities makes the solution for contact much more difficult. An improved *excitation phase* would include the following:

- Start both the work roll and the strip at the strip entry velocity at time zero,
- Use a smooth function to generate interim prescribed work-roll angular displacements,
- End the *excitation phase* with the work-roll rotating at the calculated neutral-point tangential velocity.

The next simulation step after the *excitation phase* ends maintains the prescribed work-roll velocity and lets the strip seek dynamic equilibrium.

3.5.3 The Stand Groups Affected by Additional Work-roll Deformation

Figure 3.15 is the superposition of the deformed strip coordinates and the undeformed work roll radius with its center at the deformed work roll center at simulation termination. The difference between the two curves (labeled "Difference") is a combination of the work roll and

the strip-elastic deformation. Because the strip is in a plastic state though out most of the work roll and strip contact area (see Figure 3.14), the elastic strip recovery is nearly constant over the area of contact, so this leaves any prominent feature a work-roll deformation. The work-roll deformation under labels d_1 and d_2 in Figure 3.15 are also the locations of higher work-roll stress (m_1 and m_2). The deformation at d_1 and d_2 could flatten out to give the work roll a shape more consistent with Hitchcock's formula [13] without the extra momentum currently present.
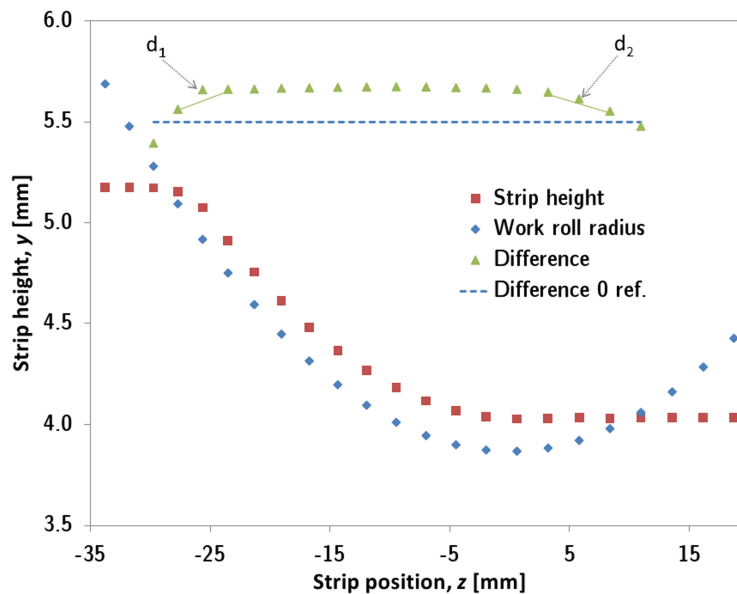
Figure 3.15: Stand group 5 deformed strip and undeformed work roll profile with relative difference.

Figure 3.16 compares the work roll deformation profile for all four stand groups 1, 3, 5, and 7. All four have the prominent feature d_1 shown in Figure 3.15. There is the same buckling of the strip that produces extra strip center height in combination with feature d_1.
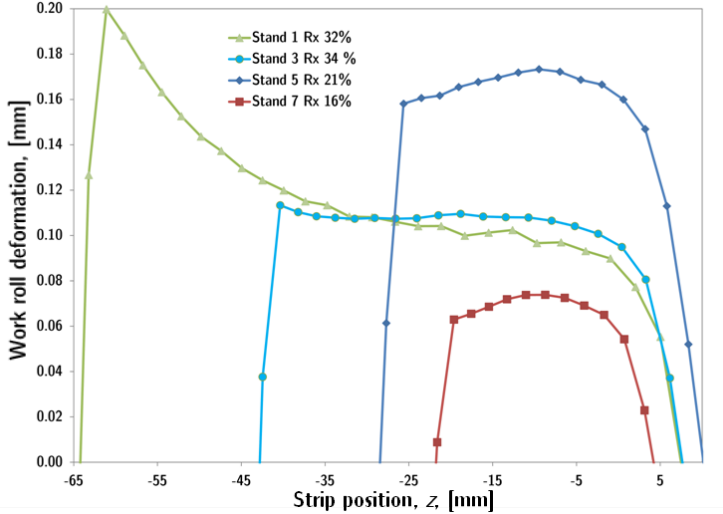
Figure 3.16: A comparison of work-roll contact deformation at the four-stand groups.

Chapter 4

Steady-State Dynamics Model

4.1   2DOF Lumped Mass Model

4.1.1   Exponential Decay of Strip Exit Height

Figure 4.1 is the Fast-Fourier Transform, FFT, for the same five samples from the 6.4 [mm] excitation analysis plus the FFT of an exponential function that represents a simple case of critical damping,

$$(h_{x0} - h_x)/h_{x0} \approx e^{-a\,\Delta z} \tag{4.1}$$

where a is a handpicked value that minimized the differences between one of the five samples. The FFT for four of the samples and the FFT for the analytical curve are in good agreement. The FFT for fastest excitation multiple of 0.5 is the exception. The good agreement of the critically damped system and the steady-state exit height data support the use of the 2DOF system seen in Figure 3.9.

4.1.2   Equations of Motion

Once the *excitation phase* ends and the strip and roll stack are free to seek steady state, the simulation runs without any external vertical forces. The 2DOF model shown in Figure 3.9 has initial vertical position and a zero vertical velocity after the *excitation phase* ends. The two equations of motion are

$$\ddot{U}_{2,br} = \frac{-C_{RS}}{M_2}(\dot{U}_{2,br} - \dot{U}_{2,wr}) - \frac{C_{std}}{M_2}\dot{U}_{2,br} - \frac{K_{RS}}{M_2}(U_{2,br} - U_{2,wr}) - \frac{K_{std}}{M_2}U_{2,br} \tag{4.2}$$

$$\ddot{U}_{2,wr} = \frac{C_{RS}}{M_1}(\dot{U}_{2,br} - \dot{U}_{2,wr}) - \frac{C_{stp}}{M_1}\dot{U}_{2,wr} + \frac{K_{RS}}{M_1}(U_{2,br} - U_{2,wr}) - \frac{K_{stp}}{M_1}U_{2,wr} \tag{4.3}$$
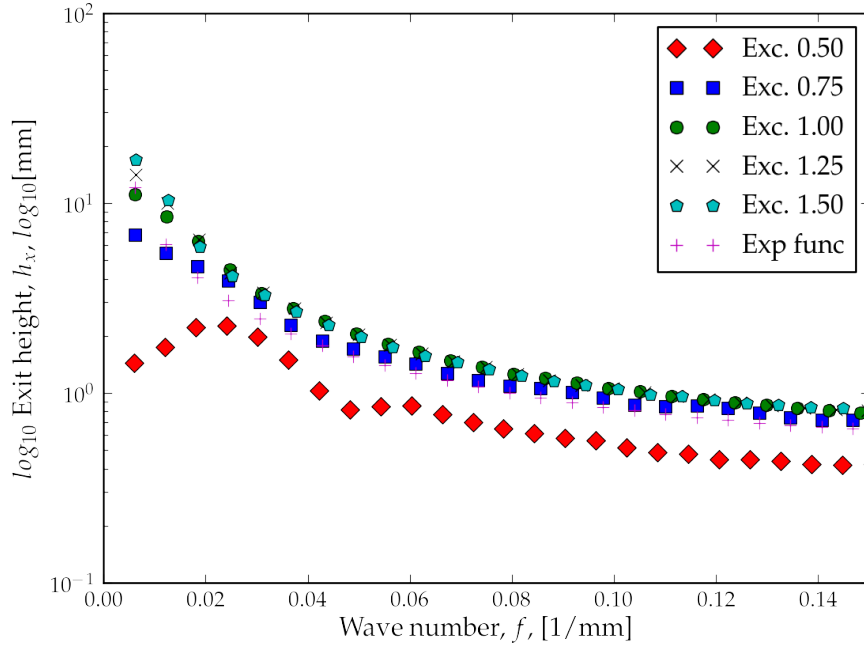
Figure 4.1: A FFT of the five samples used in excitation analysis compared to the damping term in a single degree of freedom system.

where the variables are illustrated in Figure 3.9. The equations of motion in state space after a change of variables are

$$\dot{y_1} = y_2 \tag{4.4}$$

$$\dot{y_2} = \ddot{U}_{2,br} = \frac{-C_{RS}}{M_2}(y_2 - y_4) - \frac{C_{std}}{M_2}y_2 - \frac{K_{RS}}{M_2}(y_1 - y_3) - \frac{K_{std}}{M_2}y_1 \tag{4.5}$$

$$\dot{y_3} = y_4 \tag{4.6}$$

$$\dot{y_4} = \ddot{U}_{2,wr} = \frac{C_{RS}}{M_1}(y_2 - y_4) - \frac{C_{stp}}{M_1}y_4 + \frac{K_{RS}}{M_1}(y_1 - y_3) - \frac{K_{stp}}{M_1}y_3 \tag{4.7}$$

or in more compact matrix form:

$$\dot{\mathbf{y}} = [\mathbf{A}]\{\mathbf{y}\} + [\mathbf{B}]\{\mathbf{u}\} \tag{4.8}$$

$$\mathbf{z} = [\mathbf{C}]\{\mathbf{y}\} + [\mathbf{D}]\{\mathbf{u}\} \tag{4.9}$$

where matrices are enclosed in square brackets and vectors in curly braces. The matrix $[\mathbf{A}]$ is

$$[\mathbf{A}] = \begin{pmatrix} 0 & 1 & 0 & 0 \\ -\frac{K_{RS}}{M_2} - \frac{K_{std}}{M_2} & -\frac{C_{RS}}{M_2} - \frac{C_{std}}{M_2} & \frac{K_{RS}}{M_2} & \frac{C_{RS}}{M_2} \\ 0 & 0 & 0 & 1 \\ \frac{K_{RS}}{M_1} & \frac{C_{RS}}{M_1} & -\frac{K_{RS}}{M_1} - \frac{K_{stp}}{M_1} & -\frac{C_{RS}}{M_1} - \frac{C_{stp}}{M_1} \end{pmatrix} \quad (4.10)$$

The deformation of the strip, h_x, at the contact boundary with the work roll is the desired information, $U_{2,wr}$, so $y_3 = U_{2,wr} = h_x$. Since data from one of the outputs is available, the $[\mathbf{C}]$ matrix is

$$\mathbf{C} = \begin{pmatrix} 0 & 0 & 1 & 0 \end{pmatrix} \quad (4.11)$$

4.1.3   The Single Output Solution

Given that $det([\mathbf{A}])$ is not zero, to solve this system: first use the fact that a rotational transform, $[\mathbf{P}]$, exists and it is not a function of time, such that,

$$[\mathbf{A}][\mathbf{P}] = [\mathbf{P}][\mathbf{\Lambda}] \quad (4.12)$$

where $[\mathbf{\Lambda}]$ is a diagonal matrix of eigenvalues and $[\mathbf{P}]$ is a matrix of the eigenvectors. Letting

$$\{\mathbf{y}\} = [\mathbf{P}]\{\hat{\mathbf{y}}\} \quad (4.13)$$

and substituting into Equations 4.8 and 4.9 yields

$$[\mathbf{P}]\{\dot{\hat{\mathbf{y}}}\} = [\mathbf{A}][\mathbf{P}]\{\hat{\mathbf{y}}\} + [\mathbf{B}]\{\mathbf{u}\} \quad (4.14)$$

$$\{\mathbf{z}\} = [\mathbf{C}][\mathbf{P}]\{\hat{\mathbf{y}}\} + [\mathbf{D}]\{\mathbf{u}\} \quad (4.15)$$

After solving for $\dot{\hat{\mathbf{y}}}$

$$\{\dot{\hat{\mathbf{y}}}\} = [\mathbf{P}]^{-1}[\mathbf{A}][\mathbf{P}]\{\hat{\mathbf{y}}\} + [\mathbf{P}]^{-1}[\mathbf{B}]\{\mathbf{u}\} \quad (4.16)$$

Then taking into account the lack of a forcing function, $\{u\}$, the final matrix equation for the state equation is

$$\{\dot{\hat{y}}\} = [\mathbf{\Lambda}]\{\hat{\mathbf{y}}\} \quad (4.17)$$

and the final output equation is

$$\{\mathbf{z}\} = [\mathbf{C}][\mathbf{P}]\{\hat{\mathbf{y}}\} \quad (4.18)$$

.

Since the general solution to Equation 4.17 with four eigenvalues is

$$\hat{y} = c_1 e^{\lambda_1 t} + c_2 e^{\lambda_2 t} + c_3 e^{\lambda_3 t} + c_4 e^{\lambda_4 t} \quad (4.19)$$

the final equation for the single output z with an initial displacement is

$$\mathbf{z} = c_0 + c_1 e^{\lambda_1 t} + c_2 e^{\lambda_2 t} + c_3 e^{\lambda_3 t} + c_4 e^{\lambda_4 t} \quad (4.20)$$

.

Chapter 5

Steady-State Determination

5.1 Steady-State Overview

5.1.1 Steady-State Data Points

The data extracted from each simulation is

1. the time history for the rolling load,

2. the strip centerline exit heights in the x-z plane,

3. the strip exit heights at the feather in the x-z plane,

4. the strip surface heights in all three coordinates.

The extracted data from items 1, 2, and 3 are used in the determination of the $t = \infty$ steady-state values for the rolling load, P, the strip centerline height, h_x, and the strip height at the feather, h_{ef}, respectively. The process used for this determination is covered in this section after a brief overview of how the extracted data from 4 is used.

The extracted data from item 4 uses selected strip cross-sections in the x-y plane for polynomial regression to define function, $xySurf(wid)$. Strip exit crown, $C_{x,2}$, is calculated with

$$C_{x,2} = xySurf(wid = 0) - xySurf(wid = wid_{fea}) \tag{5.1}$$

This estimate of strip exit crown, $C_{x,2}$ is used as an independent measure of strip exit crown, but only at stand 7 where there is no deformation beyond the strip feather width. The further development of Equation 5.1 is out-of-scope for this research.

5.1.2   Observation Level Dependent Variables

The strip exit crown calculation for each observation is

$$C_{x,1}(t = \infty) = h_x(t = \infty) - h_{xf}(t = \infty) \tag{5.2}$$

where functions $h_x(t)$ and $h_{xf}(t)$ are variations of Equation 4.20 after the coefficients and exponents are derived from a nonlinear search. $C_{x,1}(t = \infty)$, $h_x(t = \infty)$, and $h_{xf}(t = \infty)$ are the dependent variable steady-state values from one observation used to build the response surface.

5.1.3   Response Surface Crown Models

Strip exit crown can be calculated from the two response surface exits heights, h_x and h_{xf} with

$$C_x(\{\zeta\}) = h_{x,RS}(\{\zeta\}) - h_{xf,RS}(\{\zeta\}) \tag{5.3}$$

where $h_{x,RS}(\{\zeta\})$ and $h_{xf,RS}(\{\zeta\})$ are now functions of the isoparametric coordinate vector, $\{\zeta\}$. The other option explored is to build a response surface directly the strip exit crown, $C_{x,1}$, value from each observation, which is equivalent to

$$C_x(\{\zeta\}) = C_{x,RS}(\{\zeta\}) \tag{5.4}$$

Equation 5.3 is the preferred method found for calculating strip exit crown. The next chapter goes into the details on building the response surface and the isoparametric formulation.

5.1.4   Observation Level Extracted Data

Because the force history for a single exit height point on the strip is not available, all of the un-forced exit height data points are used to find the steady-state exit heights. Figure 5.1 is a plot of the data points extracted from one Abaqus simulation of both the centerline, h_x and the feather, h_{xf}, longitudinal exit heights. The strip is pressed into the work-roll starting on the right (the boxed-in area labeled "Excitation phase ..." in Figure 5.1) to set the gap and then the strip moves to the right as the strip and work roll are allowed to come to steady state. The boxed-in area labeled "In contact ..." in Figure 5.1 encloses the set of data points in contact with the work-roll after the simulation terminates and this set of data points is excluded from the steady-state search. The remaining set of deformed coordinates for all of the data points after the *excitation phase* and not in contact with the work-roll are used to determine the steady-state exit heights. The simplifying assumption is that the first data point $h_{x,0}$ (see Figure 5.1) is the time zero exit height and the remaining n data points are moving at the strip velocity, so each strip exit height point to the left is a positive time relative to time zero. The equation to compute the simulation time is,

$$t_i = (z_0 - z_i)/vel_{wr} \tag{5.5}$$

where z_i is the z coordinate for strip exit height at $h_{x,i}$, vel_{wr} is the work roll tangential velocity parameter, vel_{wr} is strip initial velocity and $z_0 \geq z_i$. The introduction of a realistic time value also allows using what is known about the time domain 2DOF system to provide a more reliable estimate of initial conditions. The set of n data points is the exit height post-excitation steady-state window.
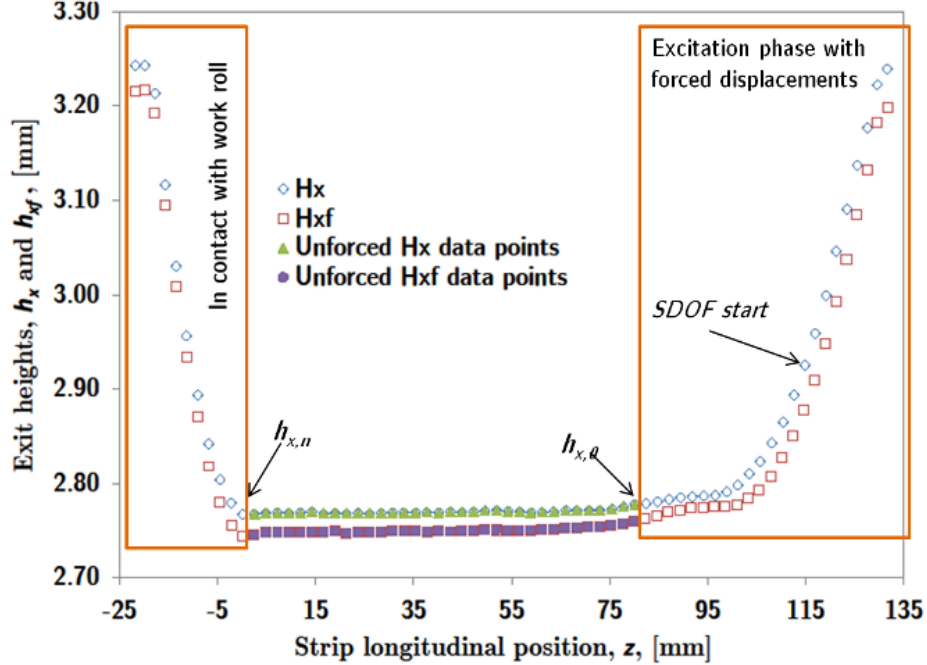
Figure 5.1: Simulation strip exit heights taken from the deformed strip.

5.2   SDOF Steady-State Model, Unconstrained Fit

The first attempt to find steady-state uses a single degree of freedom model (SDOF) as seen in Equation 5.6. This is done because the algorithm for the nonlinear root finding does not support constraints on the variables, so at least one positive exponent is very likely when using the complete set of 2DOF equations. The form of the equation used in the search is

$$0 = \sum_{i=0}^{n-1} \left((c_0 + e^{a\, t_i}(b\, cos(c\, t_i) + d\, sin(c\, t_i))) - h_{x,i} \right) \tag{5.6}$$

where c_0 is the steady-state exit height (centerline or feather), $h_{x,i}$ are the exit heights in the steady-state set, $\{SDOF\ start : h_n\}$ and a, b, c, and d are dummy variables in the nonlinear fit. Equation 5.6 is also used for the set of exit heights at the feather, $h_{xf,i}$. An added safe

guard against positive exponents is to use a small portion of the excitation curve (labeled *SDOF start* in Figure 5.1) in the nonlinear search. Prior to making this change, occasionally positive exponents appear in the result, along with an unrealistic steady-state exit height.

One difficulty with this method is that the result is sensitive to a large initial value of the exponent and can degenerate into an average of the final strip exit height data when the exponential term takes the other terms to zero. The variance of residuals is part of the data collected for both of the strip exit heights. Checking for observations with large variances make it possible to identity and make corrections. Even with the added simplifications, the SDOF model does well with most differences with 2DOF result under 2%.

Figure 5.2 are two side-by-side plots from the SDOF fit code. The left plot is from the rolling load steady-state search, which uses a modified form of Equation 5.6, and the plot on the right is the result for both of the strip exit heights. The unconnected dots plotted are from the extracted data and the continuous curves are from Equations 5.6 once the missing values are known. Also, plotted is a dotted line as a zero reference with the residues plotted relative to this reference line.
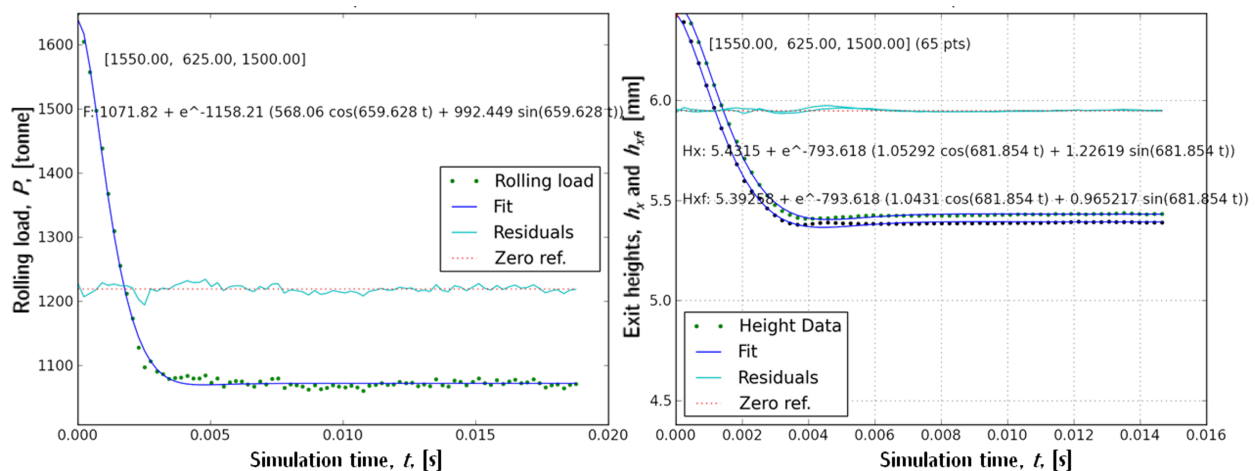
Figure 5.2: SDOF fit for both rolling load, P, and the two exit heights, h_x and h_{xf}.

5.3   2DOF Steady-State Model, Constrained Fit

5.3.1   2DOF Eigenvalues

Using the complete 2DOF solution is practical with the discovery of a L-BFGS minimization routine [17]. Equation 4.19 is used with constraints on the scalar and exponential variables. An added benefit of the constrained search is that only the post *excitation phase* points are used to determine the steady-state exit heights. It is assumed that the set of strip exit

heights in the post-excitation steady-state window are at the strip velocity specified in the model setup parameters. The starting exit height index, z_0, for the 2DOF solution is under $h_{x,0}$ in Figure 5.1, and Equation 5.5 is used to assign time values to each data point up to z_i.

A real system based on Equation 4.19 is limited to one of the following eigenvalue combinations:

- 4 real negative eigenvalues,

- a special case with duplicate negative eigenvalues (critically damped), plus 2 negative real eigenvalues or 2 complex eigenvalues in the left-half complex plane (LHP),

- 2 real negative eigenvalues and 2 complex conjugates in the LHP,

- 4 complex conjugates in the LHP,

- rigid body motion ($\lambda = 0$), plus some combination of real and complex eigenvalues in the LHP.

Rigid body modes are not possible in this simulation, so only the first four items are considered. The function to minimize can be written in the form of four exponential functions if complex numbers are allowed, but this would require complex number support in the L-BFGS routine, which has unknown support for complex types in the Python routine used. Instead, Equation 4.20 is solved as the superposition of individual special cases using real numbers.

The above four cases can be broken up into eight different combinations of three equations: sub-solution 1 for a pair of eigenvalues, sub-solution 2 for the other pair of eigenvalues and the steady-state exit height, c_0. Two of the three basic solutions are

1. 2 real negative eigenvalues,

2. a special case with duplicate negative eigenvalues (critically damped),

3. 2 complex conjugates in the LHP.

The $t = \infty$ strip exit height, c_0, is always one of the equations included in the final sum of three equations.

5.3.2 Two Negative Real Eigenvalues

For case 1 with two exponential functions, exponents A and B are related by a common pseudo-frequency, ω, and damping constant γ. Enforcing this relationship helps prevent degenerate final values, namely, $A = B$, so A and B are calculated using γ and ω with

$$A, B = \omega \pm \omega \sqrt{\gamma^2 - 1} \tag{5.7}$$

where γ is greater than one. The sub-equation is

$$real_1 = a\ e^{At} + b\ e^{Bt} \tag{5.8}$$

where a, b are scalars. The constraints on the variables are

- a and b are between $\pm 2.5(stdDev(\{y_n\}, 0, n))$ where $\{y_n\}$ is the array of strip exit heights in the post-excitation rolling window, and $stdDev$ is a function to calculate the standard deviation,

- γ is greater than or equal to 1.0 and less than some maximum damping, which is estimated at 3.0,

- ω is less the sampling frequency, $2\pi/(t_1 - t_0)$, and greater than or equal to the low frequency, $\pi/(t_n - t_0)$.

5.3.3   Duplicate Eigenvalues

If the damping factor, γ, is greater than or equal to 1.0 and $abs(\gamma - 1.0) < 10^{-8}$ then the critically damped case is used,

$$crit_1 = (a + bt)e^{\omega t} \tag{5.9}$$

where a and b are scalars. The constraints on the variables are

- a and b have the same constraints as case 1,

- γ is equal to 1.0,

- ω has the same constraints as case 1.

5.3.4   Two Complex Eigenvalues

For case three, when there two complex conjugate eigenvalues in the LHP, the under-damped frequency is calculated as

$$\omega_d = \omega_n \sqrt{1 - \gamma^2} \tag{5.10}$$

where γ is less than one and $\omega_n = \omega$. The sub-equation used is

$$compx = e^{-\gamma \omega_n t}(a\ cos(\omega_d t) + b\ sin(\omega_d t)) \tag{5.11}$$

where ω_n is the natural frequency, ω_d is the damped frequency and γ is the damping factor. The under damped constraints are

- a and b have the same constraints as case 1,

- γ is between 0.8 and 1.0

- ω has the same constraints as case 1.

5.3.5   L-BFGS Routine

A wrapper function, $twodof$, does the conditional testing and evaluations necessary to return the proper summation of: c_0 and Equations 5.8, 5.9, or 5.11. The function to minimize with the L-BFGS routine is

$$F_{min}(c_0, a, b, c, d, \gamma_1, \omega_1, \gamma_2, \omega_2, t_i, h_{x,i}) = (twodof(c_0, a, b, c, d, \gamma_1, \omega_1, \gamma_2, \omega_2, t_i) - h_{x,i})^2 \quad (5.12)$$

where $i \in \{0, 1, 2, ..., n-1\}$; a, b, γ_1 and ω_1 are used for one partial solution; and c, d, γ_2 and ω_2 are used for the other partial solution. The L-BFGS routine is passed the function to minimize, the bounds on the variables, and the gradient of the function to minimize. The gradient is calculated with the wrapper function $twodofgrad$, which uses the same input variables to determine the form of the gradient. The exit height at the feather, $h_{xf,i}$, is handled in the same manner.

Three different combinations of either over-damped (with critically damped a special case) or under-damped systems are all potential solutions. All three permutations are evaluated and the best fit returned. The mean of the residuals and the sum of the residuals squared is used in a weighted sum to pick the best of the three models.

The same kind of plots are produced as the SDOF routines, Figure 5.3 are the two plots generated from the 2DOF fit code. Red and green dots are the original data points and the solid lines are from the best solution found. The dotted line is a zero reference that the residues are plotted relative to.

A new feature with 2DOF plots is extending the analytical curves out to one-and-half times the steady-state run time to provide a visual indication of any problems with the solution. This final value, h_{prj}, is also kept for use later as a post processing check, namely, if $abs(h_{last} - h_{prj}) > 0.01$ [mm] this observation needs investigation. The observations that have exceeded this value are cases where the sinusoidal magnitude is still comparatively large after the simulation ends. This is possibly either a resonate condition, like chatter, [6], strip edge wave, strip center buckle, or an indication that the simulation time is too short.

5.3.6   Steady-State Rolling Load

The rolling-load data is already a function of time, so all of the rolling-load data points from time zero up to the end of the excitation time are excluded and the remaining data points are used in the steady-state window. A pseudo-exit height is produced by scaling the rolling-load data with stand stiffness, K_{std}, with

$$\{h_{rl}\} = \{P\}/K_{std} \quad (5.13)$$

where $\{P\}$ is the vector of the *post-excitation phase* rolling loads. The same function to minimize, Equation 5.12, employed for the exit heights is used. The results are put back in terms of force by multiplying K_{std}.
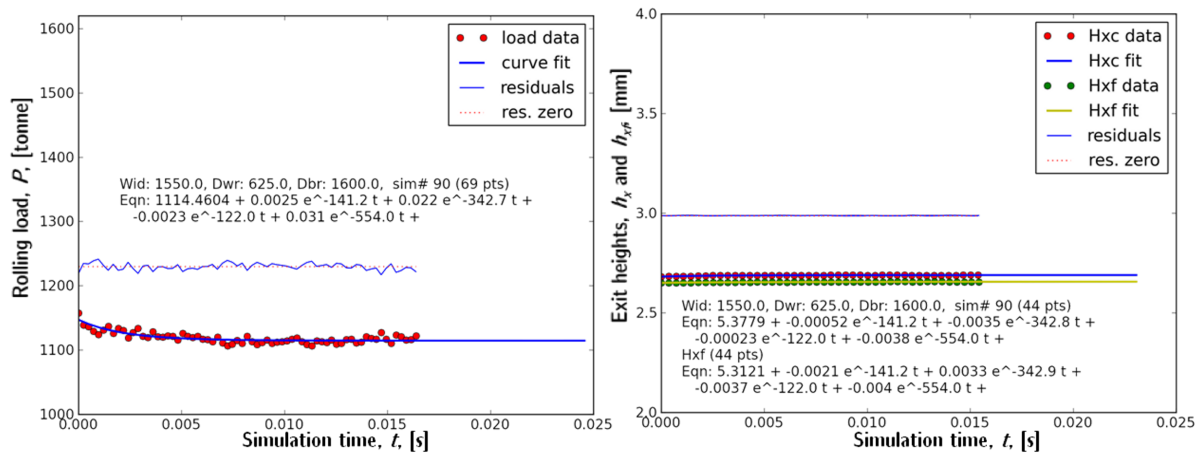
Figure 5.3: 2DOF fit for both rolling load, P, and the two exit heights, h_x and h_{xf}.

Chapter 6

Response Surface Models

6.1 Choice of Independent Variables

6.1.1 Ford and Alexander Force Equation Variables

Two of the dependent variables and four of the independent variable chosen for the response surface are used in the Ford and Alexander force equation [21],

$$P = kbL_p \left(\frac{\pi}{2} + \frac{1}{2} \frac{L_p}{(h_e + h_x)/2} \right) \qquad (6.1)$$

where b is the strip width, $k = S_y/\sqrt{3}$, S_y is the yield strength, L_p is the arc of contact, h_e is the centerline entry height including entry crown, h_x is the centerline exit height. The value for L_p is achieved by iteration, because the rolling load is unknown,

$$L_p \approx \sqrt{R'(h_e - h_x)} \qquad (6.2)$$

where R' for the first iteration is the original work radius, $d_{wr}/2$. As part of the next iteration a new estimate of the flattened radius is computed from the force estimate, P, with

$$R' = R' \left(1 + \frac{16(1 - \nu)^2}{\pi E(h_e - h_x)} \frac{P}{b} \right) \qquad (6.3)$$

where E is the work-roll modulus of elasticity and ν is Poisson's ratio. Repeated iterations are needed to get a converged force and exit-height value starting from Equation 6.1. The current procedure does not use a tolerance to end the search, but a fixed number of iterations.

6.1.2 Nine Selected Independent Variables

The minimum set of independent variables based on the Equations 6.1 through 6.3 and assuming the existence of strip crown are

- Strip width, wid [mm];
- Strip height at the feather, h_{ef} [mm] $(h_e - C_e)$;
- Strip entry crown, C_e [mm];
- Strip yield strength, S_y [tonne/mm^2];
- Work roll diameter, d_{wr} [mm].

Two other variables are chosen because they are known to influence the final exit crown value [20, 19, 12]. The independent variables are user inputs designed to control the final exit crown:

- Work-roll crown, C_{wr} [mm];
- Jacking load for work roll bending, J [tonne].

The remaining variables are chosen because they are needed in building the model or believed to have a measurable influence on exit crown, but they are not user inputs:

- FE model gap, gap [mm], (necessary to build the model),
- Backup roll diameter, d_{br} [mm], (known to influence crown [10, 22]).

One variable not chosen because it is believed to have a minimal influence on exit crown based on experience is strip velocity [14]. As the strip height is reduced the strip velocity increases, in a seven stand mill the strip velocity at the final stand is 5 to 6 times greater than the first stand. Realistic nominal strip velocities are assigned to each stand and used to set up the finite element model, but treated as fixed parameters necessary for calculating the dynamics of rolling.

6.1.3 The Four Selected Dependent Variables

Strip centerline exit height, h_x, and rolling load, P, are the two dependent variables in the Ford and Alexander equations. The strip centerline exit height, h_x, is the sum of the strip exit crown, C_x and strip exit height at the feather h_{xf}, therefore C_x and h_{xf} are also good dependent variables. The list of dependent variables is

- strip centerline exit height, h_x,
- strip exit height at the feather h_{xf},
- strip exit crown, C_x,
- rolling load, P.

Response surfaces built from C_x, h_x and h_{xf} provide the means of calculating strip exit crown using Equations 5.4 and 5.3. Rolling load, P, is not directly used to calculate strip exit crown, but is used to help validate the response surface.

6.1.4 The Choice of Strip Exit Height at the Feather

Figure 6.1, which is the transverse cross-sectional view of the strip, illustrates why the exit height at the feather, h_{xf}, is a better measurement to estimate strip exit crown than exit height at the edge, h_{xe}. Passing a curve through the 32 exit height data points between the center and feather width produces very little residual error. The last point at strip edge, h_{xe}, is approximately 0.04 [mm] away from h_{xf}. This is about twice the exit crown of 0.02 [mm].
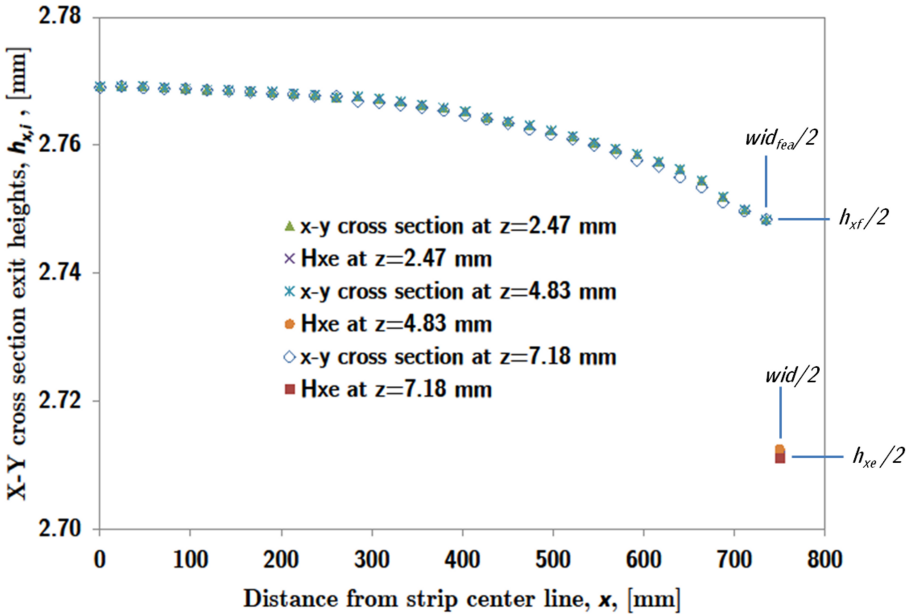
Figure 6.1: Three X-Y axis cross sections from the strip profile are used with both h_{xf} and h_{xe} identified.

Figure 6.1 is made from a stand 7 observation. The earlier stands (1 though 3) exert enough force on the strip that edge rounding extends pass the feather width (see Figure 6.30), so using a cross sectional fit fails to predict the strip exit height at the feather even if a quartic is used in place of a quadratic fit. Because of the excessive deformation at stand 1 though 3, the steady-state exit height calculations are based on the longitudinal exit height data, h_x and h_{xf}.

6.2   Response Surface Formulation

6.2.1   Design of Experiments Approach

A design of experiments approach with nine factors (variables) and two levels for each variable requires 512 experiments for a fully-factored response surface. The use of only two levels per variable assumes that a variable can be represented with a straight line (linear representation) [15, 2]. Fully factored requires that every possible combination of the two levels for each of the nine variables has an experiment, which is 2^9 or 512 permutations. If all factors have quadratic relationships then at least 3^9 or 19683 samples are needed. The number of samples or observations needed is calculated with

$$n_{obs} = max(i)max(j)...max(s) \qquad (6.4)$$

where $i, j, ..., s \in \{1, 2, ...\}$. For example, if the variable indexed with i has a linear representation and j is quadratic then $i \in \{1, 2\}$ and $j \in \{1, 2, 3\}$. The numbers of nodes is related to the number of degrees of freedom in the polynomial, using Lagrange interpolation functions:

- a linear polynomial - 2 nodes,
- a quadratic polynomial - 3 nodes,
- a cubic polynomial - 4 nodes....

Each experiment or observation for a response surface are derived from the steady-state results collected from one dynamic strip rolling simulation. The steady-state analysis (Section 5) is performed on the extracted data to produce the dependent variables: strip exit crown, $C_{x,1}$, centerline strip exit height, h_x, strip exit height at the feather, h_{xf}, and rolling load, P. Each dependent variable is now a function of the nine factors or nine-independent variables. Centerline exit height, h_x, for example, is

$$h_x = h_{x,RS}(wid, d_{wr}, d_{br}, gap, h_{ef}, S_y, C_e, C_{wr}, J) \qquad (6.5)$$

where wid, d_{wr}, d_{br}, gap, h_{ef}, S_y, C_e, C_{wr} and J are the nine-independent variables used to build the FE model. For a scaled response surface, centerline exit height is

$$h_x = h_{x,RS}(\eta_1, \eta_2, ..., \eta_9) \qquad (6.6)$$

where the η_i variables are the scaled independent variables. For an isoparametric response surface, centerline exit height is

$$h_x = h_{x,RS}(\zeta_1, \zeta_2, ..., \zeta_9) \qquad (6.7)$$

where the ζ_i variables are the transformed independent variables. The functional relationship for strip width becomes a function of more than one variable,

$$wid = wid(\zeta_1, \zeta_2, ..., \zeta_9), \qquad (6.8)$$

while the scaled width relationship is still one-to-one, as in $\eta_1 = \eta_1(wid)$.

6.2.2 The Evolution of the Sampling Methodology

Initial speculation is that the strip width *wid*, work-roll diameter, d_{wr} and backup-roll diameter, d_{br} have a cubic relationship with the remaining six variables having a linear form. A cubic function needs four observations per variable to define the curve and the linear form needs two observations. The minimum number of observations using Equation 6.4 is 4096 observations.

The collection of observations begins with the final finishing stand 7, which is also where most of the original finite element (FE) development is concentrated, so there are fewer unknowns to deal with. Stand 7 has one *gap* value in use; four perturbations of the so-call cubic variables, *wid*, d_{wr} and d_{br}; and a high and a low value for the six remaining variables.

A preliminary response surface built with a single value for the variables h_{ef}, S_y, C_{wr}, J show that cubic functions for d_{wr}, and d_{br} provides too many degrees of freedom, since a family of curves for strip exit crown does not show any consistent trends. Cubic interpolation functions are dropped in favor of quadratic or linear functions.

A revised sampling plan uses values from an existing mill setup schedule and targets collecting simulations from four out the seven stands. For each of the four stands there is one *gap* value; three perturbations of the potentially quadratic variables, *wid*, d_{wr} and d_{br}; and a high and a low value for the five remaining variables for a total of 864 observations per stand, or 3456 observations in total. This is twice as many samples as needed, but the experimental error seen in the first response surfaces is significant enough that weighted least squares becomes part of the next response surfaces.

The weights are the reciprocal of the sample variance, $1/S^2$, calculated in the steady-state fit for each of the dependent variables, h_x, h_{xf}, and P. C_x uses the sum of the sample variance for h_x and h_{xf}.

The observation samples are broken up into two groups to assign different collection priorities (see Table 6.1): *sample set 1* which is composed of a set with one gap and one entry height per stand group and it is based on the mill schedule. The other set, *sample set 2*, is composed of the same gap value, but with *sample set 1* entry heights reduced by roughly ten percent. Table 6.2 contains the perturbations for the remaining "linear" variables.

Table 6.1: Sample Sets 1 and 2 FE Gap and Edge Entry Height Values

	Sample Set 1		Sample Set 2	
Stand	**Gap [mm]**	**Entry height [mm]**	**Gap [mm]**	**Entry height [mm]**
1	23.78	40.21	23.78	32.17
3	10.04	19.05	10.04	17.20
5	5.43	10.26	5.43	8.28
7	4.38	6.43	4.38	5.90

The use of an existing schedule, instead of sampling based on the minimum and maximum

Table 6.2: Standard Sample Set Independent Variable Perturbations

Stand	C_e [mm] low	C_e [mm] high	C_{wr} [mm] low	C_{wr} [mm] high	S_y [mm] low	S_y [mm] high	J [tonne] low	J [tonne] high
1	0.201	0.300	-0.14	0.0000	0.01100	0.01364	0.00	75.76
3	0.158	0.205	-0.14	0.0000	0.01300	0.01657	0.00	123.00
5	0.090	0.100	-0.14	0.0000	0.01200	0.01922	96.88	126.01
7	0.000	0.050	0.00	0.0135	0.02038	0.02330	0.00	96.88

values for the full sample space, turns out to be a serious problem in building a usable response surface. The next subsection (6.2.3) goes into more detail about what problems are discovered building a response surface for a hot-rolling mill and how they are solved, but those solutions do not fully address the problem of using narrow ranges in values for the independent variables.

Early testing shows that the variable d_{wr} is best represented with a linear form and d_{br} is found to be linear or contributing very little to the model. Also, trend analysis for 12 yield strengths, S_y, using a typical stand 7 setup indicates that for a large range in S_y, S_y is quadratic or logarithmic, but for the narrow range of values used, a linear function works just as well. Therefore, expanding the range of the S_y is deferred, until a complete set of observations for stand groups 1, 3, and 5 are complete.

6.2.3   Hot-Rolling Mill Response Surface Issues

There are four obstacles discovered to building a response surface for a hot-rolling mill:

1. A large, 2×10^6 to 1, difference in independent variable magnitudes, I.E. $S_y \approx 10^{-3}$ [mm] and $wid \approx 10^3$ [mm].

2. A large, 10^5 to 1, difference in dependent variable magnitudes, I.E. $C_x \approx 10^{-2}$ [mm] and $wid \approx 10^3$ [mm].

3. The domain of the response surface is not rectangular. For instance, a large sample space with combinations of variable values that are either meaningless, I.E. $gap = 10.0$ [mm] and $h_{ef} = 5.0$ [mm] or unused, I.E. $gap = .1$ [mm] and $h_{ef} = 44$ [mm].

4. A narrow choice of the high-and-low values for independent variable sampling relative to the range of possible values used in a mill. Figure 6.2 is an example of this for gap and h_{ef}.

The solution to *obstacle 1* is to scale all of the independent variables to between ± 1. The scaled wid has the same magnitude as the scaled S_y. *Obstacle 2* exists for the exit crown dependent variable, C_x, but using a response surface based on exit heights h_x and h_{xf} to derive C_x changes the relative scales from 10^5 to 1 to 10^3 to 1. The *third obstacle* requires discretization where the solution space is meshed.

Three meshing solutions are possible: The first solution is to build an element about each stand or about pairs of adjacent stands. However, this breaks up a continuous space into separate elements and while this guarantees piecewise function continuity, derivative continuity requires additional constraint equations for the slopes, which is to expensive. For instance, linear interpolation requires 2 equations to find the two unknowns (the nodal values), but derivative continuity requires two more equations for the slope at each node and different interpolation functions (Hermite). The additional constraint also increases the polynomial degree from linear to cubic and it doubles the number of observations required, so this option is ruled out. The second option is rotating the axes in addition to scaling, which potentially allows a single element to be used for the entire solution space. The third option, an isoparametric representation, includes the scaling and rotation, but also allows the size of the element to change as a function of the other variables. The ability to form a non-rectangular domain with the lengths of each of the sides different makes the third option the method of choice.

Strip entry crown, C_e, and FE gap, *gap*, are examples of how the hot-rolling mill space varies as a function of the entry height at the feather, h_{ef}. The ranges for C_e and *gap* are $0.1 \leq C_e \leq 0.40$ [mm] and $20 \leq gap \leq 39$ [mm] when $h_{ef} = 40$ [mm] and the bounds are $0.0 \leq C_e \leq 0.10$ [mm] and $0 \leq gap \leq 4.0$ [mm] when $h_{ef} = 6.0$ [mm]. The isoparametric meshing accommodates this as a single element without enlarging the space at either h_{ef} endpoint.

Obstacle 4 is partially addressed with the choice of an isoparametric element for the response surface, but for some independent variable combinations, like *gap* and h_{ef}, there is still a relatively large area without observations (see Figures 6.2, 6.4, or 6.5). The best solution is to start with a isoparametric element as large as needed to cover the range in values for all seven stands and then generate coordinates for all of the observations based on either the nodal values or at the Gauss integration points. The use of nodal values is not practical in this case because many nodal combinations are close to an unused or a meaningless combination of variable values (see Figure 6.2). Because of this the Gauss points are a better choice.

The first full response surface uses all observations labeled *sample set #1* that are available (observations for $h_{ef} = 40$ [mm] have not run at this time). The least squares fit statistics for this response surface indicates a good fit, but for the worst case independent variable, the partial derivatives fluctuate between large positive and negative values, $\pm O(10^5)$. The same situation as a two-dimensional (2-D) example can be imagined using Figure 6.2 where a small amount of system error in the observations labeled *sample set #1* at a h_{ef} of 6.4 [mm], 10.26 [mm] and 19.1 [mm] will create large incline changes in the *gap* and h_{ef} plane.

A new response surface that includes *sample set #2* and 6 % of the $h_{ef} = 40$ [mm] observations is a big improvement in both the least squares fit and in the trend and magnitude of the partial derivatives. The largest partial derivatives are on the order of 10 and they have a consistent sign, except for "problem" regions, which are discussed in more detail later.
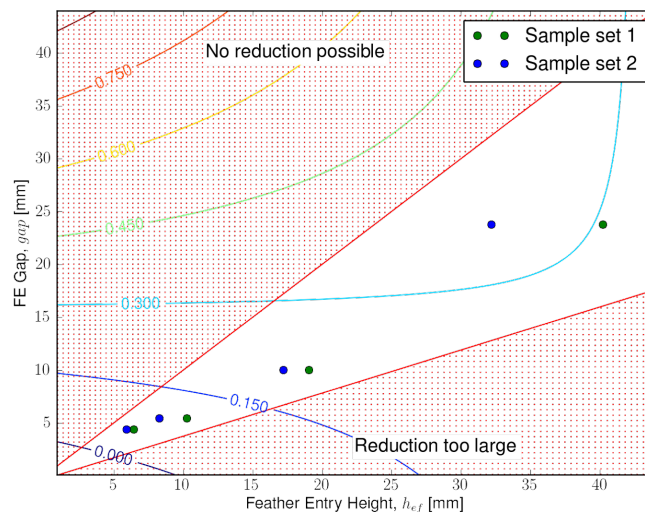
Figure 6.2: A contour plot of exit height, C_x, as a function of h_{ef} and *gap*.

6.2.4 Interpolation Introduction

The response surface is built from an orthogonal combination of linear and quadratic interpolation functions. Each independent variable defines one dimension in a n-space hyper-surface. Orthogonality requires that the set of independent variables are linearly independent and they are combined with the other variables using the tensor product.

For example, linear interpolation functions have two degrees of freedom just like the polynomial form of a line, $y(x) = mx + b$. An interpolated line using Lagrangian shape functions is

$$y_h(x) = \sum_{i=0}^{max(i)} y_{h,i} N_{h,i}(x) \tag{6.9}$$

where h is the element number, i is the node number, the nodal constant $y_{h,i}$ is the value of $y_h(x_{h,i})$, and $N_{h,i}(x)$ is the shape function. The requirements for the Lagrangian shape functions are [5]

1. The polynomial order of the original function, $y(x)$, and the shape functions, $N_{h,i}(x)$, are the same.

2. $N_{h,i}(x = x_{h,i}) = 1$ where $x_{h,i}$ is a nodal coordinate and $N_{h,i}(x = x_{h,j}) = 0$ when $i \neq j$.

3. The sum of all shape functions $N_{h,i}(x)$ are equal to 1 if the shape functions are C^0 continuous.

Figure 6.3 illustrates the C^0 property of the Lagrangian interpolation functions used. In Figure 6.3 two linear shape functions with two nodes each, $N_{h,1}$ and $N_{h,2}$ where $h \in \{1, 2\}$,

are used to create a two element mesh for a quadratic function, $y(x)$ with

$$y_1(x) \;=\; y_{1,1}N_{1,1}(x) + y_{1,2}N_{1,2}(x) \quad \{1 \geq x \geq 3\} \tag{6.10}$$

$$y_2(x) \;=\; y_{2,1}N_{2,1}(x) + y_{2,2}N_{2,2}(x) \quad \{3 \geq x \geq 5\} \tag{6.11}$$

where $y_1(x)$ is element 1 and $y_2(x)$ is element 2 and $y(x) = y_1(x) + y_2(x)$. At the common node at $x = 3$ both shape functions are piecewise continuous, C^0, but the two slopes for y_1 and y_2 are different, or not C^1 continuous. The polynomial form of the element makes it possible to get any number of derivatives within the element. A single quadratic interpolation function with three nodal values could have represented $y(x)$ exactly.
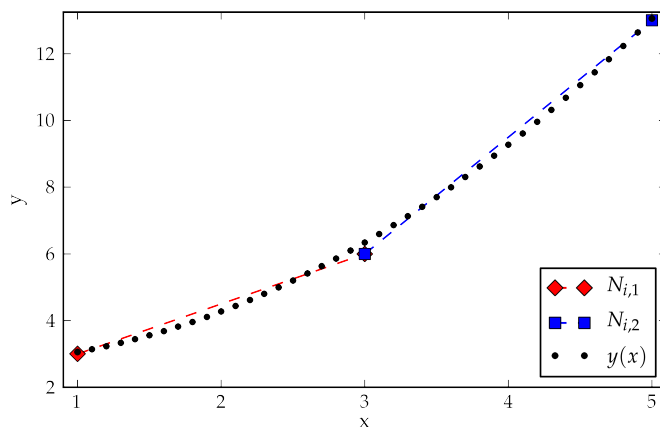
Figure 6.3: An example of a two element linear interpolation approximation of a quadratic function $y(x)$.

6.2.5   Un-scaled 2-D Example

Figure 6.2 uses independent variables *gap* and h_{ef} to illustrate a simple two-dimensional response surface example without scaling. The element boundaries are defined with the choice of the minimum and maximum values for independent variables *gap* and h_{ef}. The contours represent the value of dependent variable exit crown, $C_x(h_{ef}, gap)$. The value of both independent variables without any translation, scaling, or rotation are in terms of their natural values or natural coordinates. The shaded region labeled "No reduction possible" refers to stand gap that is larger than the strip entry height at the feather, so observations are not generated for this combination of variable values. The other shaded region labeled "Reduction too large" is a case where a practical limit is established and again no observations are planned.

The linear Lagrangian shape functions for *gap* in terms of two nodal values gap_1 and gap_2

are

$$N_{2,i}(gap) = \frac{gap_j - gap}{(gap_j - gap_i)} \tag{6.12}$$

where i and j varies from 1 to 2; and $i \neq j$. Letting $N_{1,j}(h_{ef})$ represent the linear shape function for entry height at the feather, the surface shown in Figure 6.2 is

$$C_x(gap, h_{ef}) = \sum_{i=0}^{max(i)} y_{2,i} N_{2,i}(gap) \sum_{j=0}^{max(j)} y_{1,j} N_{1,j}(h_{ef}) \tag{6.13}$$

where $i, j \in \{1, 2\}$ (both linear), the products $y_{2,i}\, y_{1,j}$ are the unknown nodal coefficients for C_x. Equation 6.13 defines the Exit crown function, $C_x(gap, h_{ef})$, as a 2-D element. Equation 6.13 in matrix form is

$$C_x(gap, h_{ef}) = [\phi_k(gap, h_{ef})]_{(1 \times 4)} \{C_{x,k}\}_{(4 \times 1)} \tag{6.14}$$

where

- brackets ([ ]) identify matrices,
- curly braces ({ }) identify column vectors,
- $C_{x,k}$ is the product of the constants $y_{2,i}\, y_{1,j}$,
- $\phi_k(gap, h_{ef})$ is the product of single variable the shape functions $N_2(gap)N_1(h_{ef})$,
- $k = (j - 1) + max(j)(i - 1) + 1$ (Equation 6.20).

Independent variable values for this example are in Table 6.1 and the exit crown values for the 2-D example are chosen arbitrarily by hand to reflect general trends for gap and strip entry height at the feather. Linear regression is used to define $C_x(gap, h_{ef})$, just for the 2-D example, as an analytic linear polynomial with one cross-term, or the equivalent of $C_x(gap, h_{ef}) = (gap\ gap_1 + gap_2)(h_{ef}\ h_{ef,1} + h_{ef,2})$.

6.2.6 Scaled 2-D Example

The result of scaling both of the independent variables to range from ± 1 is seen in Figure 6.4. The independent variable *gap* as the scaled independent variable η_2 is

$$\eta_2(gap) = 2\frac{gap - gap_{avg}}{gap_{rng}} \tag{6.15}$$

where

$$
\begin{aligned}
gap_{avg} &= (gap_1 + gap_2)/2 \\
gap_{rng} &= (gap_2 - gap_1)
\end{aligned}
$$
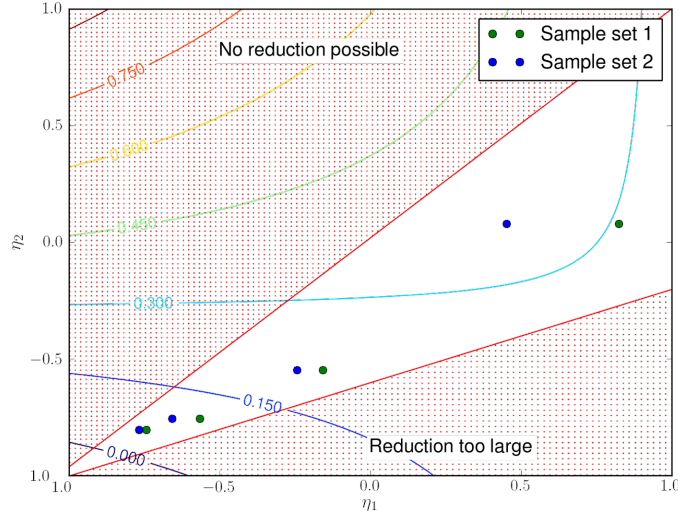
Figure 6.4: A contour plot with scaled coordinates η_1 and η_2 for scaled natural coordinates h_{ef} and *gap* respectively.

$\eta_1(h_{ef})$ is the equivalent scaling for h_{ef}. Scaling does not affect the relative size of the unused portions of the plane shaded in red in Figures 6.2 and 6.4.

The shape functions in terms of the scaled variable η are still Lagrangian. Solving Equation 6.12 in terms of η_2 with $gap_1 = \eta_{2,1} = -1$ and $gap_2 = \eta_{2,2} = +1$ simplifies to,

$$
\begin{aligned}
N_{2,1}(\eta_2) &= \frac{1}{2}(1 - \eta_2) \\
N_{2,2}(\eta_2) &= \frac{1}{2}(1 + \eta_2)
\end{aligned}
\tag{6.16}
$$

6.2.7   Isoparametric 2-D Example

Figure 6.5 shows the h_{ef} and *gap* plane after the transformation to new coordinates ζ_1 and ζ_2, including the location of the four Gauss integration points. The scaled h_{ef} axis, η_1, in this example is mapped one-to-one to the isoparametric ζ_1 axis, but this is an arbitrary choice to make the example a little easier to work.

Figure 6.6 is an overlay of the scaled and isoparametric 2-D planes, which both use coordinate ranges of ± 1. The diamonds show the two *sample sets* with an isoparametric representation and the circles are scaled representation. The transformation for the gap axis includes a rotation and a scaling as a function of h_{ef}, which makes *gap* a function of both ζ_1 and ζ_2 as seen in Figure 6.6. For the *gap* mapping, the effect of changing ζ_2 and holding ζ_1 constant only changes the value of *gap*, while changing ζ_1 and holding ζ_2 constant changes h_{ef} and *gap*.
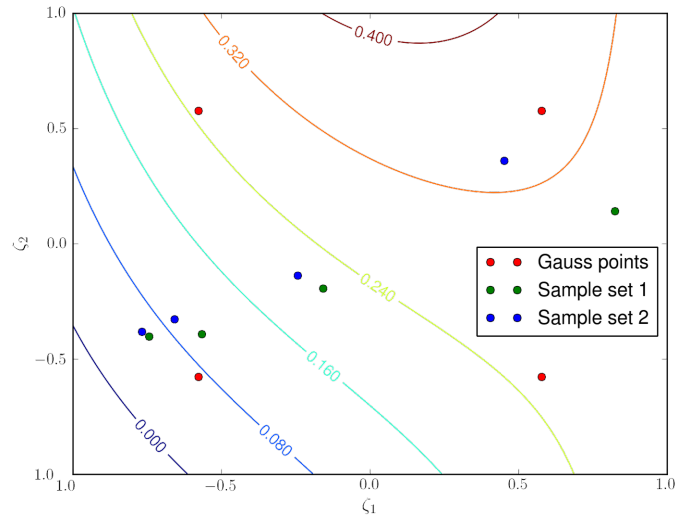
Figure 6.5: Exit crown contour plot on isoparametric coordinate plane ζ_1 and ζ_2 for transformed h_{ef} and *gap* respectively.
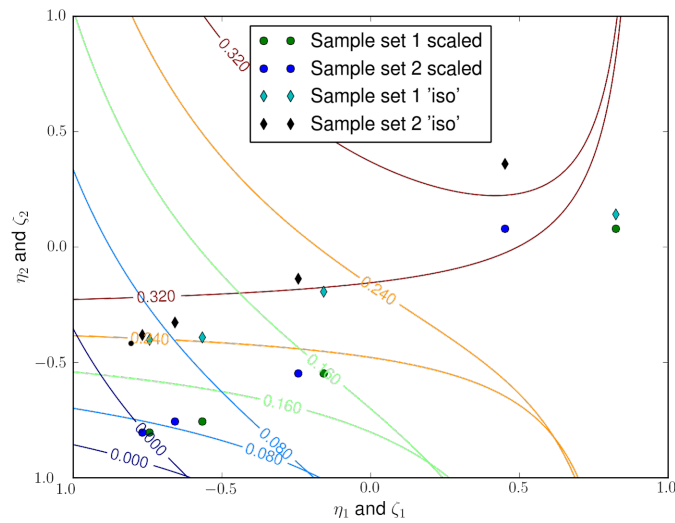
Figure 6.6: An overlay of scaled and isoparametric coordinate planes for η_1 and ζ_1 and η_2 and ζ_2.

There is some increase in separation between observations because of the isoparametric mapping, but as seen in Figure 6.5, sampling at the four Gauss points is a much better approach. Using the Gauss points to generate the natural coordinates for the four observations needed in this 2-D example is a three step process,

1. For a single linear dimension compute the two Gauss points $(\pm 1/\sqrt{3})$ or three Gauss points for quadratic dimension $(\pm\sqrt{3/5}$ and $0)$.

2. Build a coordinate vector, $\{\zeta\}$ based on all possible combinations of the index range for each dimension. For a single linear dimension,

$$\zeta_i = (-1)^i \frac{1}{\sqrt{3}} \tag{6.17}$$

   where $i \in \{1, 2\}$. For a quadratic dimension

$$\zeta_i = (i - 2)\sqrt{\frac{3}{5}} \tag{6.18}$$

   where $i \in \{1, 2, 3\}$.

3. Convert the isoparametric coordinate to natural coordinates using Equation 6.22.

Table 6.3 contains the natural coordinates for the Gauss points seen in Figure 6.5. Because there is one unusable observation, either the boundaries chosen for the isoparametric surface must change or the one observation must be forced into a usable combination and the isoparametric coordinates recomputed.

Table 6.3: The Gauss Point Mapping of Isoparametric Coordinates to Natural Coordinates.

Node	ζ_1	ζ_2	$\mathbf{h}_{ef}$ [mm]	**gap** [mm]	Description
1	-0.58	-0.58	10.01	3.78	
2	0.58	-0.58	34.89	8.34	
3	-0.58	0.58	10.01	13.59	meaningless combination
4	0.58	0.58	34.89	29.19	

6.2.8 Linear Isoparametric Interpolation Functions

The shape functions for a single linear isoparametric dimension have the same minimum and maximum as those scaled between ± 1, so they are identical to the shape functions of Equation 6.16, except for the use of ζ in place of η. Expanding ϕ_k in Equation 6.14 in terms

of the shape functions in Equation 6.12 produces the four nodal equations,

$$\phi_1(\zeta_1, \zeta_2) = \frac{1}{2}(1 - \zeta_1)\frac{1}{2}(1 - \zeta_2) \tag{6.19}$$

$$\phi_2(\zeta_1, \zeta_2) = \frac{1}{2}(1 + \zeta_1)\frac{1}{2}(1 - \zeta_2)$$

$$\phi_3(\zeta_1, \zeta_2) = \frac{1}{2}(1 - \zeta_1)\frac{1}{2}(1 + \zeta_2)$$

$$\phi_4(\zeta_1, \zeta_2) = \frac{1}{2}(1 + \zeta_1)\frac{1}{2}(1 + \zeta_2)$$

where ζ_1 and ζ_2 are the transformed h_{ef} and gap axes respectively. Node numbering and locations are mapped as shown in Table 6.4. In generic terms, the node number, k, is

$$k = (i - 1) + i_{max}(j - 1) + i_{max}j_{max}(l - 1) + ...(i_{max}j_{max}..r_{max})(s - 1) + 1 \tag{6.20}$$

where i, j, ..., r and s vary from 1 to 2 for linear dimensions or vary from 1 to 3 for quadratic dimensions and $i_{max} = max(i)$, $j_{max} = max(j)$, ..., $r_{max} = max(r)$. To calculate the total number of nodes use the maximum values for i, j, etc., in Equation 6.20.

Table 6.4: 3-D Node Numbering Example

ζ_1	ζ_2	ζ_1 **node number, i**	ζ_2 **node number, j**	**Node number, k**
-1	-1	1	1	$(1 - 1) + 2(1 - 1) + 1 = 1$
1	-1	2	1	$(2 - 1) + 2(1 - 1) + 1 = 2$
-1	1	1	2	$(1 - 1) + 2(2 - 1) + 1 = 3$
1	1	2	2	$(2 - 1) + 2(2 - 1) + 1 = 4$

Expanding Equation 6.14 in terms of the isoparametric form,

$$C_x(\zeta_1, \zeta_2) = \begin{bmatrix} \phi_1(\zeta_1, \zeta_2) & \phi_2(\zeta_1, \zeta_2) & \phi_3(\zeta_1, \zeta_2) & \phi_4(\zeta_1, \zeta_2) \end{bmatrix} \begin{Bmatrix} C_{x,1} \\ C_{x,2} \\ C_{x,3} \\ C_{x,4} \end{Bmatrix} \tag{6.21}$$

where ϕ_k are the nodal equations from the tensor product (Equation 6.19) and $C_{x,k}$ are the nodal values. The derivation of the nodal values for $C_{x,k}$ is covered in the next section (6.3). To recover the original natural coordinate values, the matrix product between the interpolation function tensor product ($[\phi_k]$ in Equation 6.21) that produces a $1 \times k$ row vector and the $k \times n$ matrix of natural nodal values is,

$$\begin{bmatrix} h_{ef} & gap \end{bmatrix} = [\phi_k(\zeta_1, \zeta_2)]_{(1 \times k)} [\{h_{ef,k}\}, \{gap_k\}]_{(k \times 2)} \tag{6.22}$$

where $\{h_{ef,k}\}$ and $\{gap_k\}$ are vectors of the natural nodal coordinates that correspond to the isoparametric coordinates, $[\zeta_{1,k}, \zeta_{2,k}]^T$ where $\zeta_{1,k} = \pm 1$ and $\zeta_{2,k} = \pm 1$ for the two linear

dimensions. The shorter notation $\{\zeta\}$ for q dimensions is used in place of $[\zeta_{1,k}, \zeta_{2,k}, ..., \zeta_{q,k}]^T$ from now on. The natural nodal values are determined from the usable area in Figure 6.2. The $\{\zeta\}$ vector for the *sample sets* are found using a gradient-based search covered in more detail later.

6.2.9   Extending the 2-D Example to 3-D

Adding independent variable *wid* to the 2-D surface to produce a 3-D volume, requires the following steps,

1. extend the tensor product with $\phi_k = N_{h,i}(\zeta_1)N_{h,j}(\zeta_2)N_{h,l}(\zeta_3)$ where $h \in \{1, 2, 3\}$, Equation 6.4 calculates the value of node number k; and i, j and l are varied depending on the number of nodes or degrees of freedom in the interpolation functions,

2. add a new column of nodal values in terms of natural coordinates to the isoparametric mapping matrix.

The use of the same interpolation functions and tensor product in Equations 6.21 and 6.22 to calculate the response surface value and the natural coordinates respectively makes this an isoparametric mapping. Using a different order of interpolation function between these two equations creates either superparametric or subparametric mapping, which is not covered.

6.2.10   Quadratic Shape Functions

Quadratic shape functions are based on a quadratic polynomial, so there are three nodes and three degrees of freedom. The new term in the isoparametric shape functions is the ζ^2 term [5] as in,

$$
\begin{aligned}
N_{l,1}(\zeta) &= \frac{1}{2}(\zeta^2 - \zeta) \\
N_{l,2}(\zeta) &= (1 - \zeta^2) \\
N_{l,3}(\zeta) &= \frac{1}{2}(\zeta^2 + \zeta)
\end{aligned}
\tag{6.23}
$$

Assuming that h_{ef} is now a quadratic dimension then there are now two new nodes in Figure 6.5 at $(0, -1)$ and $(0, +1)$. Using Equation 6.20 with $i_{max} = 3$ generates the node numbers in Table 6.5.

Table 6.5: 2-D Node Numbering Example

ζ_1	ζ_2	ζ_1 **node** **number,** i	ζ_2 **node** **number,** j	**Node** **number,** k
-1	-1	1	1	$(1-1)+3(1-1)+1=1$
0	-1	2	1	$(2-1)+3(1-1)+1=2$
1	-1	3	1	$(3-1)+3(1-1)+1=3$
-1	1	1	2	$(1-1)+3(2-1)+1=4$
0	1	2	2	$(2-1)+3(2-1)+1=5$
1	1	3	2	$(3-1)+3(2-1)+1=6$

6.2.11 Independent Variable Pre-scaling

Some of the possible functional relationships between the independent and dependent variables that can be handled with variable scaling are,

$$y = ln(x) + c$$
$$y = 1/x + c$$
$$y = \sqrt{x} + c$$

where x is the independent variable and c is a constant. All three functional relationships have to be approximated without scaling; either with a single element mesh with a high enough order polynomial to minimize the error or a multiple element mesh with enough elements to minimize the error. Using the square root as an example, let $\hat{x} = \sqrt{x}$ then $y = \hat{x} + c$ is now a linear polynomial that can be exactly represented with linear interpolation, instead of approximated.

The natural value of the independent variable is pre-scaled. This requires that the natural value in the isoparametric mapping to be pre-scaled. The steps to go from natural coordinate to the ζ coordinate using the 2-D gap and h_{ef} example with h_{ef} using square root scaling are

1. apply pre-scaling: $\widehat{gap} = gap$ and $\widehat{h_{ef}} = \sqrt{h_{ef}}$ (this step assumes that all of the values in $\{h_{ef,k}\}$ are now $\{\sqrt{h_{ef,k}}\}$),

2. do the gradient search to find the ζ coordinates.

The steps to go from the ζ coordinate to the natural coordinate is

1. compute the tensor product, $[\phi_k(\{\zeta\})]$,

2. compute $[\widehat{gap}, \widehat{h_{ef}}] = [\phi_k][\{gap_k\}, \{h_{ef,k}\}]$

3. undo the pre-scaling with: $gap = \widehat{gap}$ and $h_{ef} = \widehat{h_{ef}}^2$.

The value of the dependent variable is not affected by the pre-scaling, but the partial derivatives are affected by both the coordinate transformation and any pre-scaling. The partial

derivatives of C_x with respect to h_{ef} and *gap* require two chain rule expansions. First, expand the partials derivatives in terms of the pre-scaled variable as in

$$
\begin{aligned}
\frac{\partial C_x}{\partial gap} &= \frac{\partial C_x}{\partial \widehat{gap}} \frac{\partial \widehat{gap}}{\partial gap} \\
\frac{\partial C_x}{\partial h_{ef}} &= \frac{\partial C_x}{\partial \widehat{h_{ef}}} \frac{\partial \widehat{h_{ef}}}{\partial h_{ef}}
\end{aligned}
\tag{6.24}
$$

and then expand the partials of C_x with respect to the ζ variables using the chain rule as in

$$
\begin{aligned}
\frac{\partial C_x}{\partial \zeta_1} &= \frac{\partial C_x}{\partial \widehat{gap}} \frac{\partial \widehat{gap}}{\partial \zeta_1} + \frac{\partial C_x}{\partial \widehat{h_{ef}}} \frac{\partial \widehat{h_{ef}}}{\partial \zeta_1} \\
\frac{\partial C_x}{\partial \zeta_2} &= \frac{\partial C_x}{\partial \widehat{gap}} \frac{\partial \widehat{gap}}{\partial \zeta_2} + \frac{\partial C_x}{\partial \widehat{h_{ef}}} \frac{\partial \widehat{h_{ef}}}{\partial \zeta_2}
\end{aligned}
\tag{6.25}
$$

Putting the set of Equations 6.25 into matrix form and solving for the partials with respect to the "hatted" variables,

$$
\begin{bmatrix} \frac{\partial C_x}{\partial \widehat{gap}} \\ \frac{\partial C_x}{\partial \widehat{h_{ef}}} \end{bmatrix} = \begin{bmatrix} \frac{\partial \widehat{gap}}{\partial \zeta_1} & \frac{\partial \widehat{h_{ef}}}{\partial \zeta_1} \\ \frac{\partial \widehat{gap}}{\partial \zeta_2} & \frac{\partial \widehat{h_{ef}}}{\partial \zeta_2} \end{bmatrix}^{-1} \begin{bmatrix} \frac{\partial C_x}{\partial \zeta_1} \\ \frac{\partial C_x}{\partial \zeta_2} \end{bmatrix}
\tag{6.26}
$$

Formulating Equation 6.24 into matrix form and then substituting the result of Equation 6.26 produces,

$$
\begin{bmatrix} \frac{\partial C_x}{\partial gap} \\ \frac{\partial C_x}{\partial h_{ef}} \end{bmatrix} = \begin{bmatrix} \frac{\partial \widehat{gap}}{\partial gap} & 0 \\ 0 & \frac{\partial \widehat{h_{ef}}}{\partial h_{ef}} \end{bmatrix} \left(\begin{bmatrix} \frac{\partial \widehat{gap}}{\partial \zeta_1} & \frac{\partial \widehat{h_{ef}}}{\partial \zeta_1} \\ \frac{\partial \widehat{gap}}{\partial \zeta_2} & \frac{\partial \widehat{h_{ef}}}{\partial \zeta_2} \end{bmatrix}^{-1} \begin{bmatrix} \frac{\partial C_x}{\partial \zeta_1} \\ \frac{\partial C_x}{\partial \zeta_2} \end{bmatrix} \right)
\tag{6.27}
$$

In the final response surface square root scaling of S_y is used. Ideally quadratic interpolation should be used, but there are not enough observations with a change in S_y to do this.

6.2.12   Finding the Isoparametric Coordinates with the Gradient-Based Function Minimization Search

Prior to building the isoparametric response surface, all of the observations are made using the natural coordinates, instead of calculating the natural coordinates from the isoparametric $\{\zeta\}$ coordinate vector. Thus, a search to find isoparametric coordinates is necessary. Other reasons to search for the isoparametric coordinates are: changing the isoparametric mapping between the $\{\zeta\}$ and the natural coordinates, which invalidates any existing $\{\zeta\}$ coordinates, or the use of functions requiring a dependent variable value in terms of the

natural coordinates, for instance, $C_x(d_{wr}, d_{br}, ..., J)$. The same gradient-based search in all three cases is used to find the $\{\zeta\}$ coordinates.

Given a coordinate vector of the natural values, $\{x_{targ}\}$, a conjugate gradient search is used to minimize the function,

$$F_{min}(\{x_{targ}\}, \{\zeta\}) = (retNatCoor(\{\zeta\} - \{x_{targ}\})^T (retNatCoor(\{\zeta\} - \{x_{targ}\}) \quad (6.28)$$

where $\{\zeta\}$ is an initial estimate and function $retNatCoor$ returns a vector of natural values after calculating,

$$\{x\} = [\phi_k(\{\zeta\})]_{(1 \times k)}[\{x_{1,k}\}, \{x_{2,k}\}...\{x_{q,k}\}]_{(k \times q)} \quad (6.29)$$

where q is the number of variables in the response surface, $[\phi_k]$ is the column vector interpolation function tensor products and $\{x_{i,k}\}$ are the q row vectors of natural coordinates mapped to the isoparametric coordinates.

6.3 Weighted-Least Squares Solution of the Response Surface

6.3.1 Response Surface Form with the Nodal Values Known

The dependent variables as a function of the $\{\zeta\}$ coordinates are used to build the response surface. The tensor product for each observation, $[\phi_k(\{\zeta\})]$, is evaluated to produce k interpolation products in the form of a $1 \times k$ column vector. The concatenation of all the column vectors from n observations produces the matrix $[\Phi]$. The $[\Phi]$ matrix is the equivalent to the set of normal equations in least squares.

Strip centerline exit height, h_x, is used in the equations, but the same applies to the remaining three dependent variables: rolling load, P, strip exit height at the feather, h_{xf} and strip exit crown, C_x. If the coefficients are known then the vector of dependent variable values, $\{h_{x,RS}\}$, is calculated from

$$\{h_{x,RS}\}_{(n \times 1)} = [\Phi]_{(n \times k)}\{h_{x,k}\}_{(k \times 1)} \quad (6.30)$$

where $\{h_{x,k}\}$ is the vector of the strip centerline exit height nodal coefficients (nodal coordinates).

6.3.2 Weighted-Least Squares

If nodal coefficient matrix, $\{h_{x,k}\}$, is unknown then a weighted least squares approach is used to calculate $\{h_{x,k}\}$. Each of the dependent variables has a sample standard deviation, S, from the steady-state fit. The smaller the residuals then the smaller the standard deviation, so the inverse of the standard deviation, $1/S$, makes a good weight for this observation.

Because the observations do not depend on any other observation (they are uncorrelated), the weights matrix, $[\mathbf{W}]$, is a diagonal matrix. If the observations are correlated then $[\mathbf{W}]$ is no longer a diagonal matrix. The weights matrix is

$$[\mathbf{W}] = ([\mathbf{S}]^{-1})^T [\mathbf{S}]^{-1} \tag{6.31}$$

where $[\mathbf{S}]$ is the matrix of standard deviations. For instance, if $[\mathbf{X}'] = [\mathbf{S}]^{-1}[\mathbf{X}]$ then $[\mathbf{X}']^T[\mathbf{X}'] = ([\mathbf{S}]^{-1}[\mathbf{X}])^T[\mathbf{S}]^{-1}[\mathbf{X}]$ or after expanding the transpose operation $[\mathbf{X}]^T([\mathbf{S}]^{-1})^T[\mathbf{S}]^{-1}[\mathbf{X}]$.

A vector, $\{h_{x,obs}\}$, of observations is used in place of $\{h_{x,RS}\}$ in Equation 6.30. The weighted least squares solution is found first by pre-multiplying both sides by $[\Phi]^T[\mathbf{W}]$,

$$[\Phi]^T_{(k \times n)}[\mathbf{W}]_{(n \times n)}\{h_{x,obs}\}_{(n \times 1)} = [\Phi]^T_{(k \times n)}[\mathbf{W}]_{(n \times n)}[\Phi]_{(n \times k)}\{h_{x,k}\}_{(k \times 1)} \tag{6.32}$$

where $\{h_{x,obs}\}$ is $n \times 1$ vector, $[\mathbf{W}]$, is a $n \times n$ matrix, and $[\Phi]$ is an $n \times k$ matrix. Solving Equation 6.32 for the unknown nodal coefficients, $\{h_{x,k}\}$,

$$\{h_{x,k}\} = ([\Phi]^T[\mathbf{W}][\Phi])^{-1}[\Phi]^T[\mathbf{W}]\{h_{x,obs}\} \tag{6.33}$$

The nine-dimensional response surface used to validate the response surface has $n = 3112$ observations and because there are not any quadratic interpolations, there are $k = 512$ terms (Equation 6.4) in the tensor product. Therefore, $[\Phi]$ is a 3112×512 matrix, the coefficient vector, $\{h_{x,k}\}$ is 512×1, the vector for one dependent variable, $\{h_{x,obs}\}$ is 3112×1 and the weights matrix, W, is 3112×3112.

6.4   Function Estimation with Simple Projections

6.4.1   Variable Functional Form Estimation

The use of one-dimensional (1-D) projections or two-dimensional (2-D) projections offers a method of estimating the correct order for a given variable. The 1-D or 2-D projection offers only an estimate because of the limited size of the sets used to make predictions about a given variable. A variable that is quadratic in one area of the response surface should indicate that this is the minimum polynomial order, while finding one linear relationship at a stand group is not sufficient to end the search. None of the plots reviewed show any polynomial order greater than quadratic. An advantage to a 1-D study is a sensitivity analysis provides a good estimate of the range in values to use in sampling.

Only one independent variable changes to create the 1-D projections, while the other variables are set to nominal values for one of the stands (in 2-D projections two variables change). Ideally there is an overlap between adjacent stand groups for the changes in value of the variable under study. A stand group is the pair of adjacent stands that are represented on

the response surface using nominal variable values from just the one stand. Stand 7 and stand 6 are referred to as stand group 7, but only observations for stand seven are on the response surface. Stand 1 is its own group. Stands 2 and 3 make up stand group 3. The combination of stand 4 and 5 is stand group 5.

An example of overlap between stand groups is the strip entry height at the feather, h_{ef}, study for stand group 7 where typical ranges are $1 \leq h_{ef} \leq 7$ [mm] and $0 \leq gap \leq 4$ [mm]. A stand 5 h_{ef} might be 10 [mm], so eight samples between 5.9 [mm] and 9.2 [mm] is enough oversampling to provide a good indication of the polynomial order and study the region between stand group 5 and 7. The number of samples used here is an exception. This is done because the h_{ef} variable does not show its quadratic behavior, until a large enough change in value and the initial steps are too small. Four samples are the minimum number collected to investigate the possibility of a quadratic fit. The results are summarized starting in subsection 6.4.4.

6.4.2   Signal-to-Noise Ratios

Because the strip exit crown, C_x, is 2 orders of magnitude smaller than the two strip entry heights and C_x includes the error from both strip exit heights, building the response surface from the two strip exit heights, h_x and h_{xf}, is more accurate. The signal-to-noise ratios calculated for the linear 1-D studies (see Table 6.6) supports this. Later on, statistics from the response surface confirm the choice of the two exit heights to compute strip exit crown.

The signal-to-noise ratio is defined as the power of the signal over the power of the noise where power is defined as the mean square value of the function (typically a function of time). The signal-to-noise ratio, SNR, [4] is

$$SNR = \sqrt{\frac{S_s^2}{S_n^2}} \tag{6.34}$$

where S_s^2 is the mean square value of the signal and S_n^2 is the mean square value of the noise. The signals are the values of the dependent variables, C_x, h_x, and h_{xf}, used in the 1-D studies and the power of the noise is derived from the residual error.

Table 6.6 is a summary of the signal-to-noise ratios found from the data used in the 1-D projections and assuming a linear representation for all cases. Since a larger SNR is better, the linear fit for seven out of nine independent variables are represented better using the two strip exit heights. The seven independent variables are:

- strip width, wid,
- work-roll diameter, d_{wr},
- entry height at the feather, h_{ef},
- FE gap, gap,

- yield strength, S_y,

- entry crown, C_e,

- jacking load, J.

The 1-D fit for work-roll crown is better using strip entry crown at low strip velocities, but at the strip velocity of stand 7, the average strip exit height SNR and the strip exit crown SNR are about equal. The remaining variable, backup-roll diameter has a inconsistent SNR for strip exit crown, C_x, with only one ratio out of four greater than 10 and the SNR for the two strip exit heights is worse with the signal about equal to the noise ($SNR \approx 1$).

Table 6.6: Summary of the Signal-to-Noise Ratios for the 1-D Projections using a Linear Model

Range		Aux.	Signal-to-Noise Ratio		
wid [mm]		**d$_{\mathbf{wr}}$** [mm]	C_x SNR	h_x SNR	h_{xf} SNR
1000	1700	625	1.59	8.56	23.79
1000	1700	775	1.83	15.43	32.35
d$_{\mathbf{wr}}$ [mm]		**d$_{\mathbf{br}}$** [mm]	C_x SNR	h_x SNR	h_{xf} SNR
625	850	1450	1.29	23.78	18.08
625	850	1500	1.93	21.95	15.88
625	850	1550	6.66	40.62	65.11
d$_{\mathbf{br}}$ [mm]		**d$_{\mathbf{wr}}$** [mm]	C_x SNR	h_x SNR	h_{xf} SNR
1450	1550	625	1.00	1.36	0.94
1450	1550	700	157.84	1.00	0.89
1450	1550	775	9.80	1.02	1.08
1450	1550	850	3.11	4.92	0.96
h$_{\mathbf{ef}}$ [mm]			C_x SNR	h_x SNR	h_{xf} SNR
6.43	7.20		5.96	159.25	85.56
gap [mm]			C_x SNR	h_x SNR	h_{xf} SNR
2.44	3.48		5.3	71.15	180.63
S$_{\mathbf{y}}$ [mm]			C_x SNR	h_x SNR	h_{xf} SNR
0.0080	0.0140		3.71	15.01	16.76
C$_{\mathbf{e}}$ [mm]			C_x SNR	h_x SNR	h_{xf} SNR
0.01	0.04		3.26	13.54	4.73
C$_{\mathbf{wr}}$ [mm]		**Vel$_{\mathbf{stp}}$** [mm/s]	C_x SNR	h_x SNR	h_{xf} SNR
-0.120	0.100	1284.23	8.33	1.22	4.15
-0.130	0.110	4018.44	26.04	1.66	5.08
-0.130	0.110	6752.64	48.53	2.37	79.32
J [tonne]			C_x SNR	h_x SNR	h_{xf} SNR
20.00	80.00		9.29	19.17	94.53

6.4.3 Stand Groups 3, 5 and 7 1-D Collection Status

All of the figures that follow for this section are created from stand 7 values: $h_{ef} = 6.4337$ [mm], $gap = 3.48$ [mm], and $C_e \leq .05$ [mm]. The remaining seven variables besides h_{ef} and gap are not stand specific (Appendix A contains a table values for the plots). Additional R^2 and SNR information is collected from 1-D studies for stand groups 3 and 5, and the results are summarized in the text.

The effort to replicate the 1-D projections for stand groups 3 and 5 is not completed due to time and license constraints on running the Abaqus simulations. Only two of the stand group 5 projections are collected: a full range of h_e observations and a partial set of observations for d_{wr}. Six of the variables are complete for stand group three. Missing for both stand group 3 and 5 is confirmation of *gap* linearity.

6.4.4 The Dependent Variable Functional Form for Work-Roll Diameter

Table 6.7 summarizes the 1-D work-roll diameter projection statistics for both the linear and quadratic polynomial relationships for three different backup-roll diameters studied at stand 7. The quadratic polynomial is the best model in all cases. Figure 6.7 shows a quadratic model for a backup roll of 1450 [mm] with a very good coefficient of determination (R^2) greater than 0.998. This set of observations is the worst of the quadratic relationships between work-roll diameter, d_{wr}, and the feather, h_{xf} and centerline exit heights, h_x.

Table 6.7: Summary of the Signal-to-Noise Ratios and R^2 statistics for the work-roll 1-D Projections

d_{br} [mm]	Poly. order	h_x R^2	h_x SNR	h_{xf} R^2	h_{xf} SNR
1450	Linear	0.9982	23.78	0.9969	18.08
1450	Quadratic	0.9996	49.99	0.9985	25.69
1500	Linear	0.9979	21.95	0.9960	15.88
1500	Quadratic	0.9986	26.45	0.9999	103.59
1550	Linear	0.9994	40.62	0.9998	65.11
1550	Quadratic	0.9999	130.20	0.9999	115.78

A linear study with nominal stand group 5 values with only three observations has R^2 values between 0.996 to 0.98; and the SNR for h_x of 7.00 and h_{xf} of 15.62. Collecting more samples with a larger range in values at the stand 5 and 3 should provide confirmation that work-roll is quadratic. At this time there are not enough variations in d_{wr} at all stand groups to produce a quadratic response surface, so a linear model is being used.
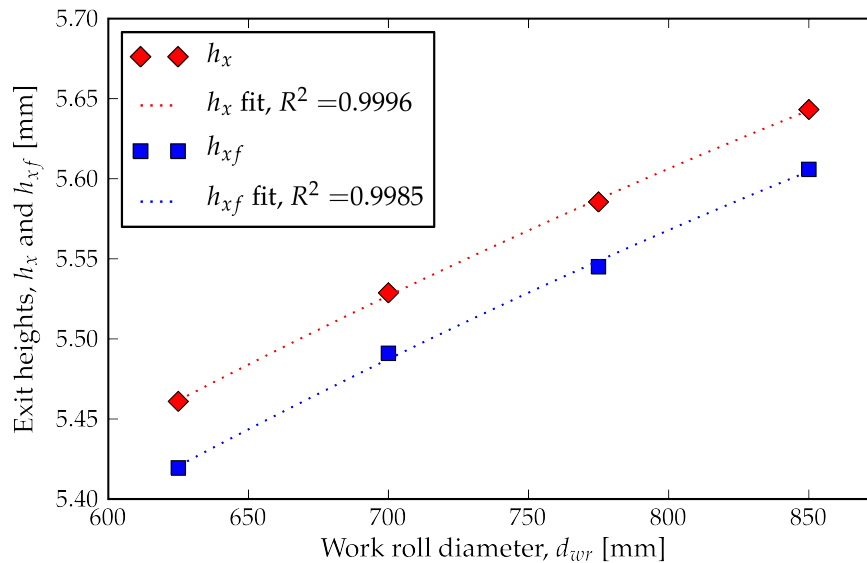
Figure 6.7: Exit heights, h_x and h_{xf}, as a quadratic function of work-roll diameter, d_{wr}.

6.4.5   The Dependent Variable Functional Form for Strip Width

Figure 6.8 shows that the two strip exit heights h_x and h_{xf} have a quadratic relationship with strip width, *wid*. Ginzburg[10] supports a nonlinear relationship for exit crown as a function of width. In Ginzburg, the strip exit crown increases as strip width increases, until a point about 70 to 80 percent of the maximum strip width. At this point, the strip exit crown reaches its peak value and begins to decrease as strip width increases. This effect is clearly seen in Figure 6.9 for the C_x plots using the two work-roll diameters, $d_{wr,1} = 625$ [mm] and $d_{wr,2} = 775$ [mm]. In each case, the peak is at about a strip width of 1200 [mm]. This same peak at 1200 [mm] and same quadratic polynomial order are also confirmed with an additional study at stand group three.

6.4.6   The Dependent Variable Functional Form for Entry Height at the Feather

Figure 6.10 shows that the two strip exit heights have a quadratic relationship with entry height at the feather, h_{ef}. Response surfaces created with a quadratic form for h_{ef} have good statistics. However, this improvement in statistics is in most part due to the additional degrees of freedom that come with using a higher-degree polynomial. These response surfaces fail realistic rolling mill constraints, namely, a good model has a increase in rolling load for decrease in *gap*, which is consistently violated with the use of a quadratic model for h_{ef}.
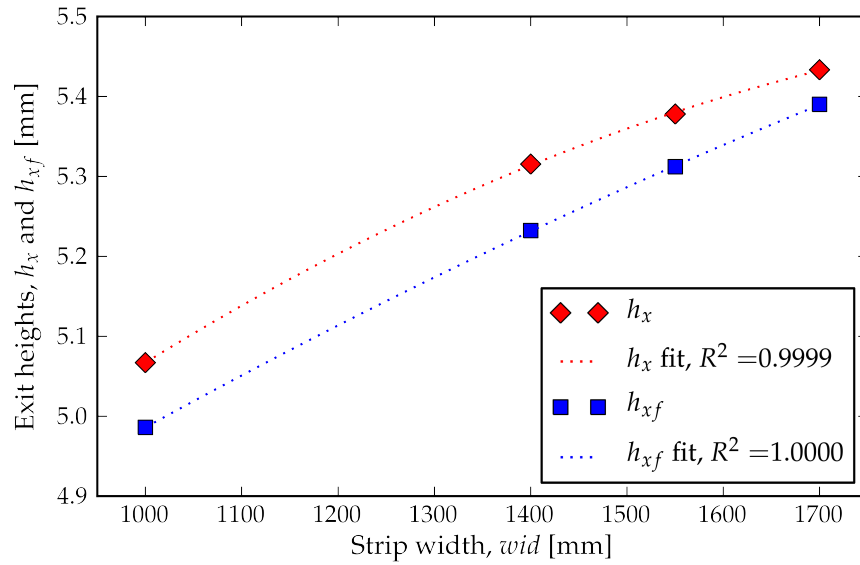
Figure 6.8: Exit heights, h_x and h_{xf}, as a function of strip width, *wid*.
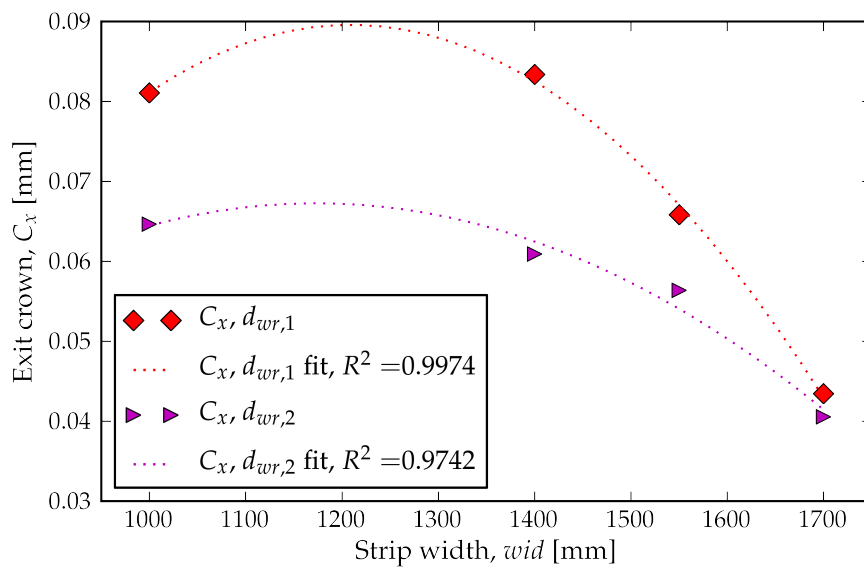
Figure 6.9: Exit crown, C_x, for two work rolls ($d_{wr,1} = 625$ [mm] and $d_{wr,2} = 775$ [mm]) as a function of strip width, *wid*.

Thus, the quadratic form requires the collection of three perturbations of entry height at the feather for each gap value on the response surface. Currently there are six different feather heights for three gaps, which are enough observations, but not the correct ratio.
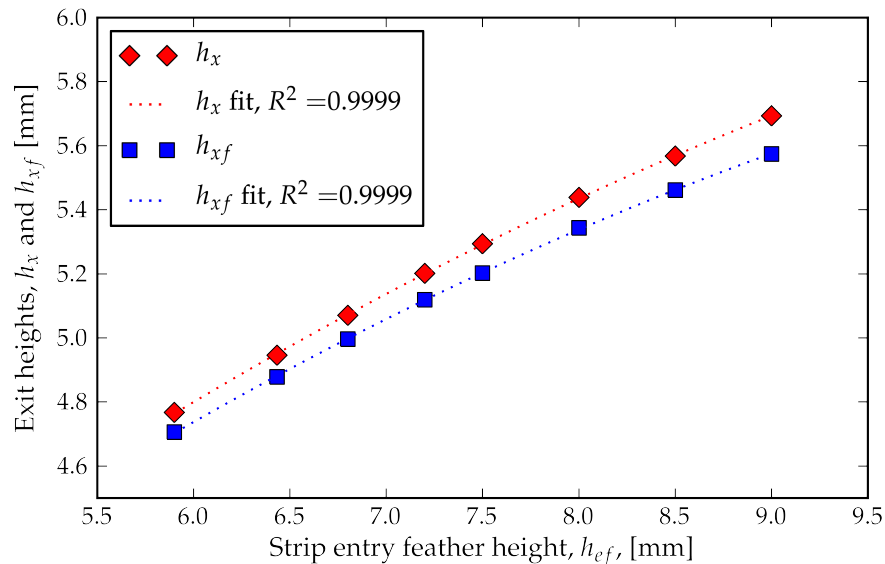
Figure 6.10: Exit heights, h_x and h_{xf}, as a function of entry height at the feather, h_{ef}.

The ratio of entry height at the feather to gap observations is not the only issue, an early 1-D projection for h_{ef} uses 4 observations: 5.9 [mm], 6.4337 [mm], 6.8 [mm], and 7.2 [mm]. The choice of any three of these four h_{ef} values does not provide enough curvature information to represent the quadratic correctly, but with h_{ef} sampled at 5.2 [mm], 7.2 [mm] and 9.2 [mm] curvature should be well represented. The same overlap in sampling is necessary at the other stand groups.

Additional studies of h_{ef} for stand group three and five confirm that h_{ef} has a quadratic form for the two exit height h_x and h_{xf}, but is also nearly linear in within a narrow range.

Until three perturbations of h_{ef} per *gap* with good separation in value are available, the response surface must be linear in h_{ef}. Square-root scaling, and logarithmic scaling options are also evaluated.

6.4.7 The Dependent Variable Functional Form for Strip Yield Strength

Figure 6.11 shows that both strip exit heights h_x and h_{xf} have a quadratic relationships with a moderately good R^2 (≥ 0.998) for strip yield strength, S_y. The two signal-to-noise ratios are 27.72 for strip centerline height, h_x, and 26.20 for strip exit height at the feather, h_{xf}.
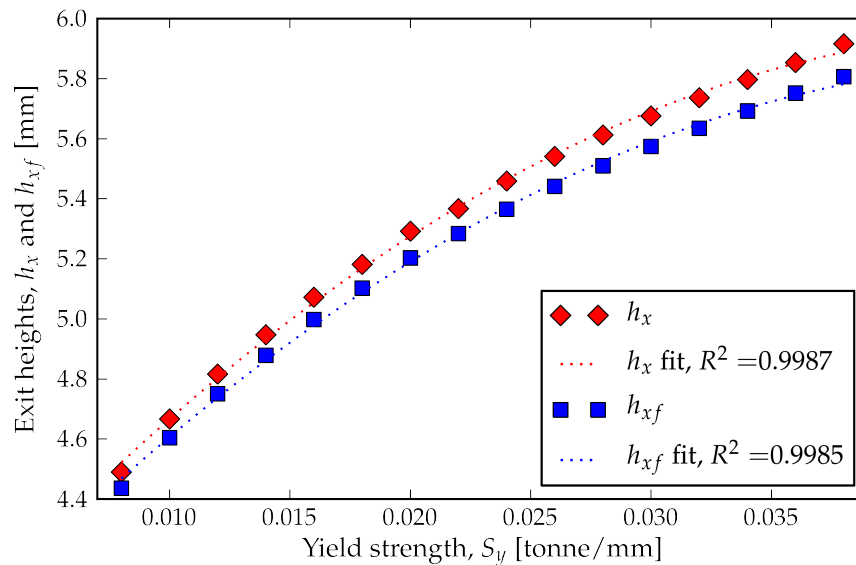
Figure 6.11: Exit heights, h_x and h_{xf}, as a function of strip yield strength, S_y.

This set of 16 observations are made after the first response surface comparison with the production model where it is determined that any valid model must have a positive change in strip exit crown for any increase in yield strength under the same conditions. This is not the case when observations with too short a run time multiplier of 3.0 are included in the response surface. Response surfaces run times for 6.4 [mm] strip have to be greater than 3.0.

The eventual determination is that in the narrow range of yield strengths, S_y, collected for each stand group a linear model for S_y works. A linear model on just the first four observations has a good R^2 of 0.9956 for h_x and 0.9964 for h_{xf} along with signal-to-noise ratios between 15 and 17. These numbers improve when the natural coordinate, S_y, is scaled by the square root first, I.E. $\widehat{S_y} = \sqrt{S_y}$. A linear model with square root scaling on the first four observations has a excellent R^2 of 0.9994 for h_x and 0.9997 for h_{xf} along with signal-to-noise ratios of 39.67 and 54.50 respectively.

The expansion of the response surface beyond stand group seven takes precedence over collecting 3 changes in S_y (Section 6.2), so a linear model or a linear model with square-root scaling are the two candidate representations for S_y.

6.4.8   Independent Variables with a Linear Functional Relationship

Three of the independent variables, *gap*, J, and C_e have linear relationships with the both of the strip exit heights, h_x and h_{xf}. Figure 6.12 shows the linearity for *gap*; Figure 6.13 for

jacking load, J; and Figure 6.14 for entry crown, C_e. Gap has excellent R^2 values at 0.9996 for h_x and 0.9999 for h_{xf}. Jacking load has a mixed result of good for h_x with $R^2 = 0.9973$ and excellent for h_{xf} with $R^2 = 0.9999$. While strip entry crown, C_e, has a good R^2 value for h_x at 0.9945 and poor for h_{xf} at 0.9552, which is consistent with both of the SNR values being under 20.00. Studies of additional samples from stand group 3 support the choice of a linear form for variables J and C_e. Additional samples for *gap* are not collected.
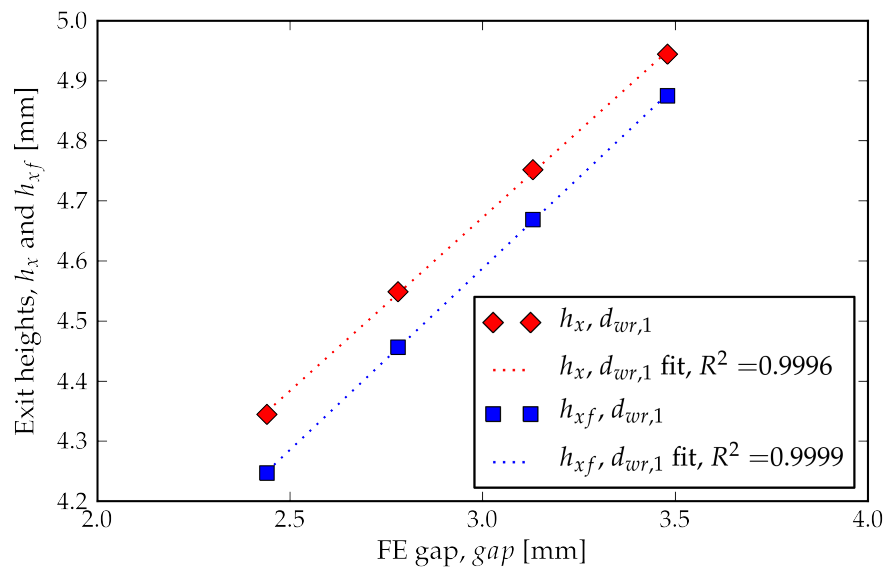
Figure 6.12: Exit heights, h_x and h_{xf}, as a function of stand gap, *gap*.

Strip centerline exit height, h_x, changes about 0.05 [mm] for the changes in *gap* and h_x changes about 0.01 [mm] over the range C_e changes. Strip entry crown, C_e, would need to change 0.17 [mm], instead of its current 0.05 [mm] range, to get h_x to change 0.05 [mm]. This should also increase the SNR for C_e and potentially correct problems on the response surface with C_e for the stand groups one, three and five, which have in many instances smaller changes in C_e. The minimum change in C_e should be different for stand group one, three and five due to different stand group sensitivities. Section 6.7 covers this in more detail.

6.4.9 The Dependent Variable Functional Form for Work Roll Crown

The inclusion of strip velocity in the one-dimensional projections for the work-roll crown, C_{wr}, is accidental, but additional observations are generated with the correct velocity in addition to the observations made with stand one and stand five strip velocities. Perturbations of
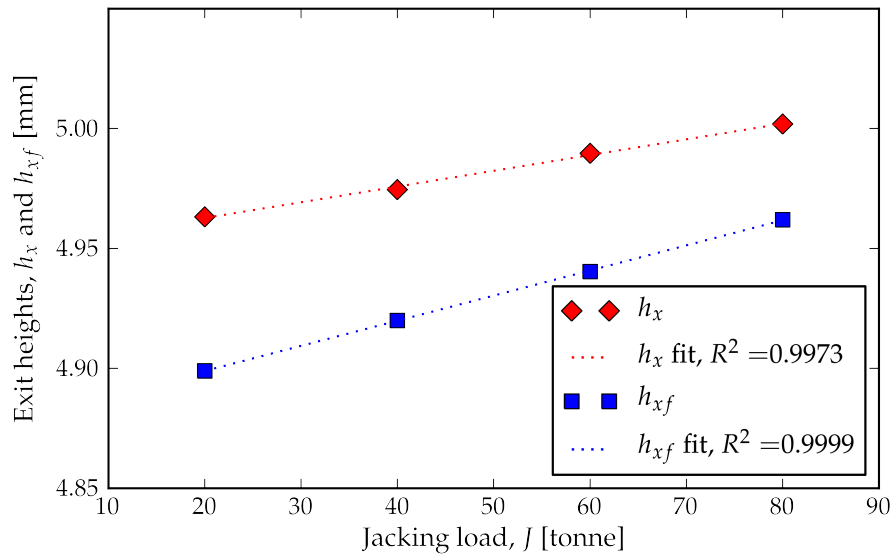
Figure 6.13: Exit heights, h_x and h_{xf}, as a function of jacking load, J.
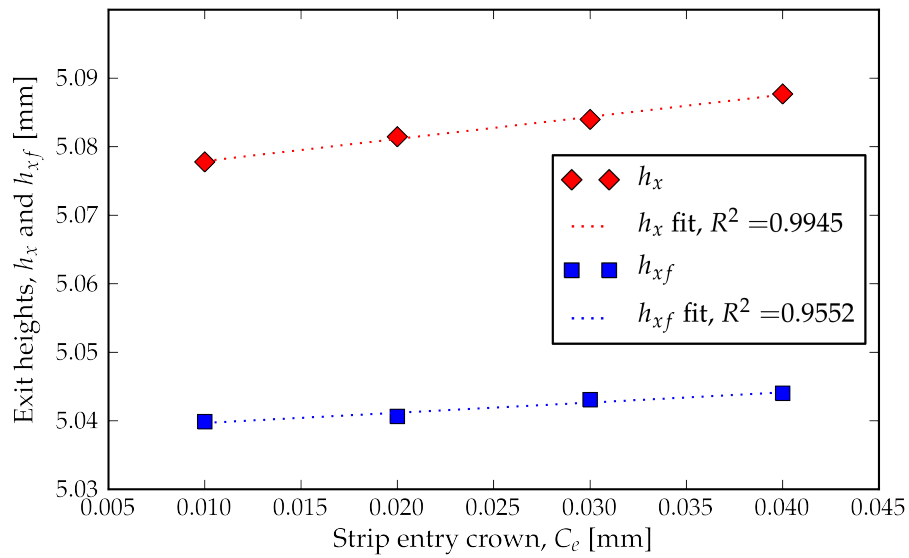
Figure 6.14: Exit heights, h_x and h_{xf}, as a function of entry crown, C_e.

the work-roll crown indicate that as strip velocity increases there is an decrease in strip height. According to Shahani *et al.*[18] increasing the work roll speed increases force and strain hardening because of the increase in strain rate, but strain-rate effects are not part of the elastic-plastic material model currently in use, so the only result is the decrease in exit height with the increase in rolling load.
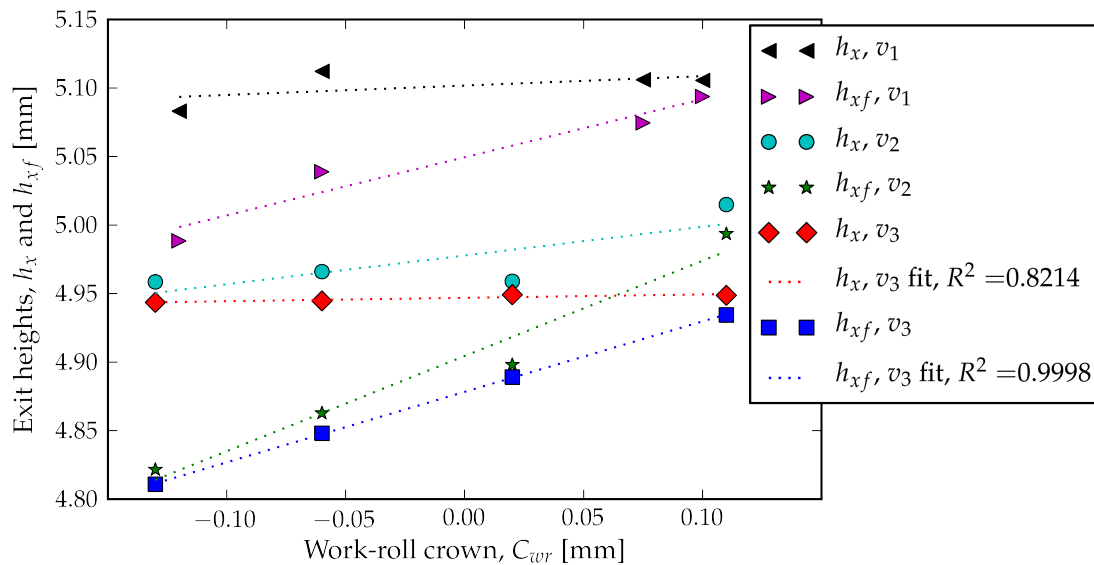
Figure 6.15: Exit heights, h_x and h_{xf}, as a function of work-roll crown, C_{wr}.

Figure 6.15 shows that both exit heights have a linear relationship. Exit height at the feather, h_{xf}, has a excellent R^2 value of 0.9998, while the R^2 value for exit height at the centerline, h_x is quite poor at 0.8214. The poor R^2 value for h_x has support with the SNR of 2.37, since a SNR ratio greater than 10.00 is required to see a R^2 greater than 0.9 based on Table 6.6. Figure 6.15 shows that h_x has very nearly a zero slope, which is equivalent to having nearly no signal.

The results for a second study at stand 7 has a R^2 value of 0.0139 for h_x again has nearly a zero slope, but a R^2 value of 1.000 for h_{xf}. However, studies at stand five and stand three clearly indicate a quadratic model for C_{wr}. The linear R^2 value of 0.9956 for h_{xf} at stand 5 changes to 0.9993 for a quadratic model, but there is no improvement of the R^2 value for h_x for either the linear or quadratic model. The stand three quadratic model R^2 values are 0.9995 for h_x and 0.9999 for h_{xf} compared to the R^2 values of the linear model of 0.9771 for h_x and 0.9981 for h_{xf}. Although, a linear models works relatively well, the best model will be quadratic for both the strip exit widths, h_x and h_{xf}.

Unlike the strip exit heights h_x and h_{xf}, a linear model for strip exit crown seen in Figure 6.16 shows an excellent R^2 statistic of 0.9995 for $C_{x,1}$ (C_x) and 0.9994 for $C_{x,2}$. $C_{x,2}$ is found using polynomial regression of the strip cross-section in the $x - y$ plane and it is used an

independent measure of strip exit crown. $C_{x,1}$ or C_x is computed using Equation 5.2. $C_{x,2}$ is only a comparable to $C_{x,1}$ at the finishing stands because the high forces found at the early stands create strip deformations beyond the wid_{fea} measurement.
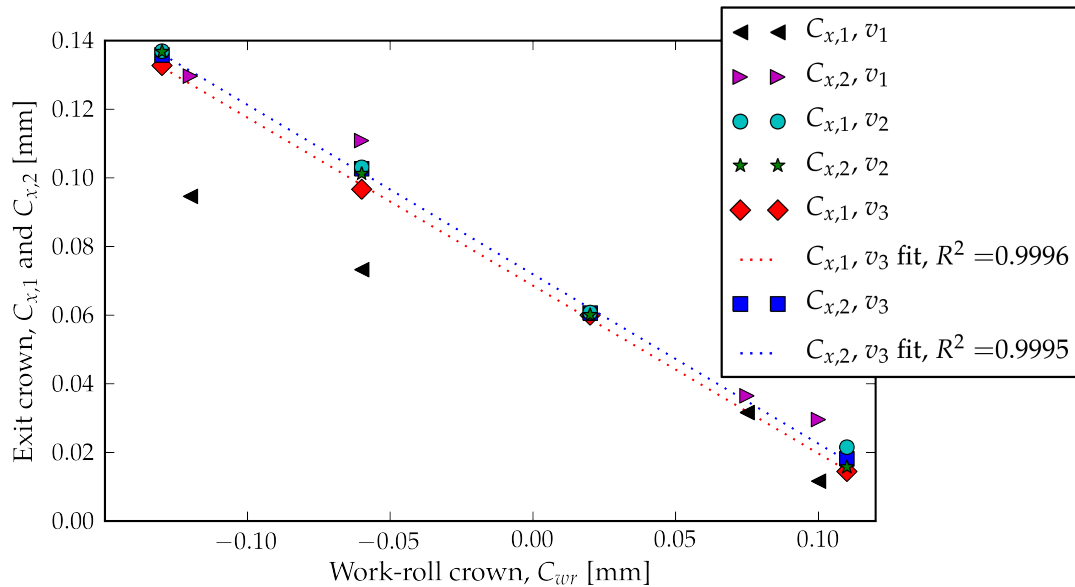
Figure 6.16: ,
$v_2 = 4018$ [mm/s], and $v_3 = 6753$ [mm/s].]Strip exit crown, $C_{x,1}$ and $C_{x,2}$ (parabolic fit), as a function of work-roll crown, C_{wr}, for strip velocities $v_1 = 1284$ [mm/s], $v_2 = 4018$ [mm/s], and $v_3 = 6753$ [mm/s].

The C_{wr} study at stand group three for the C_x variable can be either represented as a linear ($R^2 = 0.9998$) or quadratic ($R^2 = 1.0000$) model. This trend does not hold up for stand 5 where the linear model has $R^2 = 0.9676$ and the quadratic model has $R^2 = 0.9815$. The quadratic model has the better fit overall.

One note on the strip velocities v_1 and v_2, because the meshing does not change, the reduction in velocity at v_1 and v_2 results in fewer data points for the strip exit height steady-state determination. A change in model mesh parameters is required to maintain the same number of data points and without this change more variation in strip exit height is expected. Therefore, there are not any fit statistics for the v_1 and v_2 plots. These values are presented to demonstrate the effect for strip velocity only.

Quadratic is the preferred model for the C_{wr} variable, but a linear model is used on the response surface due to limitations on the perturbations of C_{wr}.

6.5   2-D Study for Backup-roll Diameter

6.5.1   The Dependent Variable Functional Form for Backup-Roll Diameter

A combination of the small effect of backup-roll diameter, d_{br} and many contradictions in the expected trend make the backup roll a difficult study for 1-D projections. The R^2 for a linear model is less than 0.9 and the SNR is only occasionally greater than 10 (see Table 6.8). Visually a quadratic form works with strip exit crown, C_x, where C_x increases as d_{br} increases from 1400 [mm] to 1550 [mm], but in about 50 percent of the cases viewed, C_x begins to decrease below the maximum C_x as d_{br} continues to increase. The large variance in the final exit height from the steady-state determination compared to the small effect of backup-roll diameter is potentially a factor responsible for this.

Table 6.8: Backup-Roll Diameter SNR and R^2 Study for Stand Group 5 for a 1-D Linear Model

d_{wr} [mm]	wid [mm]	C_x SNR	C_x R^2	h_x SNR	h_x R^2	h_{xf} SNR	h_{xf} R^2
625.00	1200.00	1.00	0.0043	4.43	0.9491	4.04	0.9388
775.00	1200.00	1.11	0.1850	19.85	0.9975	2.25	0.8023
850.00	1200.00	10.51	0.9909	8.58	0.9864	9.14	0.9880
625.00	1400.00	1.01	0.0245	7.87	0.9839	5.20	0.9630
775.00	1400.00	3.06	0.8930	38.57	0.9993	7.37	0.9816
850.00	1400.00	7.40	0.9818	5.54	0.9674	6.28	0.9747
625.00	1700.00	2.07	0.7674	2.28	0.8073	1.75	0.6726
775.00	1700.00	1.43	0.5094	10.06	0.9901	11.52	0.9925
850.00	1700.00	6.27	0.9746	8.44	0.9860	8.21	0.9852

Three effects are present for a fixed work-roll diameter, d_{wr} and a changing backup-roll diameter. There are effects due to the backup-roll diameter being varied, effects due to work roll and strip contact deformation and effects due to backup roll and work roll contact deformation. A 2-D study of d_{br} and d_{wr} should provide evidence to correlate a relationship of d_{br} and d_{wr} with C_x. The best correlation consistent with the prior studies is a quadratic relationship for work-roll diameter and linear one for backup-roll diameter.

Table 6.9 shows the individual results for the 2-D study of backup-roll diameter, d_{br}, and work-roll diameter, d_{wr}. Both strip exit heights h_x and h_{xf} in all seven studies have a R^2 greater than 0.997 and SNR greater than 20. Part of the reason of the excellent fit has to be attributed to the limited number of data points used – the number of degrees of freedom, $k = 6$, and the number of observations, $n = 9$. The degrees of freedom, $(n - k = 3)$, of the residual error are less than the number of degrees of freedom used in the fit ($k = 6$). Four or more observations are needed to correct this, but this is good evidence that backup-roll diameter needs to part of the response surface if work-roll diameter is modeled with a

quadratic polynomial.

Table 6.9: Backup-Roll Diameter SNR and R^2 Study for Stand Group 5 for the 2-D Model: $(c_1 d_{wr}^2 + c_2 d_{wr} + c_3)(c_4 d_{br} + c_5)$

Stand	wid [mm]	C_x SNR	C_x R^2	h_x SNR	h_x R^2	h_{xf} SNR	h_{xf} R^2
7	1000	11.68	0.9707	37.83	0.9972	36.63	0.9970
7	1400	6.70	0.9629	22.62	0.9967	26.20	0.9976
7	1550	4.51	0.8526	34.77	0.9975	29.37	0.9965
7	1700	3.64	0.7736	31.80	0.9970	49.73	0.9988
5	1200	3.23	0.7118	53.25	0.9989	37.99	0.9979
5	1400	3.88	0.8008	207.73	0.9999	130.41	0.9998
5	1700	19.34	0.9920	59.47	0.9992	47.84	0.9987

Figures 6.17 and 6.18 are contour plots of the strip exit crown, C_x as a function of backup-roll diameter, d_{br} and work-roll diameter, d_{wr}. The two stand 7 plots with $h_{ef} = 6.4$ [mm] and $gap = 3.48$ [mm] on the left in Figures 6.17 and 6.18 have similar contours. The two stand plots with $h_{ef} = 10.26$ [mm] and $gap = 5.43$ [mm] on the right in Figures 6.17 and 6.18 have similar contours. Although, both the stand 7 and stand 5 plots have denser contours for the strip width of 1700 [mm] seen in Figure 6.18.
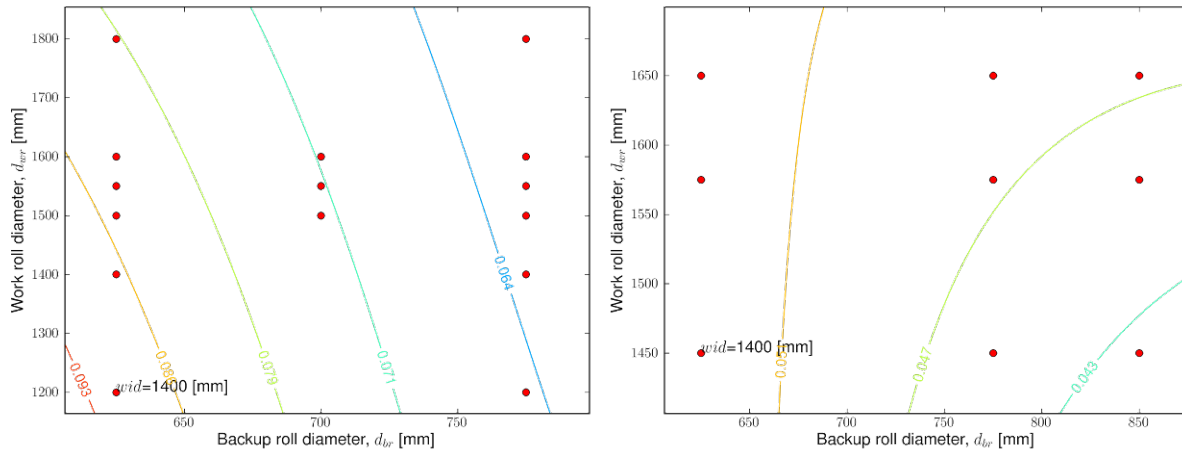
Figure 6.17: Side-by-side plots of strip exits crown, C_x as a function of backup-roll diameter, d_{br} and work-roll diameter, d_{wr}.

A linear polynomial order in d_{br} is the best case for the response surface model currently available, but this is not possible in combination with a quadratic model in d_{wr}. The response surface (identifier 9-D in Table 6.10) is built with a linear backup-roll diameter and linear work-roll diameter.
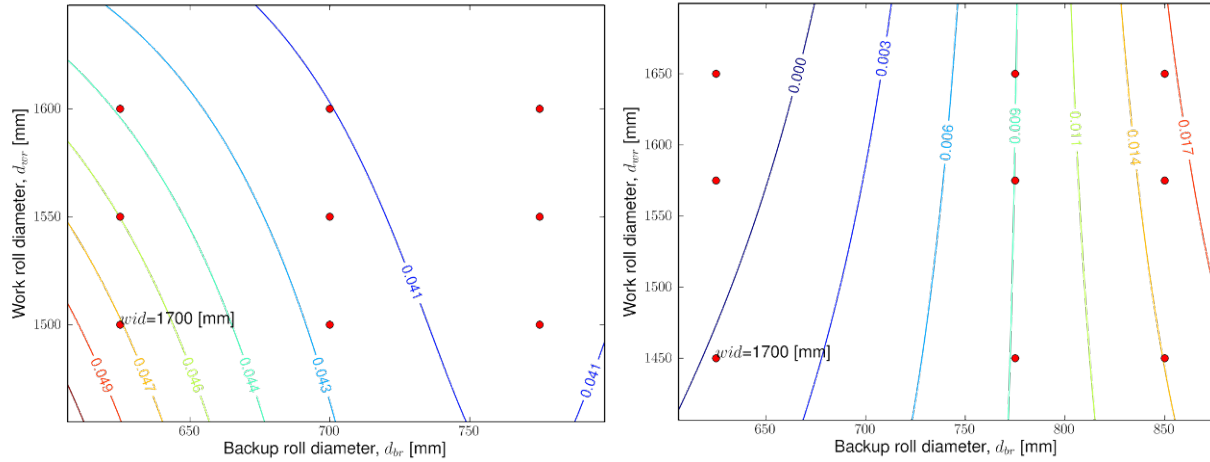
Figure 6.18: Side-by-side plots of strip exits crown, C_x as a function of backup-roll diameter, d_{br} and work-roll diameter, d_{wr}.

6.6 Validating the Response Surface Model

6.6.1 Response Surfaces Under Consideration

This section goes into the analysis of variance procedure, the F-test performed on each response surface and the method used to select the final response surface. Table 6.10 lists the independent variable form of all of response surfaces considered in this section. The letter codes are: "L" for linear (2 nodes), "Q" for quadratic (three nodes) and "N/A" to indicate that this independent variable is not used in the model. Also, the functional form of any pre-scaling in use is included. All response surfaces use the same pool of 3112 observations.

Table 6.10: Response Surface Independent Variable Form and Identifier.

Independent Variable	Response Surface Identifier			
	9-D	**8-D V1**	**8-D V2**	**8-D V3**
h_{ef} form	L	L	L, $\sqrt{h_{ef}}$	L, $ln(h_{ef})$
gap form	L	L	L	L
wid form	L	Q	Q	Q
S_y form	L, $\sqrt{S_y}$	L, $\sqrt{S_y}$	L, $\sqrt{S_y}$	L, $\sqrt{S_y}$
d_{wr} form	L	L	L	L
C_e form	L	L	L	L
C_{wr} form	L	L	L	L
J form	L	L	L	L
d_{br} form	L	N/A	N/A	N/A

6.6.2   Response Surface Dependent Variable Input

The response surfaces built from the vectors $\{h_{x,obs}\}$, $\{h_{xf,obs}\}$ and $\{P_{obs}\}$ are based on n observations and k degrees of freedom. The response surface built from the vector $\{C_{x,obs}\}$ is based on $n + n$ observations with $2k$ degrees of freedom. This is because C_x is a derived value,

$$\{C_{x,obs}\} = \{h_{x,obs}\} - \{h_{xf,obs}\} \tag{6.35}$$

and because of this, C_x includes the error from both strip exit heights, so the weights are based on the inverse of the strip exit crown variance, $S_{cx}^2 = S_x^2 + S_{xf}^2$.

6.6.3   Statistics Supporting the Functional Form Chosen

The response surface nodal values for exit height at the centerline, $\{h_{x,k}\}$, strip exit height at the centerline, $\{h_{xf,k}\}$, rolling load, $\{P_k\}$, and strip exit crown, $\{C_{x,k}\}$, are used to calculate the residuals for each dependent variable with (using h_x as an example),

$$\{r\} = \left([\Phi]_{(n \times k)}\{h_{x,k}\}_{(k \times 1)} - \{h_{x,obs}\}_{(n \times 1)}\right) \tag{6.36}$$

where $[\Phi]$ is the concatenation of n tensor products, and $\{h_{x,obs}\}$ is the vector of h_x values for n observations.

Allowing for the k degrees of freedom in the model ($2k$ for $\{C_x\}$), the sample variance [15] is defined as,

$$S^2 = \frac{\{r\}^T\{r\}}{n - k} \tag{6.37}$$

.

The following statistics are calculated from the residuals, $\{r\}$, and for comparisons to other models:

- The error mean provides an indication of how much bias is in the solution due to a lack of fit.

- The minimum and maximum of the error provides an indication of how large the potential outliers are.

- The standard deviation of the error, S, which if small compared to the mean value of the dependent variable, is an indication of a good fit.

- The ANOVA ratio, calculated as,

$$F_{\alpha,k-1,n-k} = \frac{SSR/(k-1))}{SSE/(n-k)} \tag{6.38}$$

     where SSR is the mean square regression, and SSE is the mean square residual. If $F_{\alpha,k-1,n-k} > F_{1\%,511,2344} = 1.0$ then reject the Null hypothesis, $h_{x,k} = h_{x,constant}$ [15] (the nodal values are equal to a constant).

- The signal-to-noise ratio, SNR, is defined in Equation 6.34. The signal power is derived from the vector of dependent variable values and the noise is derived from the residuals. The SNR provides a indication of how much influence the noise has on the response surface.

- The signal to noise ratio in decibels, [dB], provides the same information as SNR only in a new unit,

$$SNRdb = 20log_{10}(SNR) \tag{6.39}$$

- The condition number of the regressor matrix, $[\Phi]^T[\mathbf{W}][\Phi]$, which provides an indication of whether or not selected parts of the response surface are poorly represented. The condition number is the ratio of the largest and smallest eigenvalues of the regressor matrix,

$$C = \frac{\lambda_{k-1}}{\lambda_0} \tag{6.40}$$

where the vector of eigenvalues $\{\lambda\}$ is sorted in ascending order.

6.6.4   Response Surface Model Validation Criteria

Three criteria are used to pick the best response surface model:

1. The model with the best standard deviation of the error, S.

2. The model with the best standard deviation from cross-validating a set of observations not used in the weighted-least squares. Equation 6.36 is used to compute the residuals and most of the same statistics from the response surface creation. Using centerline exit height, h_x, as an example, the vector $\{h_{x,cross}\}$ is used in place of $\{h_{x,obs}\}$ in Equation 6.36 and $n = 1559$.

3. The final model must meet a sign constraint for the partial derivative of rolling load, P, with respect to *gap*, namely, that this partial derivative is negative.

The above criteria only selects the best model created. The next subsection goes into how to identify which variables do not contribute to the model.

6.6.5   Response Surface ANOVA Results

The ANOVA results for the four response surfaces are compared in Table 6.11. Both of the strip exit heights $h_{x,RS}$ and $h_{xf,RS}$ have the better ANOVA results compared to $C_{x,RS}$, so strip exit crown, C_x, calculated from Equation 5.3 is the better model than using $C_{x,RS}$. Also, the 8-D models created without the backup-roll diameter, d_{br}, overall have a better ANOVA statistics than the 9-D model. The 8-D V2 model is the best model based on the ANOVA statistics; but both 8-D V2 and 8-D V3 models violate the sign criteria for the partial derivatives of rolling load with respect to gap.

Table 6.11: Response Surface ANOVA Summary, $F_{\alpha,k-1,n-k}$.

R.S. Id	$\mathbf{C_{x,RS}}$	$\mathbf{P_{RS}}$	$\mathbf{h_{x,RS}}$	$\mathbf{h_{xf,RS}}$
9-D	1,084.52	10,193.19	87,648.83	90,699.32
8-D V1	2,243.42	17,666.78	198,014.64	204,825.39
8-D V2	2,243.06	31,715.01	495,644.49	561,269.58
8-D V3	1,741.19	6,221.42	106,003.81	116,227.20

6.6.6 Independent Variable Significance Testing with the ANOVA Statistic

The analysis of variance performed here involves creating a "reduced" model with one of the independent variables omitted from the 9-D response surface. Table 6.12 shows the evolution for the "reduced" response surfaces for the first five variables in Table 6.10. The response surface is built with the same 3112 observations and the same statistics are generated as the 9-D model.

Table 6.12: 9-D Response Surface Progression for the First Five Variables for "Reduced" 8-D Model Used in ANOVA Testing.

Independent Variable	Original 9-D	"Reduced" 8-D -Variable				
		8-D $-h_{ef}$	**8-D** $-gap$	**8-D** $-wid$	**8-D** $-S_y$	**8-D** $-d_{wr}$
h_{ef} form	L	N/A	L	L	L	L
gap form	L	L	N/A	L	L	L
wid form	L	L	L	N/A	L	L
S_y form	L $\sqrt{S_y}$	L $\sqrt{S_y}$	L $\sqrt{S_y}$	L $\sqrt{S_y}$	N/A	L $\sqrt{S_y}$
d_{wr} form	L	L	L	L	L	N/A
C_e form	L	L	L	L	L	L
C_{wr} form	L	L	L	L	L	L
J form	L	L	L	L	L	L
d_{br} form	L	L	L	L	L	L

The 8-D ANOVA summary for these nine reduced models are summarized in Table 6.13. The 8-D "Reduced" ANOVA result will be less than the 9-D ANOVA values in Table 6.11 row 9-D, if that variable is significant. There are four independent variables, C_e, d_{br}, C_{wr}, and J, that show a improved fit for the dependent variables P, h_x, and h_{xf} when dropped from the model. The 8-D V1, 8-D V2 and 8-D V3 response surfaces are created without backup-roll diameter, d_{br}, based on the poor d_{br} ANOVA results, the F-test result for d_{br} and the poor SNR for d_{br} in the 1-D projections.

Table 6.13: ANOVA, $F_{\alpha,k-1,n-k}$, Summary for 8-D "Reduced" Response Surfaces.

Variable removed	$\mathbf{C_{x,RS}}$	$\mathbf{P_{RS}}$	$\mathbf{h_{x,RS}}$	$\mathbf{h_{xf,RS}}$
$-gap$	664.37	1,437.21	5,178.07	4,879.71
$-wid$	265.44	1,584.43	34,147.48	29,027.55
$-d_{wr}$	1,060.93	4,350.46	65,296.41	61,223.16
$-C_e$	1,393.80	14,068.77	136,900.00	146,369.90
$-d_{br}$	2,038.49	21,909.80	194,778.44	201,579.51
$-C_{wr}$	86.53	17,902.44	171,619.65	156,425.77
$-J$	260.90	12,267.15	136,578.85	108,999.86
$-S_y$	584.50	916.36	11,360.80	12,088.16
$-h_{ef}$	158.37	399.23	371.18	374.66

6.6.7 Response Surface F-test Results

The original 9-D and "reduced" 8-D models are also used in a F-test. The Null hypothesis is that S^2 from the 9-D model is equal to S^2 from the "reduced" 8-D regression. The F-statistic is calculated with

$$F_{\alpha,a,b} = \frac{S_a^2}{S_b^2} \tag{6.41}$$

where α is the significance level (0.05), a is the number of degrees of freedom for the 9-D model ($a \geq 120$ or ∞), b is the number of degrees of freedom for the 8-D model ($b \geq 120$ or ∞) and S_a^2 and S_b^2 are sample variances for the 8-D "reduced" and 9-D model respectively [3, 15].

The F-test results are summarized in Table 6.14 and again they show that d_{br} does not contribute significantly to the strip crown model over this range of independent variables. The ANOVA test suggests that the significance of C_e, C_{wr} and J are questionable; however, the F-test identifies that just d_{br} is a superfluous variable.

Table 6.14: F-test Ratios between 9-D and 8-D "Reduced" Response Surfaces.

Variable removed	$\mathbf{C_{x,RS}}$	$\mathbf{P_{RS}}$	$\mathbf{h_{x,RS}}$	$\mathbf{h_{xf,RS}}$
$-gap$	3.13	14.04	34.89	38.35
$-wid$	7.98	12.78	5.13	6.24
$-d_{wr}$	2.03	4.67	2.68	2.96
$-C_e$	1.56	1.45	1.28	1.24
$-d_{br}$	1.07	0.93	0.90	0.90
$-C_{wr}$	24.02	1.14	1.02	1.16
$-J$	8.26	1.66	1.28	1.66
$-S_y$	3.56	21.42	15.24	14.83
$-h_{ef}$	11.10	49.83	395.43	405.70

6.6.8 Final Response Surface Model

The F-test and ANOVA results clearly indicate that the linear functional form for backup-roll diameter, d_{br}, does not significantly contribute to the crown model, at least with a linear work-roll diameter, d_{wr}. The final response surface is at least quadratic in width based on the 1-D studies and confirmed in the response surface statistics.

The square-root pre-scaling of yield strength, S_y, improved the original 9-D all linear model, so it is kept in a second round of response surface tests with the other candidate 8-D models: *8-D V1*, *8-D V2* and *8-D V3*. The first candidate is *8-D V1* with strip entry height at the feather, h_{ef}, with a linear relationship to the dependent variables. The remaining candidates are based on the preferred model for h_{ef}, being a quadratic form, so the square root (the *8-D V2* response surface) and the natural log (the *8-D V3* response surface) are also candidate response surfaces.

The final response surface model meeting all three selection criteria is quadratic in width with square root scaling of S_y. Two other models that include the square-root or the natural-log pre-scaling of h_{ef} did much better on the least squares statistics, and about the same for the cross-validation, but failed the negative sign constraint for the partial of rolling load with respect to gap by a large margin (91% positive for square root scaling of h_e and 70% positive for natural log scaling for h_e). Table 6.15 summaries the three criteria used to pick the final response surface model.

Table 6.15: Four Responses Surfaces Comparisons using Standard Deviations from Cross Validation and Weighted Least Squares and the Rolling Load Partial.

	$\mathbf{P_{RS}}$		$\mathbf{H_{x,RS}}$		$\mathbf{H_{xf,RS}}$		
	Cross Val. S [tonne]	Least Squares S [tonne]	Cross Val. S [mm]	Least Squares S [mm]	Cross Val. S [mm]	Least Squares S [mm]	Derv. Sign Req.
9-D	128.09	25.57	0.1715	0.0507	0.1726	0.0493	
8-D V1	118.24	24.49	0.1418	0.0468	0.1461	0.0456	
8-D V2	120.18	18.27	0.1648	0.0296	0.1428	0.0275	fails
8-D V3	108.38	18.2	0.1765	0.0299	0.1542	0.0277	fails

6.6.9 Interpolation Coefficient Variance Calculation

An additional method to help validate the response surface, especially as new observations are added, is to calculate the variance for each of the response surface coefficients. The larger variances could be an indication that observations are needed there. The coefficient variance is calculated with

$$S_i^2 = R_{i,i} \, S^2 \tag{6.42}$$

where $R_{i,i}$ is the diagonal of the regressor matrix and S^2 is the sample variance [2]. Setting an arbitrary maximum variance threshold, 1.0×10^{-7} in Figure 6.19, is used to identify nodes numbers, i, with a potential problem. This allows focus to be placed on those nodes without enough observations.

Iteration for each ζ variable using Equation 6.4 as a guide to the number of nodes and sequence per dimension allows the isoparametric coordinate, $\{\zeta\}$, to be built as the index, i, is incremented. The natural coordinates can be calculated with Equation 6.22 to identify what regions are underrepresented when the maximum variance tolerance threshold is exceeded.

Figure 6.19 is a plot of the variance for each strip exit crown coefficient against the 9-D response surface node number, i. Stand group 1 observations ($h_{ef} > 35.0$ [mm]) show up as a potential problem and stand group 1 is under represented with observations, since only 6 percent of the observations planned for stand group 1 are included in the any of the response surfaces. Another group missing is made up of strip reduction values greater than 60%, which are undesirable to run. This occurs because, the range of gap values for stand group 1 requires widening in order to accommodate the range of gaps for stand group 5 and 7.
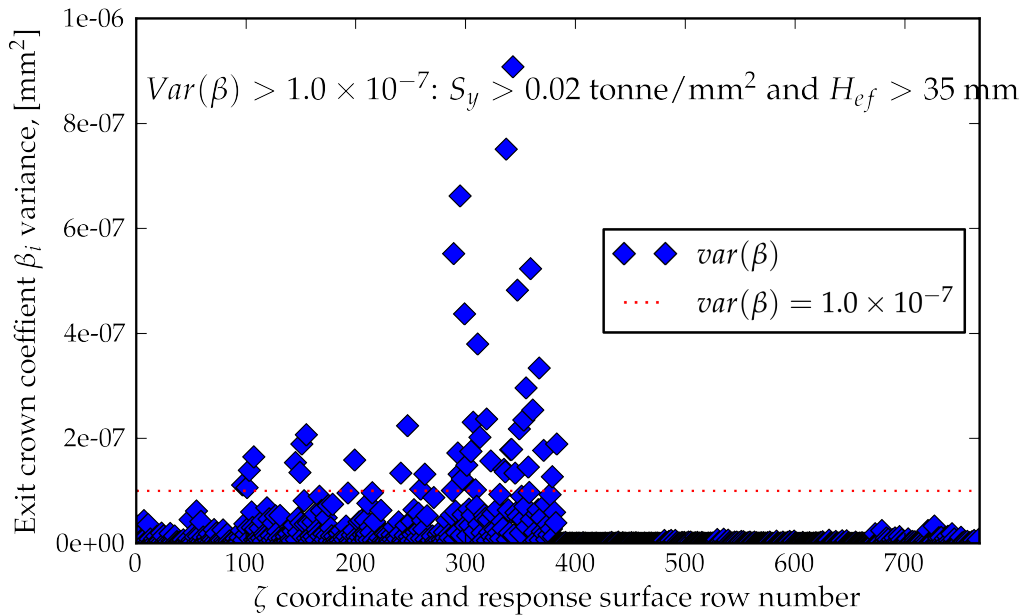
Figure 6.19: Plot of exit crown variance calculated from the regressor matrix against the response surface row number.

6.7 Response Surface and Production Model Comparisons

6.7.1 Exit Crown Prediction Models

Response-surface validation includes comparisons to a production crown model using plots of predicted strip exit crown as a function of a single independent variable with the remaining variables set to values consistent with one of the three stand groups. A comparison for the backup-roll diameter is excluded because it is not in the final model. There are three sources of strip exit crown values: the current production software (*Prod. model* in the figures), the original all linear 9-D response surface (*Lin 9D RS* in the figures), and the final 8-D response surface that is quadratic in width with square root scaling of S_y (*Quad 8D RS* in the figures). The same trends are expected to exist between the 8-D response surface and production models.

One complication in making the comparisons is that *gap* is needed for the response surface, but *gap* is not used as an input variable in the production software. The dependent variable reduction, Rx, is an input variable in the production software and in mill set up, so Rx replaces *gap* as an input variable. Reduction is calculated with

$$Rx = (h_e - h_{x,targ})/h_e \tag{6.43}$$

where $h_e = h_{ef} + C_e$ and $h_{x,targ}$ is the target centerline exit height.

A procedure is needed to search the response surface to find the natural *gap* value given a value for Rx. The other independent variables do not change while *gap* is changed to match the target Rx value. In general this procedure is:

1. Calculate the exit height required with $h_{x,targ} = (h_{ef} + C_e)(1.0 - Rx)$.

2. Estimate an initial natural *gap* value using a static force calculation and the known value for mill stretch, K_{std}.

$$gap = h_x - \frac{force(k, h_e, h_x, wid, d_{wr}, E, \nu)}{K_{std}} \tag{6.44}$$

   where k is $S_y/\sqrt{3}$, E is the work roll modulus of elasticity, ν is its Poisson's ratio and h_e is the centerline entry height.

3. Estimate the $\{\zeta\}$ vector using a simplified scaling of the natural variables with

$$\zeta_i = 2(x_i - avg_i)/rng_i \tag{6.45}$$

   where x_i is the natural value, avg_i is this variable's largest average value, and rng_i is the largest range.

4. Do a conjugate gradient search using the estimated natural *gap* and the other eight variables as the vector $\{\mathbf{x}\}$ in Equation 6.28, which returns the coordinate vector $\{\zeta\}$.

5. Interpolate the exit height, h_x, using the response surface and vector $\{\zeta\}$.

6. Calculate the partial derivative of the exit height, h_x, with respect to *gap*.

7. Use the simple linear approximation

$$gap = \alpha \frac{\partial h_x}{\partial gap} \Delta gap + gap_0 \qquad (6.46)$$

to estimate a new *gap* where gap_0 is the current estimate. The α parameter is used to control the size of the step in *gap* and picked manually to reduce the number of search iterations.

8. Test for a sufficient reduction in the error tolerance, $abs(h_x - h_{x,targ}) \leq tolerance$, and end the search if true, otherwise begin a new iteration at step 3.

9. Vector $\{\zeta\}$ now has the isoparametric response surface coordinates for the reduction requested.

A complication of the *gap* search is that the response surface result will often include a change in *gap* in addition to a change in the independent variable of interest. The effect is more pronounced for entry height at the feather. The approximate effect of changes in gap can be backed out using a linearized version of the exit crown equation:

$$C_x = C_{x0} + \frac{\partial C_x}{\partial x_i} \Delta x_i + \frac{\partial C_x}{\partial gap} \Delta gap \qquad (6.47)$$

where Δx_i is the change in the independent variable of interest relative to $x_{i,0}$, Δgap is the change in *gap* relative to gap_0, and C_{x0} is the only unknown. Solving for C_{x0} and re-calculating C_x with $\Delta gap = 0$

$$C_x = C_{x0} + \frac{\partial C_x}{\partial x_i} \Delta x_i \qquad (6.48)$$

provides an estimate of C_x without the change in *gap*.

Each independent variable comparison uses three plots from the three main stand groups simulated. Stand group 1 is omitted because there are not enough observations (see Figure 6.19) to make this region of the response surface reliable. Each stand group uses entry heights, entry crowns and yield strengths close to the nominal values used in the observations generated. This is done to avoid drawing conclusions based on extrapolation. Moving from stand 3 to stand 7 entry heights and strip crown decreases, while yield strengths increase. The range of independent variable values for each stand group are summarized in Table 6.16.

Table 6.16: Nominal Stand Group Variable Value Ranges.

Variable	3		5		7	
	Low	**High**	**Low**	**High**	**Low**	**High**
wid [mm]	1450	1700	1450	1700	1450	1700
h_{ef} [mm]	13.6	20.4	6.8	10.2	4.4	6.6
C_e [mm]	0.1398	0.2098	0.0720	0.1080	0.0389	0.0583
S_y [tonne/mm^2] $\times 10^2$	1.3260	1.9890	1.5378	2.3067	1.6949	2.5423
d_{wr} [mm]	625	850	625	850	625	850
C_{wr} [mm]	-0.10	0.05	-0.10	0.05	-0.10	0.05
d_{br} [mm]	1585.26	1585.26	1584.47	1584.47	1589.51	1589.51
Rx [mm/mm]	0.20	0.40	0.15	0.35	0.10	0.25
h_x [mm]	10.88	12.24	5.78	6.63	3.96	4.95
gap [mm]	10.210	10.210	5.430	5.430	3.983	3.983
J [tonne]	100.00	250.00	50.00	200.00	0.00	150.00

6.7.2   The Strip Exit Crown Model Comparison for Strip Width

Figure 6.20 shows that for strip width the quadratic response surface model (Quad 8-D RS) parallels the production model the best and the linear response surface does well, until a strip width of 1550 [mm]. The production model appears nearly linear, before and after the change in slope at 1550 [mm]. This change in slope occurs 35 to 40 [mm] before the backup roll edge. Neither response surface has any strip width information less than 1300 [mm], so the expected peak in strip exit crown, C_x, at around 1200 [mm] cannot be seen.

6.7.3   The Strip Exit Crown Model Comparison for Work Roll Diameter

Figure 6.21 compares the strip exit crown predictions as work-roll diameter changes. The production strip exit crown is clearly not linear, and shows that strip exit crown is directly proportional to work-roll diameter. Ginzburg [10] computes a linear ratio of change in exit crown to change in work-roll diameter,

$$K_{dw} = \frac{\Delta C_x}{\Delta d_{wr}} \tag{6.49}$$

and then plots K_{dw} against strip width and all of these finite differences are negative. The K_{dw} becomes more negative after the 1200 [mm] strip width crossing point. Corrected for changes in gap (R.S. gap const.), the final 8-D response surface predicts a negative slope for all three stand groups, while the linear model (9-D) only has a negative slope for stand group seven.
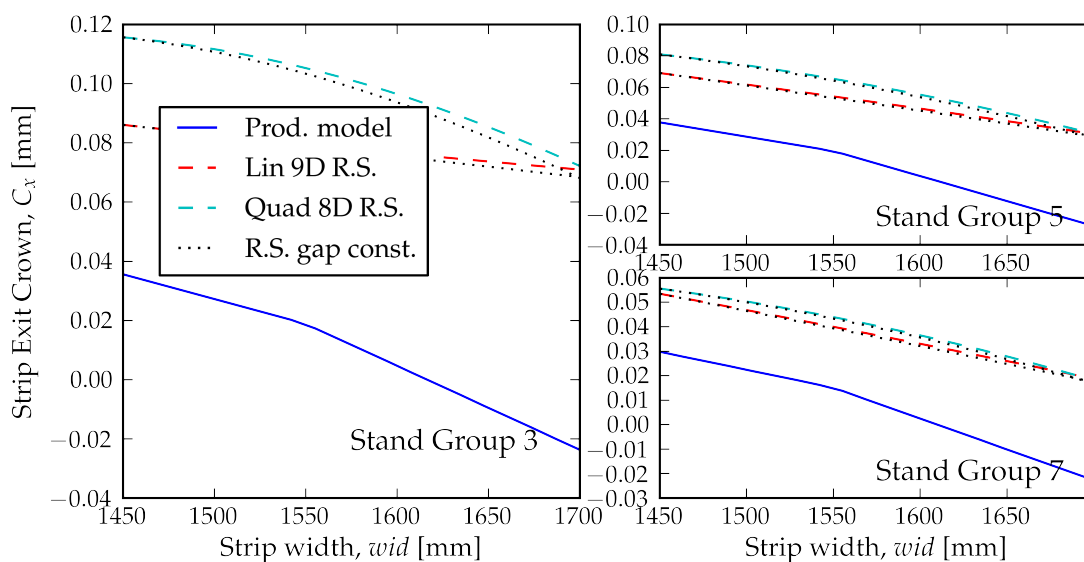
Figure 6.20: Strip exit crown comparison of the 8-D quadratic in width (Quad 8D R.S.) and 9-D all linear (lin 9D R.S.) response surfaces and production crown model for changes in strip width, *wid*, at all three stand groups. The dotted lines (R.S. gap const.) represent a estimate of crown if gap remains constant

Figure 6.21: Strip exit crown comparison of the 8-D response surface quadratic in width (Quad 8D R.S.), the 9-D linear response surface (lin 9D R.S.) and the production crown model for changes in work-roll diameter, d_{wr}, at all three stand groups. The dotted lines (R.S. gap const.) represent a estimate of strip exit crown if gap remains constant

6.7.4   The Strip Exit Crown Model Comparison for Entry Height at the Feather

Figure 6.22 shows that in both response surface models strip exit crown, C_x, have positive curvature, before eliminating the change in C_x due to changes in gap, compared to the production model with negative curvature. Since entry height at the feather, h_{ef}, is modeled as a linear dimension, the adjustment for change in gap produces much more linear curve. The response surfaces are restricted to linear form for strip entry height at the feather, h_{ef}. The quadratic trend in the production model for strip exit crown is more support a quadratic relationship between h_{ef} and the exit heights h_x and h_{xf}.

Figure 6.22: Strip exit crown comparison of the 8-D response surface quadratic in width (Quad 8D R.S.), the 9-D response surface (lin 9D R.S.) and the production crown model for changes in entry height at the feather, h_{ef}, at all three stand groups. The dotted lines (R.S. gap const.) represent a estimate of crown if gap remains constant

6.7.5   The Strip Exit Crown Model Comparison for Strip Yield Strength

Figure 6.23 shows that all three models predict increasing crown for increases in yield strength. The production model has a very linear relationship with exit crown, while both response surface models have visible curvature for stand group 3. This is due to the square root pre-scaling used for yield strength. Figure 6.24 shows the elastic-plastic yield curve used in all of the Abaqus simulations. The elliptical yield curve is similar in shape to the

Ramberg-Osgood curve provided for comparison. The equation for the elliptical yield curve is [21]

$$\sigma = b_{ell}\sqrt{1 - \left(\epsilon - \frac{S_y}{E} - \epsilon_{max}\right)^2 / \epsilon_{max}^2} + S_y \tag{6.50}$$

where ϵ_{max} is the maximum strain, $S_{y,mult}$ is a scaling factor, and $b_{ell} = \epsilon_{max}S_{y,mult} - S_y$. The equation for the Ramberg-Osgood [7] is

$$\epsilon = \frac{\sigma_y}{E} + \left(\frac{\sigma}{H}\right)^{1/n} \tag{6.51}$$

where E is modules of elasticity, H and n are a values found from fitting the empirical stress-strain data, which in this case are the data points from the elliptical stress-strain curve. A choice of a elastic linear-hardening stress-strain or elastic-perfectly plastic material model for the Abaqus simulations may produce a similar linear relationship for yield stress as seen in the production model.

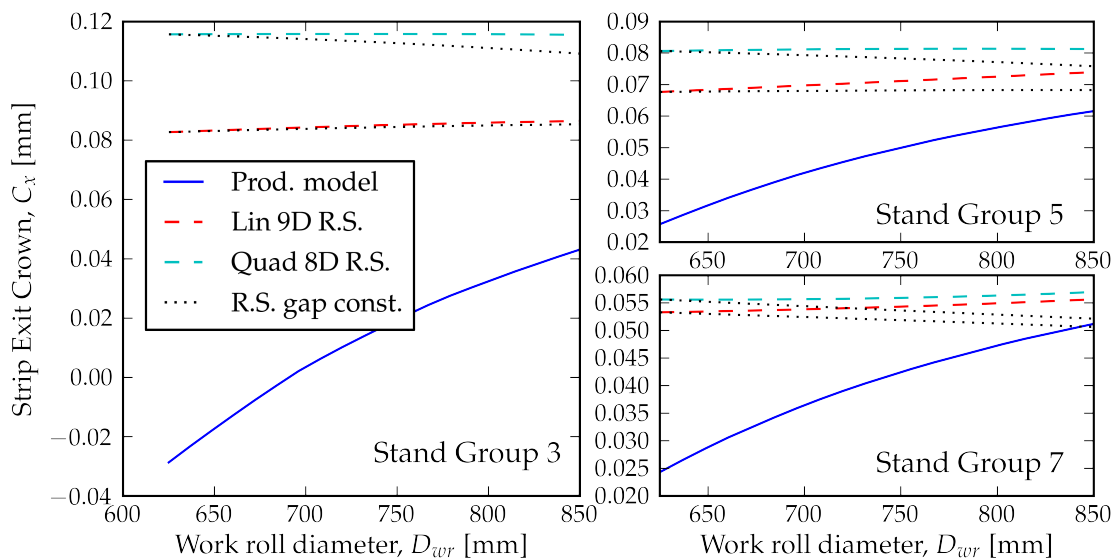

Figure 6.23: Strip exit crown comparison of the 8-D response surface quadratic in width (Quad 8D R.S.), the 9-D response surface (lin 9D R.S.) and production crown model for changes in strip yield strength, S_y, at all three stand groups. The dotted lines (R.S. gap const.) represent a estimate of crown if gap remains constant
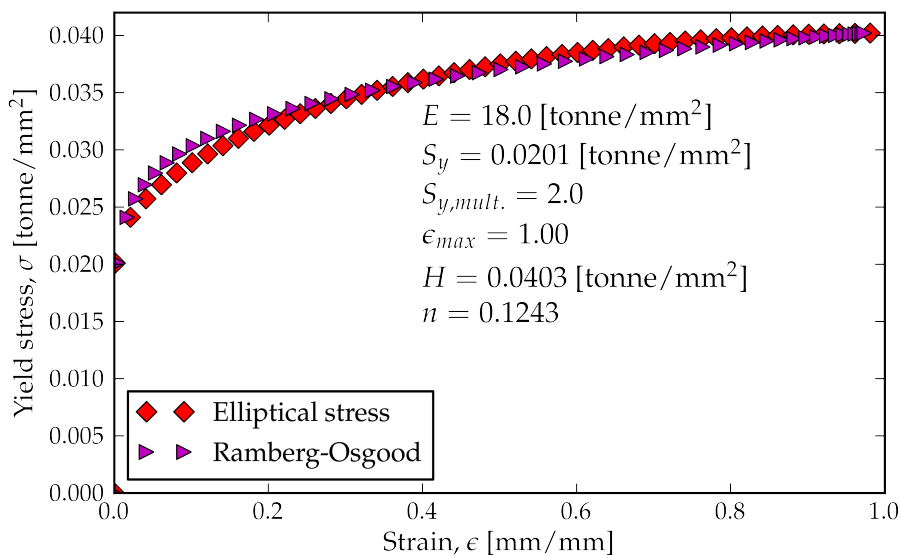
Figure 6.24: Simulation elastic-plastic elliptical yield curve and Ramberg-Osgood equivalent stress-strain curve.

6.7.6 The Strip Exit Crown Model Comparison for Stand Gap (Reduction)

Figure 6.25 shows that as gap decreases (reduction increases), both models see increases in strip exit crown and the trend for all three models is linear. The all linear (9-D) and quadratic (8-D) response surface models diverge a small amount at stand group 3 and 5, but remain parallel at stand group 7. The production model is more sensitive to reduction than the response surfaces are at stand 7.

6.7.7 Exit Crown Model Comparison for Jacking Load

Figure 6.26 for jacking load shows that all models agree as to the overall trend of the exit crown line, but not in the steepness of the slope. The two response surface models have less slope than the production model. This especially true of the quadratic in width model for stand groups 3 and 5. Additional evidence for the linear behavior for jacking load is found in *Roll Bending Methods of Control in Four-High Plate Mills* [20, 19].
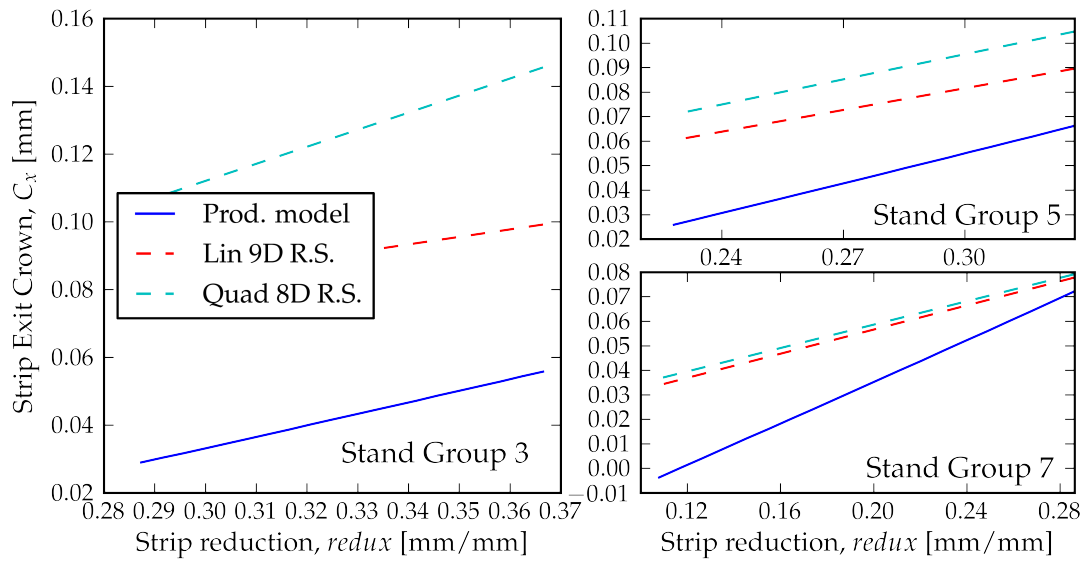
Figure 6.25: Strip exit crown comparison of the 8-D response surface quadratic in width (Quad 8D R.S.), the 9-D response surface (lin 9D R.S.) and the production crown model for changes in reduction, Rx, (gap) at all three stand groups.
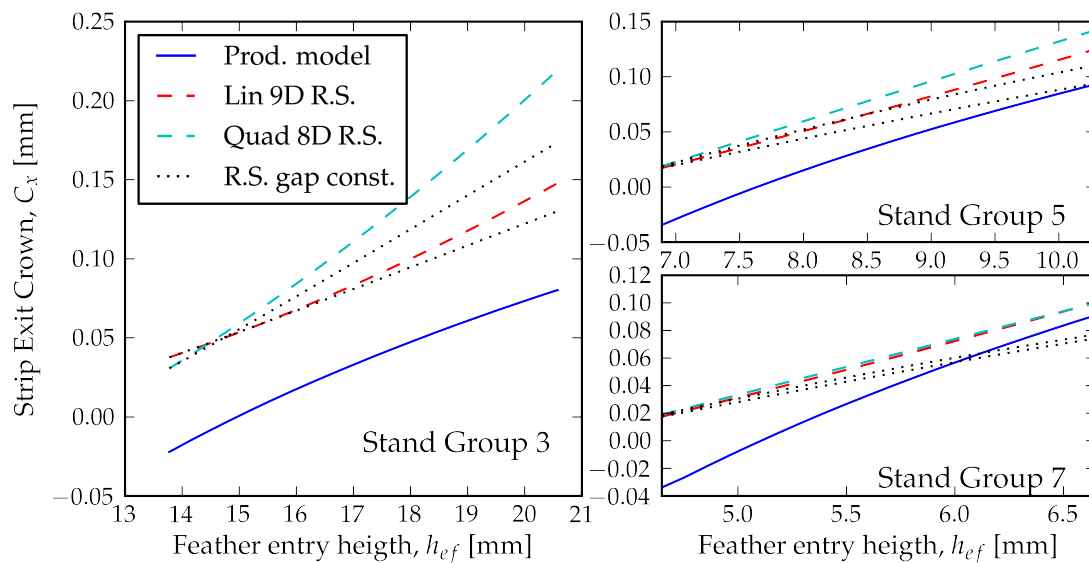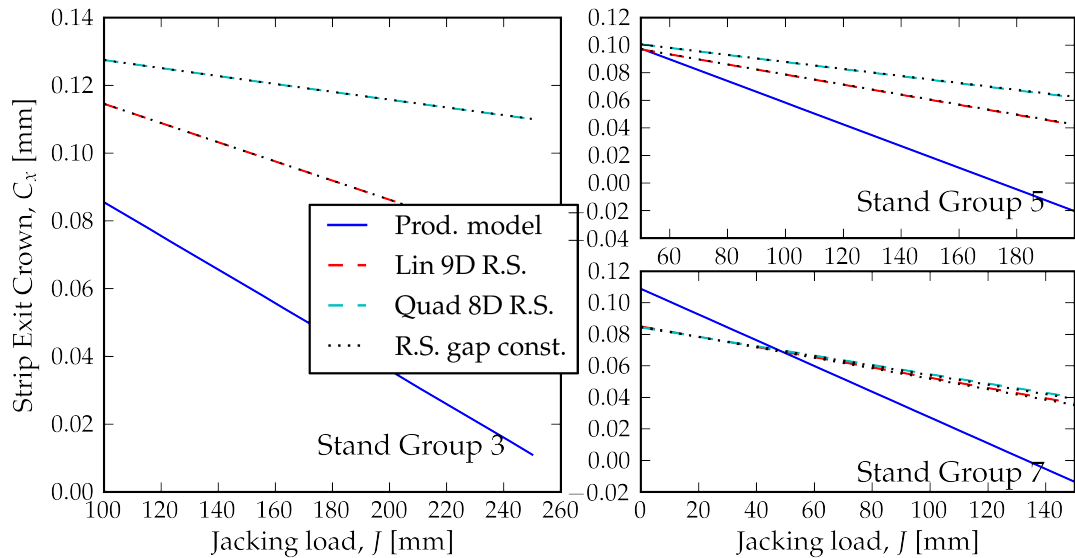

Figure 6.26: Strip exit crown comparison of the 8-D response surface quadratic in width (Quad 8D R.S.), the 9-D response surface (lin 9D R.S.) and the production crown model for changes in jacking load, J, at all three stand groups. The dotted lines (R.S. gap const.) represent a estimate of crown if gap remains constant

6.7.8   Exit Crown Model Comparison for Work Roll Crown

Figure 6.27 for work-roll crown shows an overall slope agreement, but the two response surfaces are slightly steeper in slope. Both response surface models over predict the strip exit crown, which is a consistent trend for all of independent variables with the possible exception of jacking load.
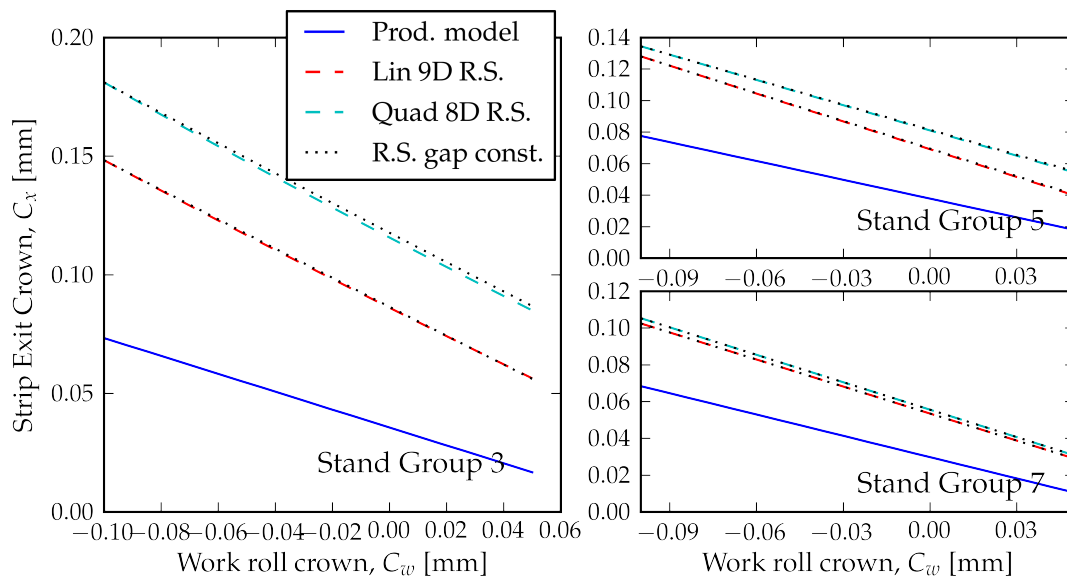
Figure 6.27: Strip exit crown comparison of the 8-D response surface quadratic in width (Quad 8D R.S.), the 9-D response surface (lin 9D R.S.) and production crown model for changes in work-roll crown, C_{wr}, at all three stand groups. The dotted lines (R.S. gap const.) represent a estimate of crown if gap remains constant

6.7.9   Exit Crown Model Comparison for Strip Entry Crown

Figure 6.28 for stand group 3 shows that both response surfaces predict less strip exit crown, C_x, as strip entry crown, C_e, increases in contradiction to the production model. The stand group 5 plot shows that the quadratic model agrees well with the production model, while the linear model expects strip exit crown losses when strip entry crown increases. All models agree for stand group 7 that strip exit crown is directly proportional to strip entry crown, but the linear 9-D model predicts less slope than the other two models.

Figure 6.29 starts at stand group 7 and varies h_{ef} with the ratio of h_{ef} to C_e held constant. A negative slope is expected when the response surface begins to break down. For strip reductions of 15 and 25 percent (ratios 0.15 and 0.25) and a S_y of 0.0212 [tonne/mm^2] the C_x trends are both good and the curves are both relatively flat, but for the same strip
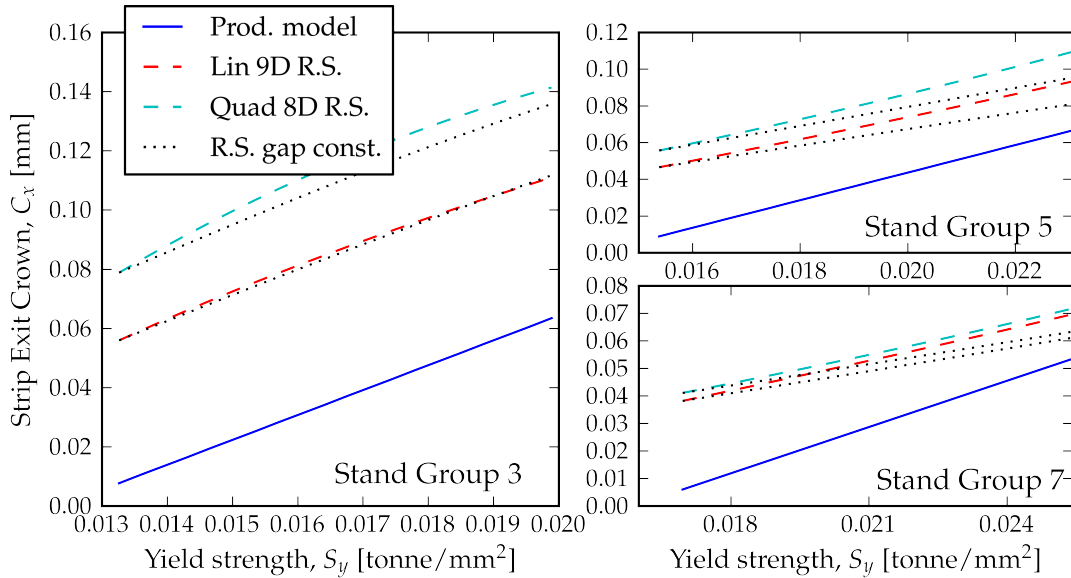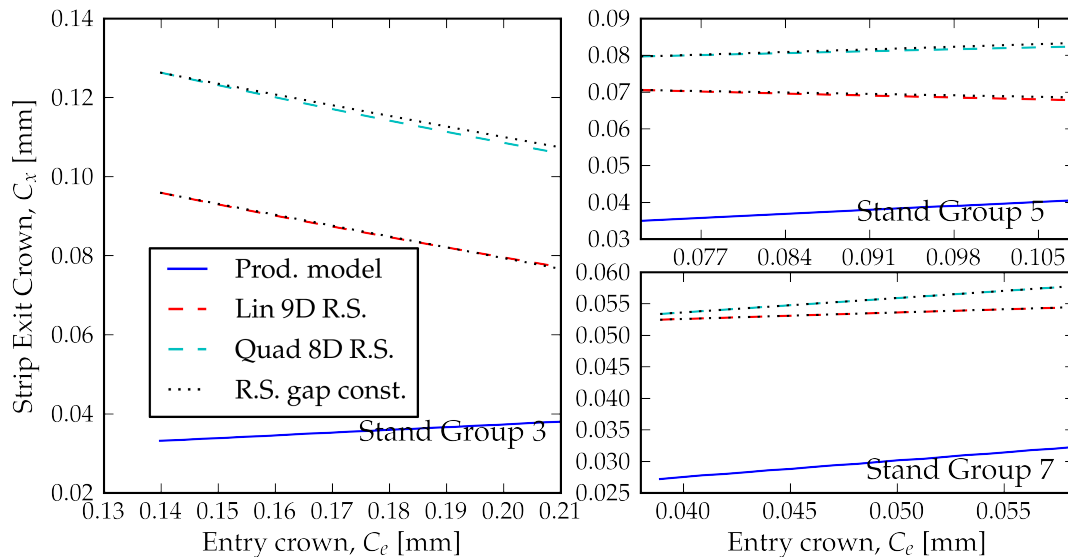
Figure 6.28: Strip exit crown comparison of the 8-D response surface quadratic in width (Quad 8-D R.S.), the 9-D response surface (lin 9-D R.S.) and the production crown model for changes in entry crown, C_e, at all three stand groups. The dotted lines (R.S. gap const.) represent a estimate of crown if the gap remains constant

reductions and a relatively soft, S_y of 0.0110 [tonne/mm^2], both C_x trends start off negative. Then the curve for a reduction of 25 percent takes an upturn into a positive slope before flattening out and approaching a slope of zero. The 15 percent reduction line takes the same upturn, but never goes very far with a positive slope before rolling off into negative values.

The use of a constant reduction as h_{ef} grows allows the gap variable to grow along with h_{ef}, which means the stand changes as h_{ef} changes. The two curves for the $S_y = 0.0212$ [tonne/mm^2] may become less steep as each one moves further away from the stand 7 "region", but neither one trends downward with a negative slope. The soft strip curve, $S_y = 0.0110$ [tonne/mm^2], starts as a problem at stand 7 and gets progressively worse, improves and then gets worse. The poor starting trend is likely due to the lack of S_y observations below 0.0212 [tonne/mm^2] in the stand 7 observations.

Noting that there is no reason to believe that a positive change in C_e will result in a negative change in C_x, all of the finite differences should be positive. The number of negative finite differences as a percentage is 1.7% for stand 7, 40.8% for stand 5 and 41.8% for stand 3. The small percentage of negative finite difference for the stand 7 data explains why starting with stand 7 nominal values and varying just one variable at a time (except *gap*), the plots have consistent trends and comparisons with the production model agree as to general trends.

Looking at stand groups 5 and 3 specifically ($h_{ef} > 7$ [mm] and $gap > 4$ [mm]), the response
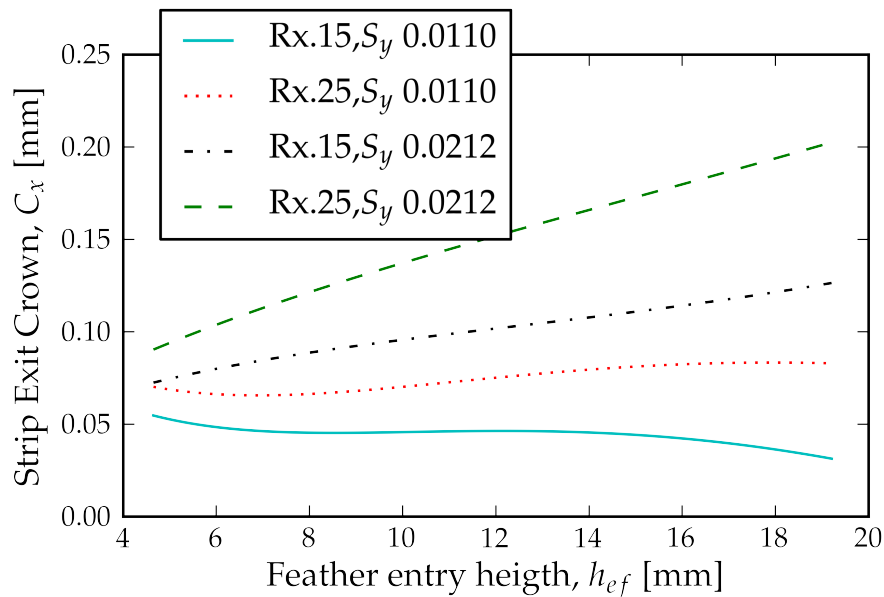
Figure 6.29: Exit crown versus h_{ef} using the final response surface with two reductions and two yield strengths and C_e maintained at constant proportion to h_{ef}.

surface for values of the strip exit crown near points where observations are made return reasonable values, but the further away from these observations the larger the error. The problem as expressed in terms of a Taylor series approximation in one variable, C_e, is

$$C_x(C_e) = C_{x0} + \frac{\partial C_x}{\partial C_e}(C_e - C_{e0})... \tag{6.52}$$

where C_{e0} is the value strip entry crown for the observation, and C_{x0} is the strip exit crown for this observation at $C_x(C_e = C_{e0})$. So only values of C_e close to C_{e0} will produce a reasonable C_x value.

Table 6.17 is calculated using the average strip entry crown, C_e, sensitivity, $\Delta C_x/\Delta C_e$ [mm/mm], from the production model for each stand group. The C_x increment in Table 6.17 is the value found for jacking load in the 1-D study, 0.05 [mm] plus 0.01 [mm] for a more conservative estimate. The hypothesis is that the 0.06 [mm] change in C_x represents the amplitude of the signal, so the same change in C_x for the C_e will improve the SNR and solve the problem on the response surface with many of the partials of C_x with respect to C_e being negative.

Table 6.17: Estimate of The Strip Entry Crown, C_e, Range Based on Production Exit Crown Sensitivity for C_e.

Stand Group	$\mathbf{C_{e,0}}$ [mm]	Current $\mathbf{C_{e,1}}$ [mm]	Prod. Model $\mathbf{\Delta C_x / \Delta C_e}$ []	Target $\mathbf{\Delta C_x}$ [mm]	$\mathbf{\Delta C_e}$ [mm] Needed	Target $\mathbf{C_{e,1}}$ [mm]
7	0.0000	0.0500	0.20	0.06	0.30	0.3000
5	0.0900	0.1000	0.10	0.06	0.60	0.6900
3	0.1580	0.1748	0.05	0.06	1.20	1.3580

6.7.10 The Response Surface and Over Prediction of the Strip Exit Crown

The strip exit crown returned from the response surface is greater than that predicted by the production model in almost all of the comparisons. Figure 6.30 uses a stand group three observation to show two locations that can be used to calculate exit height. The response surface, which uses the steady-state model for the two strip exit heights, locates the exit height at the feather at $h_{xf,1}$, while a crown prediction model based on work-roll-to-strip contact, like the polynomial fit shown in Figure 6.30 for calculating crown, will see a value closer to $h_{xf,2}$. If the assumption is that the production model selects a value close to $h_{xf,2}$ then the location of $h_{xf,1}$ is almost always less than $h_{xf,2}$, especially in the early stand groups 1 and 3. Therefore, the over prediction in strip crown model in the response surface and production comparisons are for the most part due to the differences in calculating the strip exit height at the feather. This is mathematically the equivalent to

$$\begin{aligned} C_{x,prod} &= h_x - h_{xf,2} \\ C_{x,obs} &= h_x - h_{xf,1} \end{aligned} \tag{6.53}$$

where $C_{x,prod}$ is the production-like strip exit crown and $C_{x,obs}$ is the proposed model for strip exit crown calculated for each observation. The majority of the cases seen at stand groups 1, 3 and 5 are $h_{xf,2} > h_{xf,1}$, so solving Equations 6.53 for $h_{xf,2}$ and $h_{xf,1}$ respectively and substituting back into the inequality and simplifying: $C_{x,obs}$ is greater than $C_{x,prod}$.

This also raises the question of which strip exit crown calculation is better to use in a mill setup. The accepted practice is to shape the crown at the early stands to achieve a desirable ratio between the strip exit crown and the strip exit height. This ratio cannot change in the final finishing stands without affecting flatness [23], which is defined as [11]

$$U = \frac{L - L'}{L} \times 10^5 \tag{6.54}$$

where L' is the deformed strip surface length, which follows the strip buckle or wave contour, and L is the length of strip measurement assuming perfect flatness. The use of the wrong profile to calculate C_x distorts the crown to height ratio and the projected downstream flatness. Thus, C_x can be based on
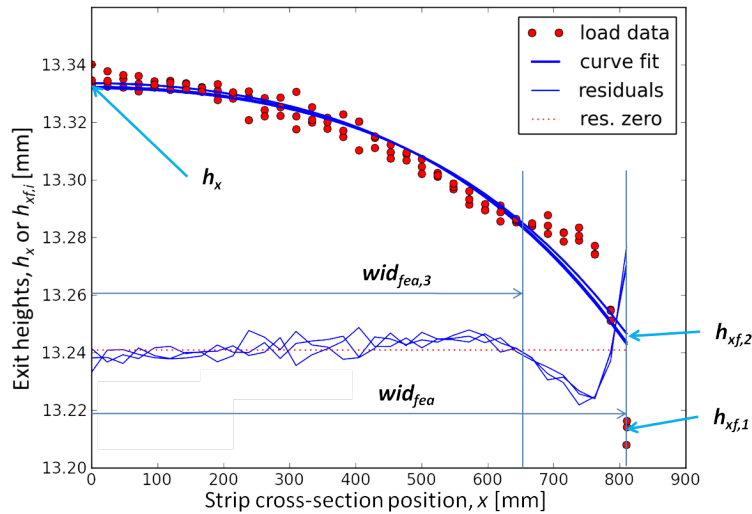
Figure 6.30: The effect of two exit heights at the feather, $h_{xf,1}$ and $h_{xf,2}$ on calculated strip exit crown.

1. $h_{xf,2}(wid_{fea,3})$ if ignoring any feather deformation is important,
2. $h_{xf,2}(wid_{fea})$ if an average of the feather deformation is important,
3. $h_{xf,1}$ if the deformation is found important to preserve.

It is out of scope for this research to pick a verify unit-strip crown or develop cases 1 or 2, but this is a reasonable explanation for some of the response surface and production model differences found in the model comparisons.

Chapter 7

Summary, Conclusions, and Recommendations

7.1 Summary

7.1.1 Dynamic Simulation Loading

A model of the actual method employed to feed the strip through the roll stack and the method employed in the FE model is compared. The prescribed displacements used for the FE model reduces simulation time to reach steady state and it maximizes strip node and work-roll node alignment at the onset. The disadvantage is that the strip initial velocity is higher than the same strip rolled in a real mill.

Some suggestions are made for the excitation times (the time duration for prescribed displacements to set gap) and the simulation damping multiplier to use in future setups for the 1.5 [mm] strip simulations, which unlike the 6.4 [mm] strip needs additional damping and longer excitation times. The two parameter values found are a starting point for additional sampling to determine a workable combination of multipliers.

7.1.2 Force Distribution under the Work Roll

The stress distribution under the work roll identifies the location of the neutral point and supports the empirical curves seen in Orowan's work. Although, the granularity of the mesh gives too much emphasis to the maximum stress point under the roll and Orowan[16] uses annealed aluminum, which is much softer than the simulations of steel rolling here.

7.1.3   Steady-state Model

FFT analysis of the exit heights out of the simulation provides evidence of the exponential decay of the longitudinal exit heights. The equations of motion are developed using a 2DOF lumped-mass model for the roll-stack and strip. The state-space solution for the equations of motion is solved assuming a single output. This is done because the time history for the backup roll is not available. The exit heights and rolling load are determined after minimizing a function based on the 2DOF equations using the simulation data points that start after the *excitation phase* ends and the un-forced steady-state run time begins.

The first effort to determine the steady-state values is based on the equation for a 1DOF system and an unconstrained nonlinear curve fit, which does a reasonable job. However, the variance is higher because a portion of the *excitation phase* is used. The final method to find steady-state values uses the 2DOF equations in combination with a constrained gradient-based minimization routine, L-BFGS. The variance is greatly improved and only the post *excitation phase* data points are used. The equations are formulated in terms of real numbers, instead of allowing complex exponents.

7.1.4   Sampling Methodology

The evolution of the sampling method is explained. The lessons learned are to determine the maximum ranges expected and to pick sample values close to those maximum values or potentially use even a larger range for insensitive variables. Next intermediate samples are collected either to complete a quadratic relationship or to check for a linear or higher functional form. The final lesson learned is to avoid concentrating too many observations in any one area.

7.1.5   Response Surface Results

Comparing the 9-D model to the 8-D "reduced" response surface model with the ANOVA test provides an indication when an independent variable does not make a significant contribution, but not necessarily the cause of the problem. Dropping entry crown with its large number of contradictory observations improves the ANOVA results, but this is a sampling issue not a poor variable choice.

The smallest ANOVA in the 8D results is for the variable that contributes the most to the fit, so the major contributor is h_{ef} and then in order *gap*, S_y, *wid* and d_{wr}. The F-test identifies variables that do not add to the model and it provides the same indication of which variable contributes the most. The F-test, unlike the ANOVA test, selects only the backup-roll diameter as a non-contributing variable.

7.1.6   1-D Projection Results

Most of the results from the 1-D projections are completed too late to guide the sampling methodology in more productive directions, but the use of backup-roll diameter is marginal at best when used in combination with a linear work-roll diameter. However, the 2-D projection for backup-roll diameter with a linear model and work-roll diameter with a quadratic model does provide evidence that backup-roll diameter can make a significant contribution.

A study of the effect of varying C_e, J and C_{wr} could have identified the signal-to-noise problem early enough to correct the sampling plan. Work-roll crown, C_{wr}, needs additional study for a possible quadratic polynomial order.

Support for Ginzburg's finding that crown peaks at 70 to 80 percent of a stands maximum width is found in the 1-D projections for strip width. Strip velocity is found to have a significant effect on exit height; however, the elastic-plastic model does not include work-hardening or strain-rate effects.

7.1.7   Model Comparison Results

The main result from the production and response surface comparisons is that both the all-linear 9-D and quadratic-in-width 8-D response surfaces over-predict the strip exit crown. The production model uses a strip crown value closer to that calculated from a parabola fit to the strip surface, while the response surface uses the strip crown value based on longitudinal strip exit height data points. Because the steady-state longitudinal exit height value at the feather for most stands is less than the same exit height for the parabolic fit, the response surface over predicts strip exit crown. The overestimation is the most pronounced at the entry stands (stand groups 1 and 3) where the larger force creates deformations beyond the strip feather, so the longitudinal exit height is even less than the parabolic fit.

7.2   Conclusions and Recommendations

Calculating the strip exit crown from the two response surface exit heights is the best exit crown model, but needs the strip entry velocity or equivalent as a independent variable. Not including strip entry velocity and deriving strip exit crown directly from a strip exit crown response surface can be done, but with a sacrifice in accuracy. Additional testing is needed to determine if strip entry velocity is a linear or quadratic variable.

It is recommended that the material model used include both the work-hardening and strain-rate effects. A better choice in place of the elliptical yield curve is a Ramberg-Osgood material model with strain rate and strain hardening and this model would not increase run time significantly. Adding temperature and carbon content are also options.

The following four variables are quadratic:

- Entry feather height, h_{ef},
- Strip width, wid,
- Yield strength, S_y,
- Work-roll diameter, d_{wr}.

Large variations in h_{ef} and S_y are needed to capture the quadratic shape. For wid, sampling near the minimum and maximum strip width of a stand and picking the third wid at the break point where C_x peaks is recommended.

The linear variables found:

- Entry crown, C_e,
- Finite element gap, gap,
- Jacking load, J,
- Backup-roll diameter, d_{br}.

C_e needs a large perturbation relative to values typically seen in industry to get the C_x R^2 value near 0.999. J needs to utilize the full range at the finishing stands and potentially larger values than that with the stiffer yield strengths. The less sensitive the variable, the larger the perturbation needs to be. Another option for the less sensitive independent variables is to make them a model parameter and excluding them from the response surface.

The independent variable that is most likely quadratic:

- Work-roll crown, C_{wr}.

Although, C_{wr} is potentially quadratic, a linear representation works well for the finishing stands, so trading accuracy for fewer required observations is an option. The minimum number of observations, assuming a linear polynomial form for strip entry velocity and work-roll crown is $3^4 2^6$ or 5184 observations.

Simulation improvements include adding steady-state controls to the Abaqus model. The current simulation runs for a fixed calculated time, which for most simulations is enough time; however, some of the runs require more time. Padding the run time and introduction steady-state controls accommodates both of the above situations. Abaqus steady-state control would terminate the run when the change in exit height meets the yet to be determined tolerance.

Another important improvement is incorporating time history into the strip exit height data. This would eliminate the need to make assumptions about the strip velocity at a particular data point. One possible source of time information is the simulation work-roll centerline position and the simulation time, which has the added advantage of identifying the strip location at the end of the *excitation phase*.

The parabolic or polynomial strip exit crown profile is potentially a better value to use

in calculating the ratio of strip crown to strip height and the existing data files provide a means to test this. The unknowns are whether or not to include the strip deformation up to the feather or to exclude it from the polynomial fit. Ignoring the deformation can be accomplished with an increase the feather offset based on empirical data or to develop an algorithm to detect the start of the feather deformation.

Based on numerical methods developed to calculate rolling force like those of Freshwater [8, 9], the neutral angle can be estimated. Once the neutral angle is found good estimates for the work-roll tangential velocity and strip exit velocity can be found. Prescribed horizontal velocities are then used to start the work roll and strip at the same velocity as a new addition to the *excitation phase*.

The 2-D work roll and backup roll study demonstrates the ability of the finite element model to capture the marginal effects of changing the backup-roll diameter. Other effects that are worth investigation are strip edge wave and strip center buckle, since simulation of the rolling dynamics are part of the finite element model. This could potentially result into the development of a unit-strip curve similar to that found by Wang [22].

The response surface model and production model disagree as to the expected trends for the strip entry crown and the work-roll diameter. Response surface sampling is the cause behind the lack of agreement for strip entry crown and it can be corrected. The response surface agrees with Ginzburg on the expected trend for work-roll.

A major advantage of the response surface is that rolling load is decoupled from the determination of strip exit height, so an seven stand optimal search only requires using dependent variables strip centerline exit height and strip exit height at the feather in the constraint equations and equation to minimize.

Bibliography

[1] J. M. Alexander. On the theory of rolling. *Proceeding of the Royal Society of London*, A326:535–563, July 1972.

[2] G. E. P. Box and N. R. Draper. *Empirical Model-Building and Response Surfaces*. Wile Series in Probability and Mathematical Statistics. John Wiley & Sons, New York, 1987.

[3] G. E. P. Box, W. G. Hunter, and J. S. Hunter. *Statistics for Experimenters*. Wile Series in Probability and Mathematical Statistics. John Wiley & Sons, New York, 1978.

[4] R. E. Collins. *Mathematical Methods for Physicists and Engineers*. Dover, Mineola, NY, 2nd edition, 1999.

[5] R. D. Cook, D. S. Malkus, M. E. Plesha, and R. J. Witt. *Concents and Applications of Finite Element Analysis*. John Wiley & Sons, Inc., 111 River St., Hoboken, NJ, 4th edition, 2002.

[6] S. A. Domanti and D. L. S. McElwain. Cold rolling of flat metal products: Contribution of mathematical modelling. *Institute of Mechanical Engineers*, 212:73–83, 1998.

[7] N. E. Dowling. *Mechanical Behavior of Materials, Engineering Methods for Deformation, Fracture and Fatigue*. Pearson Prentice Hall, Upper Saddle River, NJ, 3rd edition, 2007.

[8] I. J. Freshwater. Simplified theories of flat rolling-i the calculation of roll pressure roll force and roll torque. *International Journal of Mechanical Science*, 38(6):633–648, August 1996.

[9] I. J. Freshwater. Simplified theories of flat rolling-ii comparison of calculated and experimental results. *International Journal of Mechanical Science*, 38:649–660, August 1996.

[10] V. B. Ginzburg. Profile and flatness of flat rolled products - part ii. United Engineering, Inc., 948 Fort Duquesne Boulevard, Pittsburgh, PA, 1995.

[11] R. M. Guo. Optimal profile and shape control of flat sheet metal using multiple control devices. *IEEE Transactions on Industry Applications*, 32(2):449–457, March/April 1996.

[12] R. M. Guo. A mathematical model for strip profile prediction using influence coefficients and boussinesq's equations. *Transactions of the ASME*, 119:220–226, May 1997.

[13] J. H. Hitchcock. Elastic deformation of rolls during cold rolling. *ASME Report of Special Research Committee on Roll Neck Bearing*, pages 33–41, June 1935.

[14] IPSS. interview by author. Roanoke, VA, Jan 2011.

[15] A. I. Khuri and J. A. Cornell. *Response Surfaces, Designs and Analyses*, volume 81 of *Statitics: Textbooks and Monographs*. ASQC Quality Press, New York, 1987.

[16] E. Orowan. The calculation of roll pressure in hot and cold flat rolling. *Proceedings of the Institute of Mechanical Engineers*, 150(4):140–167, 1943.

[17] P. Lu R. H. Byrd and J. Nocedal. A limited memory algorithm for bound constrained optimization. *SIAM Journal on Scientific and Statistical Computing*, 16(5):1190–1208, 1995.

[18] A. R. Shahani, S. Setayeshib, S.A. Nodamaiea, M.A. Asadic, and S. Rezaiec. Prediction of influence parameters on the hot rolling process using finite element method and neural network. *Journal of Materials Processing Technology*, 209:1920–1935, 2009.

[19] K. N. Shohet and M. F. Boyce. Static model tests of roll bending methods or crown control. *Journal of Iron and Steel Institute*, pages 1099–1103, Nov 1968.

[20] K. N. Shohet and N. A. Townsend. Roll bending methods of control in four-high plate mills. *Journal of Iron and Steel Institute*, pages 1088–1098, Nov 1968.

[21] D. E. Slaughter. Strip crown prediction: Developing a refined dynamic roll-stack model for the hot rolling process. Master's thesis, Virginia Polytechnic Institute and State University, Blacksburg, VA, May 2009.

[22] R. Wang, Q. Yang, A. He, J. Shao, and H. Bian. Strip shape control capability of hot wide strip rolling mills. *Journal of University of Science and Technology Beijing Mineral, Metallurgy, Material*, 15(1):91, February 2008.

[23] X. Wang, A. He, Q. Yang, Z. Xie, and H. Yang. Study and application of crown feedback control in hot strip rolling. *Journal of University of Science and Technology Beijing*, 14(2):190, April 2007.

Appendices

Appendix A

1-D Projection Data

Table A.1: 1-D Projection Data for Change in Strip Width, wid, and Exit Heights, h_x and h_{xf}.

wid [mm]	h_{ef} [mm]	C_e [mm]	S_y [tonne/mm^2]	d_{wr} [mm]	C_{wr} [mm]	d_{br} [mm]	J [tonne]	gap [mm]	h_x [mm]	h_{xf} [mm]
1000	6.4300	0.05	0.020400	625	0.0135	1600	0.00	3.48	5.0670	4.9860
1400	6.4300	0.05	0.020400	625	0.0135	1600	0.00	3.48	5.3155	5.2321
1550	6.4300	0.05	0.020400	625	0.0135	1600	0.00	3.48	5.3779	5.3121
1700	6.4300	0.05	0.020400	625	0.0135	1600	0.00	3.48	5.4334	5.3900
1000	6.4300	0.05	0.020400	775	0.0135	1600	0.00	3.48	5.1911	5.1265
1400	6.4300	0.05	0.020400	775	0.0135	1600	0.00	3.48	5.4285	5.3676
1550	6.4300	0.05	0.020400	775	0.0135	1600	0.00	3.48	5.5033	5.4469
1700	6.4300	0.05	0.020400	775	0.0135	1600	0.00	3.48	5.5691	5.5285

Table A.2: 1-D Projection Data for Change in Strip Entry Height at the Feather, h_{ef} and Exit Heights, h_x and h_{xf}.

wid [mm]	h_{ef} [mm]	C_e [mm]	S_y [tonne/mm^2]	d_{wr} [mm]	C_{wr} [mm]	d_{br} [mm]	J [tonne]	gap [mm]	h_x [mm]	h_{xf} [mm]
1400	6.4337	0.00	0.014000	625	0.0000	1500	0.00	3.48	4.9455	4.8782
1400	5.9000	0.00	0.014000	625	0.0000	1500	0.00	3.48	4.7678	4.7059
1400	6.8000	0.00	0.014000	625	0.0000	1500	0.00	3.48	5.0704	4.9962
1400	7.2000	0.00	0.014000	625	0.0000	1500	0.00	3.48	5.2015	5.1191
1400	7.5000	0.00	0.014000	625	0.0000	1500	0.00	3.48	5.2935	5.2020
1400	8.0000	0.00	0.014000	625	0.0000	1500	0.00	3.48	5.4383	5.3433
1400	8.5000	0.00	0.014000	625	0.0000	1500	0.00	3.48	5.5677	5.4616
1400	9.0000	0.00	0.014000	625	0.0000	1500	0.00	3.48	5.6928	5.5740

Table A.3: 1-D Projection Data for Change in Work-roll Diameter, d_{wr}, and Exit Heights, h_x and h_{xf}.

wid [mm]	h_{ef} [mm]	C_e [mm]	S_y [tonne/mm²]	d_{wr} [mm]	C_{wr} [mm]	d_{br} [mm]	J [tonne]	*gap* [mm]	h_x [mm]	h_{xf} [mm]
1700	6.4300	0.00	0.021200	625	0.0135	1450	0.00	3.48	5.4610	5.4195
1700	6.4300	0.00	0.021200	700	0.0135	1450	0.00	3.48	5.5288	5.4910
1700	6.4300	0.00	0.021200	775	0.0135	1450	0.00	3.48	5.5855	5.5451
1700	6.4300	0.00	0.021200	850	0.0135	1450	0.00	3.48	5.6432	5.6058
1700	6.4300	0.00	0.021200	625	0.0135	1500	0.00	3.48	5.4714	5.4196
1700	6.4300	0.00	0.021200	700	0.0135	1500	0.00	3.48	5.5273	5.4887
1700	6.4300	0.00	0.021200	775	0.0135	1500	0.00	3.48	5.5907	5.5522
1700	6.4300	0.00	0.021200	850	0.0135	1500	0.00	3.48	5.6401	5.6041
1700	6.4300	0.00	0.021200	625	0.0135	1550	0.00	3.48	5.4683	5.4262
1700	6.4300	0.00	0.021200	700	0.0135	1550	0.00	3.48	5.5287	5.4894
1700	6.4300	0.00	0.021200	775	0.0135	1550	0.00	3.48	5.5841	5.5482
1700	6.4300	0.00	0.021200	850	0.0135	1550	0.00	3.48	5.6386	5.6079

Table A.4: 1-D Projection Data for Change in FE Gap, *gap* and Exit Heights, h_x and h_{xf}.

wid [mm]	h_{ef} [mm]	C_e [mm]	S_y [tonne/mm²]	d_{wr} [mm]	C_{wr} [mm]	d_{br} [mm]	J [tonne]	*gap* [mm]	h_x [mm]	h_{xf} [mm]
1400	6.4300	0.00	0.014000	625	0.0000	1500	0.00	3.48	4.9444	4.8751
1400	6.4300	0.00	0.014000	625	0.0000	1500	0.00	3.13	4.7520	4.6688
1400	6.4300	0.00	0.014000	625	0.0000	1500	0.00	2.78	4.5488	4.4566
1400	6.4300	0.00	0.014000	625	0.0000	1500	0.00	2.44	4.3447	4.2467

Table A.5: 1-D Projection Data for Change in Strip Entry Crown, C_e, and Exit Heights, h_x and h_{xf}.

wid [mm]	h_{ef} [mm]	C_e [mm]	S_y [tonne/mm²]	d_{wr} [mm]	C_{wr} [mm]	d_{br} [mm]	J [tonne]	*gap* [mm]	h_x [mm]	h_{xf} [mm]
1700	6.4300	0.04	0.014000	625	0.0000	1500	0.00	3.48	5.0877	5.0440
1700	6.4300	0.03	0.014000	625	0.0000	1500	0.00	3.48	5.0840	5.0431
1700	6.4300	0.02	0.014000	625	0.0000	1500	0.00	3.48	5.0815	5.0406
1700	6.4300	0.01	0.014000	625	0.0000	1500	0.00	3.48	5.0778	5.0399

Table A.6: 1-D Projection Data for Change in Jacking Load, J and Exit Heights, h_x and h_{xf}.

wid [mm]	h_{ef} [mm]	C_e [mm]	S_y [tonne/mm^2]	d_{wr} [mm]	C_{wr} [mm]	d_{br} [mm]	J [tonne]	gap [mm]	h_x [mm]	h_{xf} [mm]
1400	6.4300	0.00	0.014000	625	0.0000	1500	80.00	3.48	5.0018	4.9619
1400	6.4300	0.00	0.014000	625	0.0000	1500	60.00	3.48	4.9897	4.9403
1400	6.4300	0.00	0.014000	625	0.0000	1500	40.00	3.48	4.9746	4.9199
1400	6.4300	0.00	0.014000	625	0.0000	1500	20.00	3.48	4.9631	4.8989

Table A.7: 1-D Projection Data for Change in Yield Strength, S_y and Exit Heights, h_x and h_{xf}.

wid [mm]	h_{ef} [mm]	C_e [mm]	S_y [tonne/mm^2]	d_{wr} [mm]	C_{wr} [mm]	d_{br} [mm]	J [tonne]	gap [mm]	h_x [mm]	h_{xf} [mm]
1400	6.4300	0.00	0.008000	625	0.0000	1500	0.00	3.48	4.4902	4.4365
1400	6.4300	0.00	0.010000	625	0.0000	1500	0.00	3.48	4.6662	4.6038
1400	6.4300	0.00	0.012000	625	0.0000	1500	0.00	3.48	4.8165	4.7503
1400	6.4300	0.00	0.014000	625	0.0000	1500	0.00	3.48	4.9472	4.8782
1400	6.4300	0.00	0.016000	625	0.0000	1500	0.00	3.48	5.0721	4.9975
1400	6.4300	0.00	0.018000	625	0.0000	1500	0.00	3.48	5.1814	5.1027
1400	6.4300	0.00	0.020000	625	0.0000	1500	0.00	3.48	5.2919	5.2032
1400	6.4300	0.00	0.022000	625	0.0000	1500	0.00	3.48	5.3673	5.2840
1400	6.4300	0.00	0.024000	625	0.0000	1500	0.00	3.48	5.4592	5.3653
1400	6.4300	0.00	0.026000	625	0.0000	1500	0.00	3.48	5.5410	5.4412
1400	6.4300	0.00	0.028000	625	0.0000	1500	0.00	3.48	5.6121	5.5099
1400	6.4300	0.00	0.030000	625	0.0000	1500	0.00	3.48	5.6760	5.5742
1400	6.4300	0.00	0.032000	625	0.0000	1500	0.00	3.48	5.7364	5.6345
1400	6.4300	0.00	0.034000	625	0.0000	1500	0.00	3.48	5.7973	5.6927
1400	6.4300	0.00	0.036000	625	0.0000	1500	0.00	3.48	5.8536	5.7519
1400	6.4300	0.00	0.038000	625	0.0000	1500	0.00	3.48	5.9160	5.8069

Table A.8: 1-D Projection Data for Change in Work-Roll Crown, C_{wr} and Exit Heights, h_x and h_{xf}.

wid [mm]	h_{ef} [mm]	C_e [mm]	S_y [tonne/mm^2]	d_{wr} [mm]	C_{wr} [mm]	d_{br} [mm]	J [tonne]	gap [mm]	h_x [mm]	h_{xf} [mm]
Strip velocity		1284.23 [mm/s]								
1400	6.4300	0.00	0.014000	625	-0.1200	1500	0.00	3.48	5.0800	4.9900
1400	6.4300	0.00	0.014000	625	-0.0600	1500	0.00	3.48	5.1100	5.0400
1400	6.4300	0.00	0.014000	625	0.0750	1500	0.00	3.48	5.1100	5.0700
1400	6.4300	0.00	0.014000	625	0.1000	1500	0.00	3.48	5.1100	5.0900
Strip velocity		4018.44 [mm/s]								
1400	6.4300	0.00	0.014000	625	-0.1300	1500	0.00	3.48	4.9600	4.8200
1400	6.4300	0.00	0.014000	625	-0.0600	1500	0.00	3.48	4.9700	4.8600
1400	6.4300	0.00	0.014000	625	0.0200	1500	0.00	3.48	4.9600	4.9000
1400	6.4300	0.00	0.014000	625	0.1100	1500	0.00	3.48	5.0200	4.9900
Strip velocity		6752.64 [mm/s]								
1400	6.4300	0.00	0.014000	625	-0.1300	1500	0.00	3.48	4.9400	4.8100
1400	6.4300	0.00	0.014000	625	-0.0600	1500	0.00	3.48	4.9400	4.8500
1400	6.4300	0.00	0.014000	625	0.0200	1500	0.00	3.48	4.9500	4.8900
1400	6.4300	0.00	0.014000	625	0.1100	1500	0.00	3.48	4.9500	4.9300

Table A.9: 2-D and 1-D Projection Data for Change in Backup-roll Diameter, d_{br} and Exit Heights, h_x and h_{xf}.

wid [mm]	h_{ef} [mm]	C_e [mm]	S_y [tonne/mm^2]	d_{wr} [mm]	C_{wr} [mm]	d_{br} [mm]	J [tonne]	gap [mm]	h_x [mm]	h_{xf} [mm]
1700	6.4300	0.00	0.021186	625	0.0135	1450	0.00	3.48	5.4610	5.4195
1700	6.4300	0.00	0.021200	625	0.0135	1500	0.00	3.48	5.4714	5.4196
1700	6.4300	0.00	0.021200	625	0.0135	1550	0.00	3.48	5.4683	5.4262
1700	6.4300	0.00	0.021200	700	0.0135	1450	0.00	3.48	5.5288	5.4910
1700	6.4300	0.00	0.021200	700	0.0135	1500	0.00	3.48	5.5273	5.4887
1700	6.4300	0.00	0.021200	700	0.0135	1550	0.00	3.48	5.5287	5.4894
1700	6.4300	0.00	0.021200	775	0.0135	1450	0.00	3.48	5.5855	5.5451
1700	6.4300	0.00	0.021200	775	0.0135	1500	0.00	3.48	5.5907	5.5522
1700	6.4300	0.00	0.021200	775	0.0135	1550	0.00	3.48	5.5841	5.5482
1700	6.4300	0.00	0.021200	850	0.0135	1450	0.00	3.48	5.6432	5.6058
1700	6.4300	0.00	0.021200	850	0.0135	1500	0.00	3.48	5.6401	5.6041
1700	6.4300	0.00	0.021200	850	0.0135	1550	0.00	3.48	5.6386	5.6079